Biocompatible Inorganic Nanocrystals for Fluorescence and CT Imaging

Dissertation zu Erlangung des Doktorgrades der Naturwissenschaft (Dr. rer. nat.)

an der naturwissenschaftlichen Fakultät IV
- Chemie und Pharmazie -
der Universität Regensburg

vorgelegt von

Anna Hezinger

aus Neu-Ulm

im April 2010

Diese Doktorarbeit entstand in der Zeit von Januar 2006 bis April 2010 am Lehrstuhl für Pharmazeutische Technologie der Universität Regensburg.

Diese Arbeit wurde angeleitet von Prof. Dr. Achim Göpferich

Promotionsgesuch eingereicht am:		19.04.2010
Kolloquiumstermin:		23.04.2010
Prüfungsausschuß:	Vorsitzender:	Prof. Brunner
	Erstgutachter:	Prof. Göpferich
	Zweitgutachter:	Prof. Wegener
	Drittprüfer:	Prof. Pfitzner

„石の上に三年“

”Three years on the rock”
- Expect to work at something
for three years before you see results-

(Japanese Proverb)

Science is always wrong.
It never solves a problem
without creating ten more.

(George Bernard Shaw)

Acknowledgements

It is a pleasure to thank all those who made this thesis possible.

Most importantly, I have to thank **Prof. Dr. Achim Göpferich** for providing this interesting thesis and the excellent working conditions at his chair.
Also, I appreciate the very much all the help and support, all the fruitful discussions and numerous suggestions of my supervisor **Dr. Jörg Tessmar** throughout this work.
The financial support fort his work by the **BMBF "NanoforLife"** project Nanogel and the **Bayer Schering Pharma AG** is gratefully acknowledged.

I would like to show my gratitude to **Angelika Kühn** (Uni. Regansburg. Department of Zoology) for providing the TEM equipment, furthermore **Dr. Markus Drechsler** (Uni. Bayreuth, Department of Marcomolecular Chemistry II) for the Cryo-TEM measurements, **Angelika Berié** for measuring the ICP-OES samples, **Dr. Harald Huber** (Uni. Regensburg, Department for Microbiology) for providing the ICP-OES device and **PD Dr. Andreas Schreyer** (Uni. Medical Center Regensburg) for the CT measurements.

I am indebted to many of my present and former colleagues at the institute for the working atmosphere and all the help throughout this work. Most of all, I owe my deepest gratitude to my lab colleagues in the "Chicken Farm". **Cornelia Rose** for all the days and nights working together on our project and **Annina Seitz** for always being our "middleman" for all intents and purposes, and of course both for all the fun in the lab, coffee breaks and girls´ nights.

This thesis would not have been possible unless my good friends **Dr. Alexander "***Dr. Pavolv***" Schätz**, **Dr. Florian "***Flo***" Sahr**, **Klaus "***Harrarar***" Harrar**, **Dr. Markus "***Der General***" Hager**, **Katrin "***d´Gschubste***" Ulbrich**, **Dr. Alexander "***Ein Bißchen***" Tereshchenko**, **Dr. Cornelia "***Conny***" Dreher**, **Dr. Johannes "***Hans***" Hunger**, and most of all, **Dr. Matthias "***Dr. Ignaz***" Stich**, he knows why, and **Benjamin "***Benno***" Gruber**. Thanks for all the fun we had, for all the advice and backup, for just "being there" in hard times.

Finally, special thanks to my parents, **Elke** und **Dieter Traub** und **Eva** und **Dieter Hezinger**, for all the emotional and financial support, and moreover for always believing in me.

Table of Contents

1. Nanoparticles in molecular imaging 8

1.1. Luminescence Imaging 10

1.1.1. Principles of luminescence 10

1.1.2. Nanoparticles as contrast agents in luminescence imaging 12

1.2. CT Imaging 13

1.2.1. Principles of CT contrast 13

1.2.2. Nanoparticles as contrast agents in CT imaging 15

1.3. Aim of the work 15

1.4. References 17

Part I Quantum Dots

2. Quantum Dots - Introduction and General Aspects 19

2.1. Introduction 20

2.2. Quantum Dots 21

2.2.1. Optical Properties 22

2.2.2. Synthesis 23

2.3. Biocompatible Quantum Dots 24

2.3.1. Effects of surface coating 26

2.3.2. Ligand Exchange Strategies 30

2.3.3. Ligand Capping Strategies 35

2.3.4. Application of surface coatings 39

2.4. Conclusion 42

2.5. Future Outlook 43

2.6. References 44

3. Quantum Dots - Materials and Methods 53

3.1. Quantum Dots 54

3.2. Dihydrolipoic acid 54

3.3. Synthesis of amino Poly(ethylene glycol)mercaptoundecyl ether 54

3.4. Coating of Quantum Dots 54

3.5. Fluram assay 55

3.6. Cytotoxicity Test 55

3.7. Syntheses of Quantum Dots 55

3.7.1. Synthesis of Cadmium selenide Quantum Dots 55

3.7.2. Synthesis of Cadmium selenide/Zinc sulfide Core/Shell Quantum Dots 56

3.7.3. Synthesis of Cadmium telluride Quantum Dots 56

3.7.4. Synthesis of Cadmium telluride/Cadmium selenide Core/Shell Quantum Dots 57

3.7.5. Synthesis of Cadmium telluride/Cadmium zinc sulfide Core/Shell Quantum Dots 58

3.8. Syntheses of Ligands 58

3.8.1. Synthesis of Dihydrolipoic acid 58

3.8.2. Synthesis of amino Poly(ethylene glycol)$_{750}$ mercaptoundecyl ether 59

3.9. Coating of Quantum Dots 62

3.9.1. Coating of Quantum Dots with Dihydrolipoic acid 62

3.9.2. Coating of Quantum Dots with Poly(ethylene glycol) mono-11-mercaptouncedyl ether derivatives 63

3.10. Analysis of particles 63

3.10.1. Spectroscopic analysis 63

3.10.2. Analysis of composition 65

3.10.3. Size analysis with photon correlation spectroscopy 65

3.10.4. Size and concentration calculation 65

3.10.5. Morphologic analysis with transmission electron microscopy/Cryo-transmission electron microscopy 66

3.10.6. Amino group determination with a modified Fluram® assay 67

3.10.7. Cytotoxicity Test 68

3.11. References 70

4. Quantum Dots - Results 71

4.1. Cadmium Selenide based Quantum Dots 72

4.2. Cadmium Telluride based Quantum Dots 73

4.2.1. CdTe Quantum Dots 73

4.2.2. CdTe/CdSe Quantum Dots 73

4.2.3. CdTe/CdZnS Quantum Dots 74

4.2.4. Optimisation of CdTe/CdZnS Quantum Dot synthesis 76

4.3. Dihydroliponic acid coated CdTe/CdZnS Quantum Dots 84

4.4. Poly(ethyleneglycol)mercaptoundecylether coated CdTe/CdZnS Quantum Dots 85

4.4.1. Non functionalized Quantum Dots 85

4.4.2. Amino-functionalized Quantum Dots 88

4.4.3. Cytotoxicological investigation of water-soluble Quantum Dots 89

4.5. References 93

5. Quantum Dots - Discussion 95

5.1. Discussion **96**

5.2. References **100**

Part II Gadolinium Oxide Nanoparticles

6. Gadolinium Oxide Nanoparticles - Introduction and General Aspects 101

6.1. Introduction **102**

6.2. Synthesis of doped Gadolinium Oxide Nanoparticles **103**

6.3. Physical and toxicological properties of Gadolinium Oxide Nanoparticles **104**

6.3.1. Optical properties *104*

6.3.2. MRI and CT active properties *106*

6.3.3. Neutron capture properties *108*

6.3.4. Toxicological properties *108*

6.4. Coating of Gadolinium Oxide Nanoparticles **109**

6.5. Applications of Gadolinium Oxide Nanoparticles and conclusion **112**

6.6. References **115**

7. Gadolinium Oxide Nanoparticles - Materials and Methods 121

7.1. Particles synthesis **122**

7.2. Cytotoxicity test **122**

7.3. DEG-mediated Synthesis of Gadolinium Oxide Particles **122**

7.3.1. Synthesis of sub-10 nm Gadolinium Oxide particles *122*

7.3.2. Coating of sub-10nm Gadolinium Oxide particles with Silica *123*

7.3.3. Synthesis and coating of Gadolinium Oxide Nanoparticles 123

7.4. Synthesis of doped Gadolinium Oxide Nanoparticles 124

7.4.1. Combustion synthesis 125

7.4.2. Precipitation synthesis 125

7.4.3. Coating of particles 126

7.5. Analysis of particles 126

7.5.1. Spectroscopic analysis 126

7.5.2. Size and zeta potential analysis with PCS 127

7.5.3. Morphological analysis with TEM 127

7.5.4. Determination of gadolinium content 127

7.5.5. Analysis of crystal structure with P-XRD 127

7.5.6. Determination of radio-opaqueness with CT Imaging 128

7.5.7. Cytotoxicity test 128

7.6. References 130

8. Gadolinium Oxide nanopartilces - Results 131

8.1. DEG mediated synthesis of Gadolinium Oxide Nanoparticles 132

8.1.1. Synthesis and coating of sub-10 nm Gadolinium Oxide particles 132

8.1.2. Synthesis and coating of Gadolinium Oxide Nanoparticles 133

8.2. Annealing based Gadolinium Oxide Nanoparticles 139

8.2.1. Combustion synthesis 139

8.2.2. Precipitation synthesis 141

8.2.3. Cytotoxicity tests of Gadolinium Oxide Nanoparticles with different coatings 148

8.3. References 152

9. Gadolinium Oxide Nanoparticles - Discussion 153

9.1. Discussion 154

9.2. References 161

10. Summary and Conclusion 162

10.1. Summary 163

10.1.1. Quantum Dots 163

10.1.2. Gadolinium Oxide Nanoparticles 165

10.2. Conclusion 167

11. Abbreviations and Acronyms 168

12. Supplement 174

13. Curriculum Vitae and List of Publications 176

Chapter 1

General Introduction

Nanoparticles in molecular imaging

Molecular imaging – the ability to "see" within the living human body and understand its biological complexities for the treatment of disease – is one of the most exciting and rapidly growing fields of biomedical research. It involves the non-invasive study of biological processes in vivo at the cellular and molecular level. The key role for chemists is the design of suitable imaging probes that make molecular processes visible, quantifiable, and traceable over time, aiming to probe molecular abnormalities as cause for many different deseases. A closely connected, and also fast growing field, is the application of different imaging techniques in living subjects, ranging from in vitro cell based tests to in vivo whole body scanning. Nowadays, a lot of different imaging methods can be utilized, such as positron emission tomography (PET), single photon emission computed tomography (SPECT), ultrasound (US), optical (particularly fluorescence) imaging, magnetic resonance imaging (MRI), and computed tomography (CT). Each method differs in terms of sensitivity and resolution, and different imaging techniques are, in general, complementary rather than competitive. The choice of modality depends on constitution and size of the sample as well as nature of the question that is to be addressed.

In parallel to the imaging techniques, during the last decade, nanotechnology developed into a fast growing research area, involving chemistry, biology, medicine, engineering, and more. Within this field, nanoparticles emerged as important players, with applications ranging from contrast agents in medical imaging to smart probes for analytical testing. The nanoparticulate systems used are typically smaller than a few hundred nanometers and are comparable to the size of large biological molecules such as enzymes, receptors, or antibodies. They also have a number of specific properties that distinguish them from bulk materials simply by virtue of their size, such as chemical reactivity, energy absorption, and biological mobility [1-3]. The application of nanoparticles as contrast agents and reporters for molecular imaging applying and combining these different imaging systems suggests itself due to their many advantages over organic molecules. They give higher contrasts due to their higher on-site concentration, and a greater diversity of functionalization and modification possibilities due to the versatility of surface chemistry. Moreover, the combination of different modalities to investigate the fate of one nanoparticle gives a powerful tool in molecular imaging. The most important features of imaging probes are the in vitro and in vivo stability, resistance to metabolic degradation, and non-toxicity, completed by an adequate solubility in biological environment.

In the case of fluorescent contrast agents, high resistance against photobleaching, high brightness, and an emission in the NIR range of 650 – 900 nm is desirable. For CT imaging

probes, a high radiodensity is required. All these exigencies can be met by combing different features in only one particle, giving the possibility of multimodal molecular imaging. Inorganic nanoparticles can provide high luminescence and reduced photobleaching as well as high radiodensity by their mere inorganic composition. Moreover, they exhibit high resistance against disintegration in biological environment due to their particulate character. Their physicochemical properties, as well as the ability for targeting and molecular recognition, can easily be influenced by the applied surface coating. This general introduction will give a short overview of nano-scaled devices in luminescence and CT imaging and their essential features for successful application.

1.1. Luminescence Imaging

Visible light is the most versatile radiation for imaging. It enables for non-invasive measurements and creates contrast by intensity, wavelength, polarization, coherence, interference [4-6], lifetime, and nonlinear effects. Out of the optical imaging techniques available, fluorescence based methods have emerged as one of the most powerful tools in in vitro and small animal in vivo imaging. This fact is founded in the availability of highly sensitive detection techniques and separation of excitation and emission, reducing background noise due to scattering. Nevertheless, an inherent problem of fluorescence imaging is the penetration depth of light into the body, which is limited to only a few centimeters, depending on the wavelength used.

1.1.1. Principles of luminescence

Optical fluorescence strongly depends on the inherent property of the fluorophore used. Upon excitation by a quantum of specific energy, three fundamental electronic processes have to be considered: (a) the absorption of light energy, associated with an electron transfer to an excited state; (b) radiationless decay within and from the excited state and (c) emission of radiation with various wavelengths, longer than the excitation wavelength itself. The difference between the wavelength required for excitation and the wavelength of the emitted light is known as the Stokes´ shift corresponding to the radiationless energy loss within the excited state. A representative method for illustrating these electronic processes is the Jablonski diagram (see figure 1).

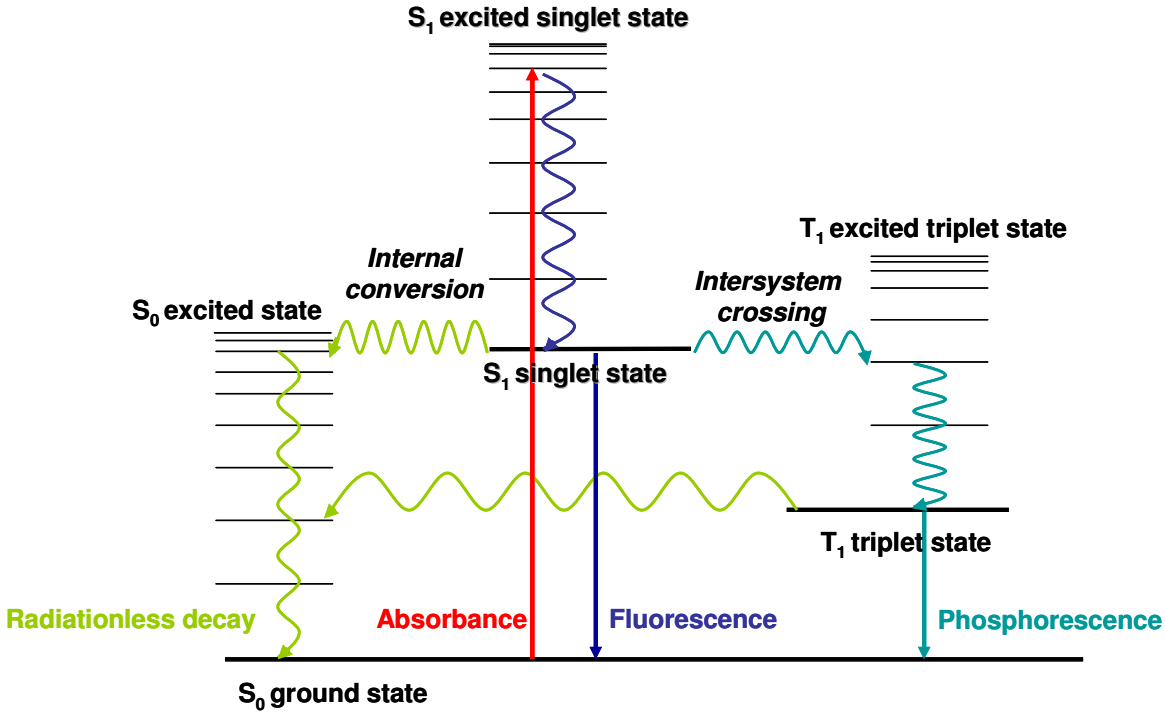

Figure 1: Jablonski diagram for illustration of electronic processes

Two basic pathways for radiative decay of an excited molecule, have to be considered. The first one is fluorescence, including vibronic relaxation of an excited singlet S_1-state to the S_1-ground state, followed by the emission of the residual energy as a photon to the S_0 ground state. This process only occurs in states of the same multiplicity, in most cases form the S_1 to S_0. Considering quantum mechanics, it is a spin-allowed process, thus resulting in short luminescence lifetimes. The second pathway, phosphorescence, involves intersystem crossing form a singlet to a triplet state, known to be an efficient crossing between states of different multiplicity, due to spin-orbit coupling. Nevertheless, it is a spin-forbidden process with therefore much longer lifetimes. Furthermore, it is known to be much more probable for $S_n \rightarrow T_n$ than for $T_n \rightarrow S_{n-1}$, but strongly dependent on the molecule. Besides this light emitting processes, there are also some non-radiative pathways of energy loss shown in figure 1 [7,8]. The luminescence quantum yield is, in addition to the absorption coefficient and lifetime, perhaps the most important property of a fluorophore.

$$Q = \frac{\Gamma}{\Gamma + k_{nr}} \tag{1}$$

Q quantum yield

Γ rate of luminescence of the fluorophore [1/s]

k_{nr} rate of non radiative processes [1/s]

It is defined as the number of emitted photons relative to the number of absorbed photons, as shown in equation 1. The emissive rate Γ represents the rate of the fluorophore's luminescence; whereas k_{nr} includes all processes depopulating the excited singlet state in a non-radiative way. As can be seen from equation 1, the quantum yield reaches nearly unity, if the rate of non-radiative decay k_{nr} is very small. This is the case for an "ideal" fluorophore. One example meeting this postulate is rhodamine and its derivatives and other laser dyes [7-10].

A more detailed explanation of the luminescence behavior of the particulate flourophores, quantum dots sand doped gadolinium oxide nanoparticles, will be given in the respective introduction chapters (2.3 and 6.3.1).

1.1.2. Nanoparticles as contrast agents in luminescence imaging

As already mentioned, the fundamental barriers of optical imaging in tissue is the poor penetration depth and resolution, due to high light scattering, autofluorescence and high absorption by omni-present hemoglobin in the mid visible range. Near-infrared light of 650 – 900 nm, achieves the highest tissue penetration due to minimal absorbance by surface tissue in this spectral region. This fact is founded in hemoglobin, water and lipids having their lowest absorption coefficients in the NIR region [11,12].

In order to overcome most of these problems and to obtain adequate contrast in the images, the signal-emitting material has to be accumulated at the site of interest. Herein, nanoparticles can contribute the unique property to concentrate a higher fluorophore amount at one specific point. Moreover, they offer the possibility to tune the emission wavelength with retaining their physicochemical properties and vice versa. This makes them suitable for a wide range of applications, by simply changing e.g. the surface bound targeting molecules or their inherent emission wavelength. Additionally, they can be used for multiplexed imaging applications, were the same nanoparticles with different surface coatings and emission wavelengths can be detected simultaneously. In the last decade, a huge variety of different types of luminescent nanoparticles were developed. Nevertheless, some of the particles already match most, or even all of the desirable properties describes above. Therefore, they proved to be more promising than others finding broad access to modern fluorescence imaging. Two of the most prominent nanoparticular systems are luminescent doped silica or polymer nanoparticles and semiconductor quantum dots [13,14].

1.2. CT Imaging

The discovery of X-ray radiation by Wilhelm C. Röntgen in 1895 revolutionized the practice of medicine and offered the first suitable imaging method for medical applications in the patient [15,16]. Physicians instantly recognized the importance of this discovery for medical diagnosis since it was now was possible to externally visualize the internal anatomic structures. Although computed tomography X-ray imaging (CT) also employs the same X-ray radiation for generating an image, this is very different from direct X-ray projection imaging, as Röntgen developed it. Computed tomography instead produces cross-sectional images and provides very good contrast resolution and adequate spatial resolution. Moreover, not only hard tissues like bone and cartilage can be investigated, but also the differentiation between softer tissues is possible. Nevertheless, the possibilities to acquire contrasted molecular images are the same as in direct projection X-ray imaging. In CT, however, contrast molecules can be pinpointed in three dimensions to millimeter accuracy, allowing a higher resolution then the mere two dimensional projections [17].

1.2.1. Principles of CT contrast

When an X-ray beam transverses matter both absorption and deflection of photons will occur. The reduction in beam intensity, due to these processes, defines the degree of X-ray attenuation, as shown in equation 2.

$$I = I_0 e^{-\mu x} \tag{2}$$

I transmitted X-ray intensity

I_0 incident X-ray intensity

μ mass attenuation coefficient of the absorber [cm^2/g]

x thickness of matter [cm]

In CT, the linear X-ray attenuation coefficient of an investigated voxel (volumetric pixel) is measured directly, and hence a CT number is defined as

$$CTnumber = \frac{K(\mu_p - \mu_w)}{\mu_w} \tag{3}$$

K magnification constant

μ_p linear attenuation coefficient of a pixel [cm^2/g]

μ_w linear attenuation coefficient of water [cm^2/g]

When K is 1000, then the CT numbers are called Houndsfield units (HU).

The attenuation is based on three interactions between the radiation and the transversed matter: (a) coherent scattering, (b) the photoelectronic effect and (c) the Compton effect. Considering these three processes, the coherent scattering, producing scattered radiation, is insignificant compared to the other both and can therefore be neglected.

$$\mu = \omega + \tau + \delta \tag{4}$$

μ mass attenuation coefficient [cm^2/g]

ω coherent scattering [cm^2/g]

τ photoelectron effect [cm^2/g]

δ Compton effect [cm^2/g]

The contribution of the photoelectronic effect to X-ray attenuation is high with low-energy radiation and with absorbers of high atomic numbers. The probability for Compton scattering depends on the number of electrons in the outer shell and is independent of the atomic number. This effect is responsible for most of the scattered photons, which both increase noise and decrease contrast. In fact this is more likely for absorbers of low atomic number, whereas at high atomic numbers the photoelectron effect dominates.

This fact is founded in the photoelectronic effect resulting from the interaction of the X-ray photons with inner shell electrons. When an incident photon impacts an electron with energy greater than the binding energy of the encountered electron, it can eject the electron from its orbital. Since all energy is consumed in this process, the incident photon is absorbed and disappears. The ejected electron (a so-called free electron) is reabsorbed immediately, followed by the filling of the vacant electron "place" in the inner shell by an electron of the outer shell. This produces another characteristic X-ray emission. The Compton scattering arises from the interaction of an X-ray photon with an outer shell electron. When an X-ray photon with high energy collides with an outer shell electron, whose binding energy is relatively low, it will expel the electron from its orbital. The photon itself will be deflected as scattered energy. The quantity of Compton scattering decreases as the X-ray photon energy increases. As a result, the radiation exposure with scattered photons and therefore also the overall exposure, is lower with high energy X-rays [18].

1.2.2. Nanoparticles as contrast agents in CT imaging

Contrast enhancement results largely from the photoelectron effect due to high atomic numbers of the atoms used. Several theoretical and experimental investigations have demonstrated the superior X-ray contrast enhancing ability of heavy metal elements [19-24]. Furthermore, the condensation of these elements with high atomic number, optimal atomic numbers lie between 58 and 66 for tungsten tube driven X-ray sources, could even gain more contrast. Therefore, inorganic nanoparticles composed of heavy metal elements can provide the tool for molecular CT imaging, combining high contrast with the possibility to add targeting molecules. Unfortunately, there are very few examples of nanoparticular CT contrast agents in literature [25-32], due to the overpowering position of the inexpensive and nontoxic water-soluble iodinated contrast agents (Z = 53). Nevertheless, over the last one hundred years, some macro- and microparticular formulations of heavy metals composites were developed, and some also employed, for X-ray projection and computed tomography X-ray imaging [18]. However, all these formulations display certain drawbacks, as the inappropriate size for i.v. application or the adverse effects due to inherent heavy metal toxicity.

1.3. Aim of the work

Acting on the assumption of the increasing demand on nanoparticlular contrast agents for luminescence and CT imaging, as well as the possibility of combining both to overcome the limitations of each, the enhancement of existing and development of new particles is a promising field of research.

As already mentioned, the development of nanoparticular contrast agents in the field of luminescence imaging is quite advanced. Considering the existent systems, the enhancement of quantum dots systems, especially in terms of emission wavelength and size of the coated particles, appears to be the most promising approach. Due to the broad range of possible applications, the requirements for semiconductor quantum dots in terms of stability, size, water-solubility as well as biocompatibility have grown tremendously in recent years. In order to satisfy all these demands, different strategies with polymers as capping agents have been used (chapter 2). The aim of this work was the development of an easy synthesis strategy leading to long-term stable, long-wavelength emitting, and biocompatible quantum dots as versatile label for biological experiments and for the development and characterization of new drug delivery systems (part I of the thesis). Therefore, an optimization of the synthesis parameters was carried out, aiming at long emission wavelengths and high quantum yields

(chapter 4.1&4.2). Subsequently, different functionalized and non -functionalized surface ligands were applied, intending to produce water-dispersable non-toxic and functionizable quantum dots (chapter 4.3&4.4).

In contrast to luminescence imaging, the field of nanoparticular CT imaging agents is a quite new area of research, attracting growing attention with the evolving molecular imaging techniques. Even more, the fabrication of bi- or multimodal contrast agents, is an exiting new research subject (chapter 6). They enable for overcoming the resolution limitation of CT imaging and the penetration problem of luminescence imaging. Considering the requirements for nanoparticular contrast agents, the development of doped gadolinium oxide nanoparticles is most promising (part II of the thesis), giving even the possibility of MR imaging and neutron capture therapy. To reach this goal, first of all, a synthesis strategy yielding differently coated nanoparticles of different sizes for CT imaging applications were applied (chapter 8.1). Nevertheless, to realize the bimodality of the particles, another preparation route was utilized. Herein, water-dispersable particles of varying sizes and emission wavelengths could be produced (chapter 8.2).

1.4. References

[1] Y. Volokitin, J. Sinzig, L. Jongh, G. Schmid, M. Vargaftik and I. Moiseev, Quantum-size effects in the thermodynamic properties of metallic nanoparticles, Nature 384 (1996) 621--623.

[2] P.J. Reynolds. On Cluster and Clustering, Elsevier Science Publisher, Amsterdam (1993).

[3] J. Shi, S. Gider, K. Babcock and D. Awschalom, Magnetic clusters in molecular beams, metals, and semiconductors, Science 271 (1996) 937--941.

[4] S. Demos, H. Radousky, R. Alfano, Deep subsurface imaging in tissues using spectral and polarization filtering, Opt. Express 7(1) (2000) 23--8.

[5] A. K. Dunn, H. Bolay, M. A. Moskowitz, D. A. Boas, Dynamic imaging of cerebral blood flow using laser speckle, J. Cereb. Blood Flow Metab. 21(3) (2001) 195--201.

[6] G. J. Tearney, M. E. Brezinski, B. E. Bouma, S. A. Boppart, C. Pitris, J. F. Southern, J. G. Fujimoto, In vivo endoscopic optical biopsy with optical coherence tomography, Science 276 (5321) (1997) 2037--9.

[7] J.R. Lakowicz, Principles of Fluorescence Spectroscopy, 2th Edition, Kluwer Academic/Plenum Publishers, New York (1999).

[8] F. Engelke, Aufbau der Moleküle, Eine Einführung, 3th Edition, Teubner Studienbücher, Stuttgart (1996).

[9] B. Valeur, Molecular Fluorescence, Wiley-VCH, Weinheim (2002).

[10] S. G. Schulman, Fluorescence and phosphorescence spectroscopy: physicochemical principles and practice, Pergamon Press (1977).

[11] K. Licha, C. Hessenius, A. Becker, P. Henklein, M. Bauer, S- Wisniewski, B. Wiedenmann, W. Semmler, Synthesis, characterization, and biological properties of cyanine-labeled somatostatin analogues as receptor-targeted fluorescent probes, Bioconjugate Chem 12(1) (2001) 44--50.

[12] R. Weissleder, A clearer vision for in vivo imaging, Nat. Biotechnol. 19(4) (2001) 316--317.

[13] P. Sharma, S. Brown, G. Walter, S. Santra, B. Moudgil, Nanoparticles for bioimaging, Adv. Colloid Interface Sci. 123-126 (2006) 471--485.

[14] W. Cai, X. Chen, Nanoplatforms for targeted molecular imaging in living subjects, Small 3(11) (2007) 1840--1854.

[15] W. C. Roentgen, On a New Kind of Rays, Sitzungsber. Phys. Med.Ges. Wurzburg 137 (1895) 132--1141.

[16] R. L. Eisenberg, Radiology, An Illustrated History; Morsby-Year Book: St. Louis (1992).

[17] K.J. Mortele, J. McTavish, P.R. Ros, Current techniques of computed tomography. Helical CT, multidetector CT, and 3D reconstruction, Clin. Liver Dis. 6(1) (2002) 29--52.

[18] S.-B. Yu, A.D. Watson, Metal-Based X-ray Contrast Media, Chem. Rev. 99(9) (1999) 2353--2377.

[19] R.W. Katzberg, Urography into the 21st century: new contrast media, renal handling, imaging characteristics, and nephrotoxicity, Radiology 204(2) (1997) 297--312.

[20] W. Krause, D. Niehues, Daniela, Biochemical characterization of x-ray contrast media, Invest. Radiol. 31(1) (1996) 30--42.

[21] H. Katayama, K. Yamaguchi, T. Kozuka, T. Takashima T, P. Seez P, K. Matsuura, Adverse reactions to ionic and nonionic contrast media. A report from the Japanese Committee on the Safety of Contrast Media, Radiology 175(3) (1990) 621-628.

[22] B.L. McClennan, Adverse reactions to iodinated contrast media. Recognition and response, Invest. Radiol. 29 Suppl 1 (1994) 46-50.

[23] T. Almen, Contrast agent design. Some aspects on the synthesis of water soluble contrast agents of low osmolality. Theor. Biol. 24(2) (1969) 216-26.

[24] T. Almen, The etiology of contrast medium reactions, Invest. Radiol. 29 Suppl 1 (1994) 37--45.

[25] E.R. Wisner, A. Theon, S.M. Griffey, G.L. McIntire, Long-term effect of irradiation on lymph node uptake of interstitially delivered nanoparticulate contrast media, Invest. Radiol. 35(3) (2000) 199--204.

[26] G.L. McIntire, E.R. Bacon, K.J. Illig, S.B. Coffey, B. Singh, G. Bessin, M.T. Shore, G.L. Wolf, Time course of nodal enhancement with CT X-ray nanoparticle contrast agents: effect of particle size and chemical structure, Invest. Radiol. 35(2) (2000) 91-96.

[27] E.R. Wisner, R.W. Katzberg, D.P. Link, S.M. Griffey, C.M. Drake, A.R. Vessey, D. Johnson, P.J. Haley, Indirect computed tomography lymphography using iodinated nanoparticles to detect cancerous lymph nodes in a cutaneous melanoma model, Academ. Radiol. 3(1) (1996) 40--48.

[28] E.R. Wisner, R.W. Katzberg, S.M. Griffey, C.M. Drake, P.J. Haley, A.R. Vessey, Indirect computed tomography lymphography using iodinated nanoparticles: time and dose response in normal canine lymph nodes, Academ. Radiol. 2(11) (1995) 985--993.

[29] E.R. Wisner, R.W. Katzberg, P.D. Koblik, J.P. McGahan, S.M. Griffey, C.M. Drake, P.P. Harnish, A.R. Vessey, P.J. Haley, Indirect computed tomography lymphography of subdiaphragmatic lymph nodes using iodinated nanoparticles in normal dogs, Academ. Radiol. 2(5) (1995) 405--412.

[30] E.R. Wisner, R.W. Katzberg, P.D. Koblik, D.K. Shelton, P.E. Fisher, S.M. Griffey S M, C. Drake, P.P. Harnish, A.R. Vessey, P.J. Haley, Iodinated nanoparticles for indirect computed tomography lymphography of the craniocervical and thoracic lymph nodes in normal dogs, Academ. Radiol. 1(4) (1994) 377--384.

[31] F. Hyafil, J.-C. Cornily, J.E. Feig, R. Gordon, E. Vucic, V. Amirbekian, E.A. Fisher, V. Fuster, L.J. Feldman, Z.A. Fayad, Noninvasive detection of macrophages using a nanoparticulate contrast agent for computed tomography, Nat. Med. 13(5) (2007) 636--641.

[32] O. Rabin, P.J. Manuel, J. Grimm, G. Wojtkiewicz, R. Weissleder, An X-ray computed tomography imaging agent based on long-circulating bismuth sulphide nanoparticles, Nat. Mater. 5(2) (2006) 118--122.

Chapter 2

Quantum dots - Introduction and General Aspects

A. F.E. Hezinger, A. M. Goepferich, J. K. Tessmar: Polymer coated quantum dots. Handbook of Nanophysics: Nanoparticles and Quantum Dots, Chapter 36, in press

A.F.E. Hezinger, J. Teßmar, A. Goepferich: Polymer coating of quantum dots – A powerful tool toward diagnostics and sensorics. European Journal of Pharmaceutics and Biopharmaceutics 68, 138-152 (2008).

2. Introduction and General Aspects

2.1. Introduction

In the last decade, colloidal quantum dots have drawn tremendous attention as a new class of fluorophores for a wide range of diagnostic and sensoric applications. Their unique optical properties lead to major advantages in fluorescence detection and imaging in molecular and cell biology [1]. Linking these inorganic semiconductor nanoparticles to biological molecules like peptides [2], proteins [3-5] and DNA [6,7] was achieved just as well as adapting them for the development of multicolor fluorescent labels in in-vitro and in-vivo imaging [8,9]. Successful sensing applications of these systems were developed for analytes, like small ions and more complex molecules, like sugars or neurotransmitters [10,11,12]. The most commonly used quantum dots are of the cadmium chalcogenide group due to ease of synthesis and handling. Their inherent optical properties emerge from their semiconductor nature and are namely the bright and stable fluorescence and the broad excitation spectra with high absorption coefficients. These unique properties are the reason why quantum dots have significant advantages over common organic dyes and genetically engineered fluorescent proteins in many biological and biomedical applications. Compared to organic dyes they offer possibilities like multiplexed imaging and long-term investigations, e.g. for cell uptake studies and in-vivo imaging, due to their tunable emission wavelength and an increased photostability up to several months [4,8]. Nevertheless, quantum dot surfaces have to be protected and functionalized to provide biocompatibility, biostability and suitable surface functions for these applications.

A major step toward the applicability of the nanoparticulate systems for sensorics and diagnostics is therefore the design of an adequate coating of their inorganic surface. This coating should provide three functions, a chemical and physical stabilization of the quantum dots the ability to modify them for a wide range of applications by attaching certain surface groups as well as suppressing the toxicity. The beginning of this continuous evolution was made with the first water-soluble quantum dots coated with mercaptopropionic acid, already applicable to chemical functionalization utilizing the free carboxylic group (figure 1). These quantum dots were further improved by a rapid development of a wide range of polymeric ligands and amphiphilic polymers coordinating on top of the nanocrystal surface. These polymer and ligand coatings are focused on the different facets of the biological applications and even extend into new fields of relevance, like the technique of lifetime imaging or special applications, such as single molecule detection. Consequently, various polymers and ligands

have been developed for the differing application areas. Moreover, also two fundamentally different ways of surface coating for the similar applications were adapted, each with its own advantages and disadvantages. This chapter will provide a summary and comparison of the different polymer based coating strategies and the relevant organic polymers used for the modifications.

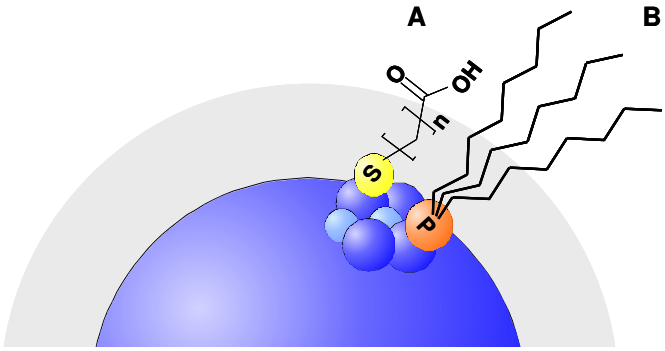

Figure 1: Schematic drawing of the quantum dot surface with (A) a hydrophilic mercaptoalkane acid applied for water-solubility and (B) a lipophilic trioctylphosphine ligand from synthesis

2.2. Quantum dots

Nowadays quantum dot probes are photostable and water-soluble nanoparticlulate systems, which display a bright luminescence and offer the possibility to tune their size and emission wavelengths [13]. All these improvements can be ascribed to a series of technological developments providing new functionalities to the inorganic materials. It has started with the first highly crystalline and monodisperse cadmium selenide nanocrystals published by Bawendi et al. in 1993 [14], synthesized in a hot coordinating solvent. This evolution was followed by improving the photostability and brightness of these quantum dots by coating them with different semiconductor materials thereby passivating the oxidation-sensitive semiconductor surface [15]. In 1998, the first synthetic approaches to water soluble semiconductor nanocrystals were published [3,4]. Today quantum dots are not only composed of cadmium selenide (CdSe) but of many other semiconducting materials derived from the II and VI elemental groups (e.g. CdTe, CdS, CdHg, ZnS) and III and V elemental groups (e.g. InAs, InP, GaAs) of the periodic table. The emissions of these quantum dots span the whole spectral range from ultraviolet to near-infrared [16-20].

Possessing a size range of 1 to 10 nm diameter, quantum dots (QDs) are so-called quasi zero-dimensional, single, mostly spherical semiconductor nanocrystals [21,22]. Due to their small dimensions, they exhibit several exciting new optical properties in addition to the classical

properties of bulk semiconductors, distinguishing them from common organic fluorescent dyes, e.g of the cyanin or rhodamine group.

2.2.1. Optical Properties

A classical attribute of quantum dots is their broadband absorption of light with increasing absorption coefficients at higher energies (i.e. smaller wavelengths) [23], which are an order of magnitude larger compared to organic dyes [24].

Furthermore, quantum dots exhibit many non-classical characteristics, as their tunable emission spectra with highly confined Gaussian distributions of the emission wavelengths. Emission peaks of CdSe quantum dots are as narrow as 25 nm full-width at half maximum (fwhm) at room temperature, unlike common organic dyes displaying asymmetric emission peaks with up to several 100 nm width. Additionally, the energetically lowest absorption peak of these dots is located only a few nanometers lower than the maximum emission wavelength. These characteristics allow an excitation of multiple QDs of different emission wavelength with only one excitation wavelength (figure 2), making multiplexed imaging of differently modified particles possible. Besides the spectral attributes, the semiconductor nature of quantum dots gives rise to a long photostability, up to several weeks or even months [25]. The slow decay rates of the exited states correspond with a long luminescence lifetime. The general luminescence lifetime of CdSe quantum dots at room temperature is composed of mulitexponetial decay rates with different lifetimes of 5 ns, 20-30 ns and 80-500ns, resulting in a general lifetime of 20-30 ns [26,27]. However, the chemical and physical cause of the multiexponential decay rates still remains vague and has to be further investigated.

The unique optical characteristics of semiconductor nanocrystals are based on an effect called quantum confinement (hence the name quantum dots), caused by the restriction of electrons and holes in all three dimensions [28]. Quantum confinement describes an effect arising in nanocrystals smaller then their so-called Bohr exciton radius. Like classical semiconductors, the nanoparticles possess a valence and a conducting band. However, in quantum dots these bands are quantisized with energy values directly related to the nanocrystal size (figure 3). This quantization of the energy results in discrete size dependent emission wavelengths of a single quantum dot. The overall energy bandgap between the valence and the conducting band changes its value dependent on the variation of nanocrystal size, and can be described similar to the quantization arising from the ‘particle in a box’ model [29]. The moment a photon enters a quantum dot, a quasi-particle is created. This so-called ‘exciton’, an electron-hole pair, is formed when the electron is promoted from the valence band to the conducting band

by energy absorption. The missing electron in the valence band leaves a hole of opposite electric charge behind. This hole is bound to the promoted electron by the Coulomb force. Upon recombination of the electron with its hole, light of a certain wavelength is emitted, corresponding to the respective badgap energy.

2.2.2. Synthesis

Among various synthesis routes leading to cadmium chalcogenide quantum dots, the high temperature synthesis in coordinating solvents is the best-investigated strategy [30]. This synthetic route for nanoparticles of high monodispersity and high crystallinity [31] is performed via the decomposition of metal-organic or organometallic precursors at elevated temperatures. The precursors are composed of an organic part coordinating or binding to the added metal or metalloid. In general, the formation of the quantum dots is carried out at high temperatures between 180 – 310° C, depending on the selected precursors and solvents. During the reaction, the chosen temperature and the reaction time determine the size of the nanoparticles, since nucleation of seed crystals and deposition of new material on existing crystals attend depending on the respective temperature of the solvent.

The reasons for the development of a broad range of synthetic strategies are the various possibilities of solvents and precursors. The chosen coordinating solvent is capable to "dissolve" the metal precursors and moreover it frequently also acts as ligand or capping agent for the resulting quantum dots (figure 1). Essential for these coordinating components are the functional groups (phosphines, phosphineoxides, amines and carboxy groups) suitable to graft on the nanocrystal surface. The attached groups stabilize the quantum dots during their formation, but they are also essential for later solubilization and capping strategies (fig. 5). Frequently, toxic and pyrophoric components, like mixtures of trioctylphosphine oxide (TOPO), trioctylphosphine (TOP) and hexadeclyamine (HDA) [32,33] are used. Nevertheless, nowadays also some other, less toxic coordinating substances, like fatty acids, or also mixtures of coordinating solvents with less pyrophoric non-coordinating solvents, like octadecene (ODE) [34,35], are utilized for nanocrystal synthesis.

However, not only the used solvents but also the used precursors have changed since the first organometallic approaches. The initially applied precursor dimethylcadmium [$Cd(CH_3)_2$] was highly toxic and pyrophoric resulting in difficult conditions for the synthesis. Most recently, Peng and Peng and other groups have applied less toxic and easier manageable cadmium precursors, like CdO or $Cd(CH_3COO)_2$; for the formation of high-quality CdX (X = S, Se, Te) quantum dots [31,36,37].

A common procedure to enhance the photoluminescence properties of CdX (X = S, Se, Te) quantum dots is the overgrowth of an additional passivating inorganic shell. This shell is composed of a second semiconducting material with a larger bandgap, e.g. ZnS or ZnSe (figure 4). The larger bandgap here provides a protection of the surface against oxidation, and additionally entraps the excitons in the core, resulting in reduced luminescence quenching caused by CdX surface defects. Furthermore, particularly Zn-containing shells exhibit a much greater affinity to thiol groups than the mere core material [38,39], which is of high importance for the later applied coating strategies leading to functionalized quantum dots. The general synthesis procedures, as well as the core formations, are all organometallic approaches in contrast to later described organic polymer coating strategies.

2.3. Biocompatible Quantum Dots

Nowadays quantum dot probes are photostable and water-soluble nanoparticlulate systems, which display a bright luminescence and offer the possibility to tune their size and emission wavelengths [13]. All these improvements can be ascribed to a series of technological developments providing new functionalities to the inorganic materials. It has started with the first highly crystalline and monodisperse cadmium selenide nanocrystals published by Bawendi et al. in 1993 [14], synthesized in a hot coordinating solvent. This evolution was followed by improving the photostability and brightness of these quantum dots by coating them with different semiconductor materials thereby passivating the oxidation-sensitive semiconductor surface [15]. In 1998, the first synthetic approaches to water soluble semiconductor nanocrystals were published [3,4]. Today quantum dots are not only composed of cadmium selenide (CdSe) but of many other semiconducting materials derived from the II and VI elemental groups (e.g. CdTe, CdS, CdHg, ZnS) and III and V elemental groups (e.g. InAs, InP, GaAs) of the periodic table. The emissions of these quantum dots span the whole spectral range from ultraviolet to near-infrared [16-20] (figure 2).

Water-solubility, high stability against oxidation and subsequent degradation, small diameters and funtionalizable groups are essential for the application of quantum dots in biological systems. Since unmodified nanocrystals exhibit extremely hydrophobic surface ligands, like trioctylphosphineoxide or hexadeclyamine resulting from the organometallic synthesis, they are not suited for biological applications due to their insolubility in aqueous media. Due to this fact, a hydrophilization of their surface is an essential prerequisite for their application in most of the here described experiments.

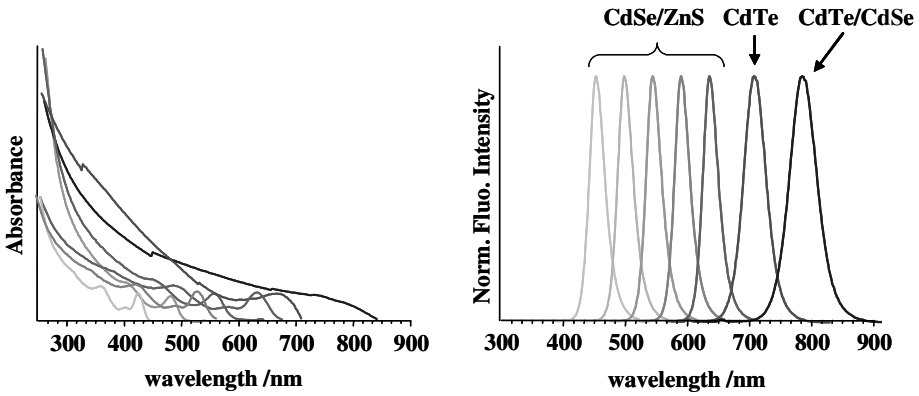

Figure 2: Absorbance and fluorescence spectra of CdSe/ZnS, CdTe and CdTe/CdSe quantum dots of various sizes

Since first reports on water-soluble QDs were published, a wide range of coating and capping strategies providing a water-soluble shell arose, having different effects on the properties of the modified particles. The strategies can be divided into two fundamentally different ways solving this problem via functional polymers. One approach completely replaces the surface bound ligands remaining from synthesis; the other only caps the present ligands on the QDs with suitable amphiphilic polymers (figure 3). Both approaches have advantages and disadvantages for the obtained water-soluble particles. Replacing the original hydrophobic surface ligands by amphiphilic ones leads to particles with a small final diameter. These composites are often only a few nanometers larger than the core quantum dots. Nevertheless, the exchange of the surface coating often results in poor quantum yields and strongly affects the physicochemical and photophysical stability of QDs in aqueous solutions. Instead, surface capping chemistries retain the original surface ligands and therefore preserve the photophysical properties of the nanocrystals. However, this approach results in particles with a final size three or four times larger than the original nanocrystal diameter.

The huge variety of different surface modifications results in quantum dots of very different optical and chemical properties. Indeed this diversity is necessary for the multiplicity of applications semiconductor nanocrystals undergo in diagnostics and sensorics. Properties like particle size and charge, as well as application relevant parameters, like chemical and photophysical stability, photoluminescence intensity and cytotoxicity have to be considered to choose the optimal system for each application.

The focus of the following chapter will be set on coating strategies with organic substances. For completeness, it has to be mentioned that there are various possibilities for inorganic coating of quantum dots with silica or titania. These coating strategies are based on the same two principles of ligand exchange or ligand capping to anchor the inorganic coating on the

nanocrystal surface. This is followed by the formation of another inorganic layer, shielding the quantum dot and rendering it water-soluble [21,40-48].

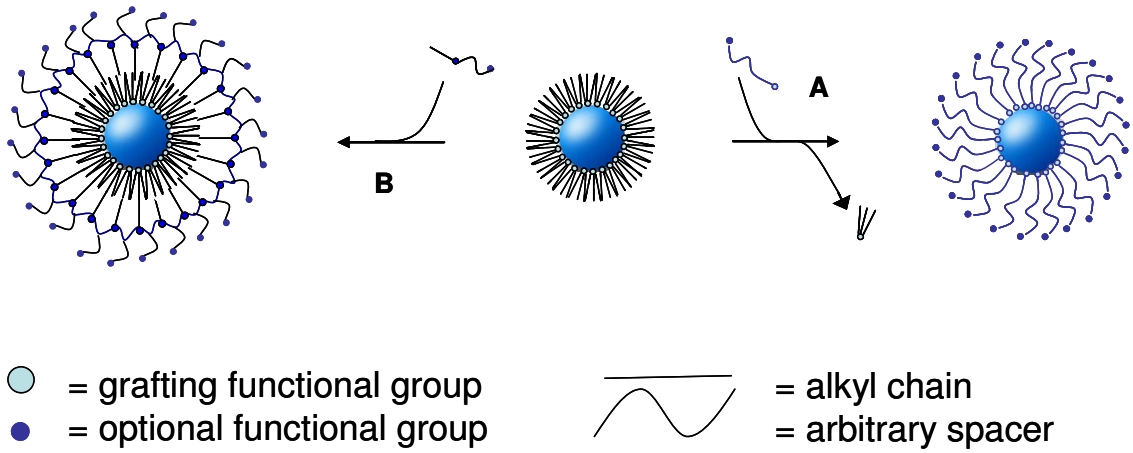

Figure 3: Scheme of the (A) ligand exchange and (B) the ligand capping strategy.

2.3.1. Effects of surface coating

Coatings can change the quantum dot properties in tree different aspects, one is the photophysical, one the physicochemical and the last is the toxicological point of view (figure 4).

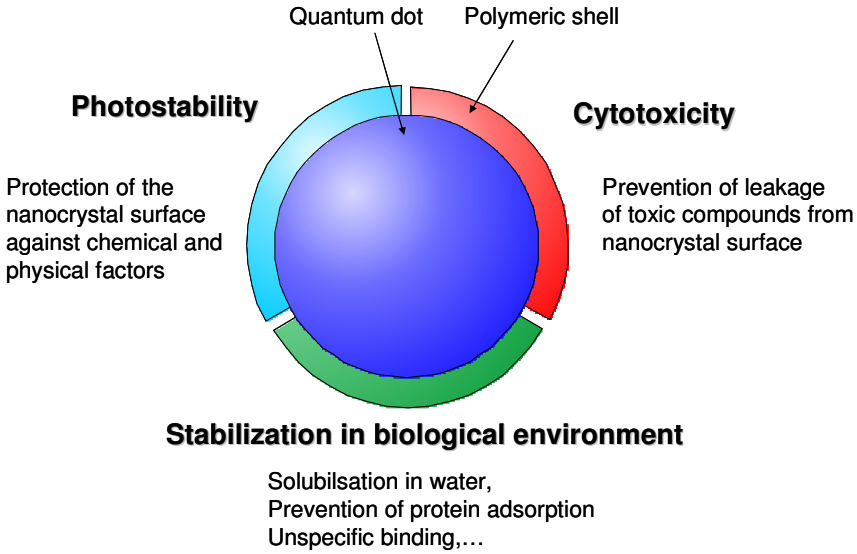

Figure 4: Functions and influences of polymeric coating on quantum dots

The affected photophysical characteristics are the emission wavelength, the quantum yield and the photostability, directly influencing each other due to the physics of the quantum dots.

The physicochemical aspects influence the size, the charge and the aggregation of quantum dots in biological environments and therefore determine the stability of quantum dot probes in biological environments. The cytotoxicity of quantum dots is an essential point to consider especially in cell cultural or in vivo applications.

Photophysical aspects

The natural quantum dot capping, resulting from synthesis, protects the surface against oxidation and can compensate surface defects. Too many surface defects result in a decrease of quantum yield, because excitons can emit their energy in a non-radiative way. Additionally, the photostability is largely influenced by the occurring photooxidation at the surface, and the larger the likelihood for an oxidation due to imperfect coating, the worse the observed photostability of the quantum dots. Finally, the occurring surface oxidation is also responsible for an effect called 'blueing' of the quantum dots, which is a shift of the emission wavelengths towards blue color [49-52]. In case the surface of a nanocrystal gets oxidized, the remaining emitting semiconductor core gets smaller (figure 5). When the core gets smaller the emission wavelength shifts to higher energies and therefore smaller wavelengths [53,54].
Consequently, the exchange of the original capping causes an increased likelihood to suffer damages due to incomplete coverage and imperfect grafting of the newly added ligands. Additionally, thiol-containing ligands used in many approaches are themselfes susceptible to oxidation of the thiol group, leading to detachment of the coating from the surface. Here again the mere capping of the initial ligands with amphiphilic polymers reduces the likelihood to suffer from surface defects and in most cases provides a much better protection against oxidation due to the much thicker shell on top of the particles.

Toxicological aspects

Having biological experiments in mind, the cytotoxicity is an tremendously important factor to be considered. quantum dot size, charge and concentration, their outer shell bioactivity and oxidative, photolytic or mechanical stress are all factors that, collectively and individually, can determine their cellular toxicity. For biological applications, it is notable that especially protection of the nanocrystal surface is not only important for the probe stability, but it is also vital to prevent leakage of cytotoxic semiconductor components from the inorganic core, e.g. due to occurring photooxidation. In addition, some coating materials can also have toxic

effects on cells on their own, if they are released from the composites, which is especially the cause for amphiphilic substances.

An oxidation of the surface happens through a variety of chemical pathways, mostly through radical reactions of oxygen combined with UV-irradiation. This leads to the formation of chalcogenoxides (e.g. SO_2, SO_3, SeO_2, TeO_2) and reduced cadmium. These chalcogenoxides can then desorb from the surface and dissolve (e.g. resulting in H_2SO_3, H_2SO_4, H_2SeO_3, TeO_2(aq)), the residual reduced cadmium is oxidized back to Cd^{2+}-ions, leading to the subsequent release of free cadmium ions [50-52] (figure 5). These soluble Cd^{2+}-ions make the biggest part of the toxic effect that is ascribed to QDs. Consequently, with increasing impermeability of the surrounding polymer shell, for these ions, the overall cytotoxicity decreases. The toxicity of the used coating material is closely related to the toxicity of the utilized polymer compuonds.

However, at the low concentrations of quantum dots needed especially for cellular experiments most reports did not find adverse effects on cell viability, morphology, function or development. Semiconductor nanocrystals are therefore not completely innocuous, but a safe range for their biological application certainly exists [55-57]. This range eventually can be further extended with increasing quantum yields of the particles and subsequently decreasing detection limits and applied amounts.

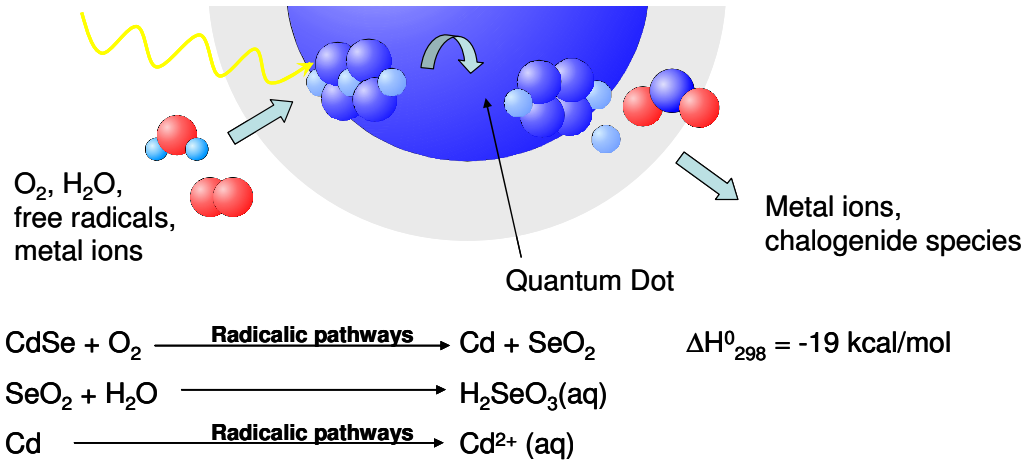

Figure 5: Schematic drawing and reaction scheme of the photooxidation on the nanocrystalsurface of CdSe.

Physicochemical aspects

The physicochemical attributes of the nanocrystals affected by different coating strategies are their size, their charge and the aggregation stability of the particle suspension in biological

systems. However, these particle attributes are often the most critical subject for the design of a new coating, as they have significant impact on the application of the quantum dots. The ligand exchange method on the one hand yields particles of a small final diameter, but together with an increased oxidation sensivity of the thiol grafting ligands. This furthermore may also result in an aggregation of the quantum dots, due to the loss of surface shielding. However, the beneficial small dimensions of the QDs with exchanged ligands prevail in some applications the comparable low stability against aggregation. The capping of the ligands on the other hand produces comparatively large polymer coated particles, which in some cases even have more than one QD inside the coating layer [58]. Nevertheless, these bigger particles provide a good chemical stabilization of the surface and a reliable protection against aggregation.

Occurring in both modification methods is the aqueous solubilization by additional charged groups on the surface. The mostly used chemical moieties are carboxyl and amino groups, which additionally offer the possibility for further functionalization with specific biomolecules. However, the use of these highly charged systems raises the risk of aggregation in biological environments caused by ionic interactions with proteins and ions present in biological fluids. The destabilization of anionic shells happens for example, caused by an increased ionic strengths of the aqueous solutions, increased temperature or complex salt mixtures, which all reduce the repulsive forces of the ionic groups. Therefore, another frequently-used technique altering the physicochemical attributes of the particles is the PEGylation of an existing polymer shell, yielding uncharged sterically stabilized colloids. This modification furthermore results in a reduced unspecific uptake in cells and moreover, prevents adsorption of proteins on the polymer shells. Also the risk of agglomeration in biological fluids is remarkably reduced [59].

2.3.2. Ligand Exchange Strategies

There are various different suitable molecules for ligand exchange, however all depend on a functional group grafting on the nanocrystal surface. Different chemical groups were utilized, mainly thiol, amine and phosphine groups. The other part of these molecules should provide the solubilization of the quantum dot. For this task, different strategies are used, like charged groups, hydrophilic spacer or combinations of both.

Thiols

Among the different strategies of ligand exchange (table 1, figure 5), various thiol ligands, including dithiols and also thiol dendrimers have been studied extensively. One of the easiest ways to obtain water-solubility is the attachment of acidic ligands as thioglycolic acid, mercaptopropionic acid or dihydrolipoic acid [60]. The introduced second functional group of the ligand, e.g. carboxy groups, provides the possibility of further functionalization steps. Additionally, these modified QDs can subsequently be covered using an oppositely charged polymer, e.g. with derivatives of poly(acrylamide) causing a stabilization of the ligand shell or by functinalisation with poly(ethylene glycols) [61].

Thiolated poly(ethylene glycol) polymers, obtained by attachment of terminal thiol groups are often synthesized for coating of quantum dots [62-66]. Main advantages of the thiolated PEGs are the easy synthesis, ease of handling and the versatile applications. Due to these facts, the PEG ligands are widely used for solubilization. An extra benefit of poly(ethylene glycol) coatings is the reduced unspecific cellular uptake of the modified uncharged particles [59] as mentioned earlier. Depending on the strived goal, varying polymer chain lengths and number of binding dentates are used. The two mainly applied types are the mono [65,66] and the bidentate [63] thiols. The latter ligand obviously grafts more effectively on the nanocrystal surface and therefore provides a much better stabilization of the nanocrystals in aqueous solution. Nevertheless, the remaining disadvantage of these simple coating agents is the reduced photoluminescence intensity of the obtained particles and the lack of long-term chemical stability of the thiol groups.

Not only synthetic polymers can attach onto a charged layer,as mentioned above, also proteins readily adsorb on it [5]. What could be a problem, some work groups turn into a benefit by attaching specific proteins on the nanocrystal surface. Furthermore, the application of engineered peptides and proteins for functional coatings of quantum dots is a fast growing field in nanocrystal modification. For these custom-designed proteins biologically relevant domains, like targeting sequences, are fused with attachment domains for the quantum dots, like thiol containing cysteine domains, cationic histidine tags [67] or the leucine zipper peptides [5]. Nevertheless, also simply thiolated proteins are utilized for direct attachment on nanocrystal surfaces providing modified nanoparticles [67]. A further improvement is the coattachment of thiolated PEGs and engineered peptides on one particle surface [69]. This method provides specific binding on the one hand, but on the other hand also reduces the adsorption of different other proteins on the quantum dots and enhances their overall biocompatibility.

Another possibility to exchange existing surface ligands is the application of grafting dendrons or dendrimers, which are three-dimensional, highly branched and almost monodisperse macromolecules [70]. Dendrons and dendrimers themselves are core-shell nanostructures consisting of a core, starting point for the step-wise polymerization, interior branch cells and an exponentially increasing number of functional groups on the surface. The mostly used dendrimers for nanocrystal capping are for example functionalized poly(amidoamine) (PAMAM) polymers [71-73]. An important attribute of these cationic PAMAM polymers is their ability to effectively penetrate cell walls, making them also useful as commercial transfection agents. The PAMAM polymers possess a large number of primary and tertiary amine groups at the surface and in the interior branches of the molecule, which are known to allow for DNA complexation and which can also graft to quantum dot surfaces, while additionally improving the fluorescent properties of the modified semiconductor nanoparticles [74]. Nevertheless, they only posses poor affinities to nanocrystal surfaces and do not offer stabilization against particle aggregation because of their charged groups. Due to this fact, the utilized PAMAM dendrimers have to be further modified with additional thiol groups, known to graft better on the surface of quantum dots. Hence, a significant improvement of their affinity to nanocrystal surfaces is achieved. Surprisingly, these dendrimer coated quantum dots even seem to transfect better than higher generation dendrons alone in first cell studies [73], which can be explained with altered particles sizes compared to the free polymers. Thus, the composites may be a promising innovation for the transfection of cells.

A new multidentate poly(acrylic acid) derivative uses not only thiol groups but also amine groups for grafting on the nanocrystal surface. For this, a denser polymer shell than with monodentate ligands can be achieved, and on that account the resulting nanocrystals display sufficiently small hydrodynamic diameters. However, also a luminescence enhancing effect of the amine groups takes place [74].

Table1: Examples of thiol ligands and polymers used for ligand exchange with their mechanism of interaction with the semiconductor and the intended application.

Ligands	Mechanisms of interaction	Applications	References
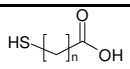 Mercaptoalkane acid	monodentate thiol bond	metal ion sensing	[108], 109], [110]
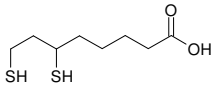 Dihydrolipoic acid	bidentate thiol bond	FRET experiments, ion sensing	[11], [12]
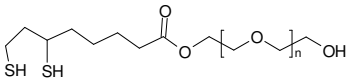 PEGylated dihydrolipoic acid	bidentate thiol bond	cancer marker detection, live cell labelling, organelle tracking	[63], [65], [66]
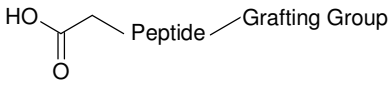 Peptide or Protein	monodentate thiol group, leucine zipper, cystein domain, histidine tag	tumor vascular imaging, intracellular targeting	[68], [69]
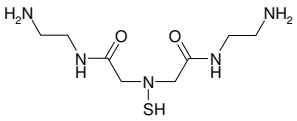 1. Generation Poly(amidoamine) dendrimer	monodentate thiol bond	transfection agent	[73]
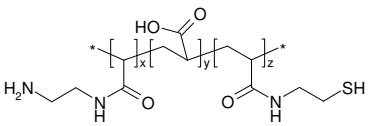 poly(acrylic acid) based multidentate polymer	multidentate thiol and/or amine bond		[74]

Amines

An alternative is the attachment of polymers to nanocrystals via the use of amines (table 2). As mentioned above, this chemical moiety is known for only a weak binding to semiconductor surfaces. However, some work groups succeeded in functionalizing quantum dots with mere amine containing polymers, like poly(ethyleneimine) (PEI) [75], also being an effective transfection agent. The PEI coated quantum dots exhibited an effective lipophilic/hydrophilic phase-transfer and a good solubility in polar solvents. However, the coatings with PEI polymers unfortunately seemed to enhance the photooxidation of the quantum dots and therefore increased the darkening of the so coated nanocrystals. Other applied amine-containing polymers are poly(N,N-dimethylaminoethyl metharcylate)s, which exhibit ternary amine groups [76-78]. It was shown that these polymers do not only effectively passivate the surface of the nanocrystals, but also provide robust colloidal stabilization in various biological environments. Additionally, the polymer-coated particles exhibit an increase in quantum yields compared to the uncoated ones, which can be ascribed to the photoluminescence enhancing effect of the amines.

Table2: Examples of amine ligands and polymers used for ligand exchange with their mechanism of interaction with the semiconductor and the intended application.

Ligands	Mechanisms of interaction	Applications	References
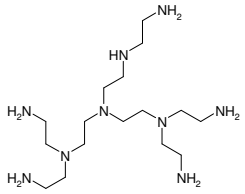 branched poly(ethyleneimine)	multidentate amine bond	transfection agent	[75]
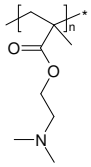 poly(N,N-dimethylaminoethyl methacrylate)	multidentate amine bond	-	[76]

Phosphines

To overcome the drawback of reduced photoluminescence intensity with all the previously described grafting groups, several phosphine-containing polymers were developed, which show more similarities to the original ligands used in synthesis (table 3). In 2003, Bawendi et al. synthesized multidentate phosphine oxide polymers [79,80] composed of three sublayers enclosing the nanocrystal, an inner phosphine layer, a liking layer between the phosphine group and an outer functionalized layer. The attachment of phosphines here provides quantum yields up to 40%, while the oligomeric outer layer can be easily modified with functional moieties, for example PEG chains [80]. Taken together, these multidentate ligands provide chemically stable and highly fluorescent quantum dots. A potential application for these particles is for example the lymph node mapping due to their exceptionally small hydrodynamic radii of 15 to 20 nm, allowing successful penetration through tissues.

Table 3: Examples of phosphine ligands and polymers used for ligand exchange with their mechanism of interaction with the semiconductor and the intended application.

Ligands	Mechanisms of interaction	Applications	References
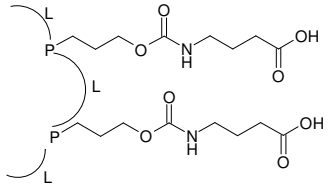 multidentate phosphine polymer	multidentate phosphine bond	lymph node mapping	[80]
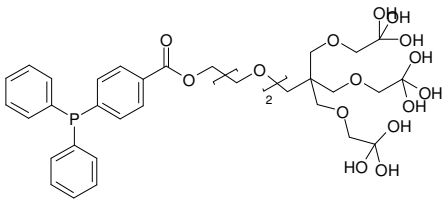 Poly(ether) dendron	monodentate phosphine bond	-	[81]

Similarly, on the sector of dendrons and dendrimers, poly(ether)s modified with aryl phosphine focal points were developed [81]. The incorporated phosphine group here provides

a strong coordination to the surface without affecting the particle´s quantum yield. Moreover, the conic shape of the attached dendrons seems to be ideal for an adsorption onto the nanoparticles, because the formation of a closely packed polymer shell is possible. These obtained shells then effectively suppress subsequent diffusion of quenching substances like oxygen or other small ions from the surrounding solution to the nanocrystal surface.

2.3.3. Ligand Capping Strategies

A wide rage of amphiphilic polymers for quantum dot surface modification was developed since the first publications describing water-solubilization using capping strategies (figure 5). Many different ways utilizing di- or triblock copolymers or other amphiphilic polymers (amphipols) were published. The common functionality of all these different polymers is the lipophilic part, intercalating between the aliphatic chains of the surface ligands, and finally covering or encapsulating the whole quantum dot with the original ligands from the synthesis still in place.

Amphiphilic polymers

One possibility is to use amphipol triblock-copolymers of poly(acrylic acid) (table 4, A), a polymer that is commercially applied to solubilize membrane proteins in aqueous solutions [82]. A few years ago, related diblock copolymers were developed for the preparation of biocompatible semiconductor nanocrystals in large scale. The used polymer shell here is composed of octylamine-modified poly(acrylic acid) additionally crosslinked with lysine (table 4, B). The modified QDs can further be improved by PEGylation of the carboxylic groups to reduce unspecific binding [83,84].

Another polymer type, which is used for quantum dot functionalization, are the amphiphilic poly(maleic anhydride-alt-1-olefin)s with different alkyl chain lengths (table 4, C) [85-87], which can be further cross linked with a diamine to stabilize the shell, or functionalized with PEG. Also a poly(isobuthylene-alt-1-maleic acid) functionalized with dodecylamine is synthesized for capping of quantum dots (table 4, D) [88]. All these amphipols have a hydrophilic backbone with attached hydrophobic side chains, interacting with the aliphatic chains of the ligands present on the nanocrystal surface, bridging between the lipophilic surface ligands and the hydrophilic solution. Solubilization of the nanoparticles in water is mainly funded in the carboxylic groups of acrylic or maleic acid, forming the backbone of the amphipol shell. The shell architecture with the functional group then provides the possibility

for further functionalization with antibodies or proteins, suitable to target cancer cells, using standard carbodiimide chemistry [83].

Table 4: Examples of amphiphilic polymers used for quantum dot capping with their application.

Capping polymers	**Applications**	**References**
A 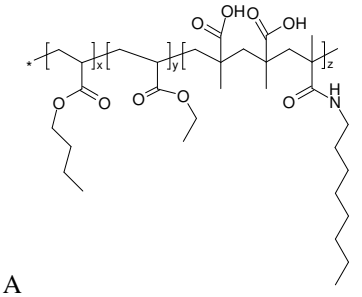 Triblock copolymer	-	[82]
B 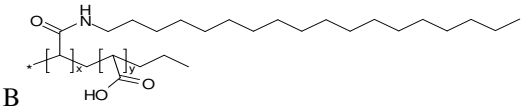 Poly(acrylic acid) derivate	multiphoton imaging in vivo, labelling of cancer markers and cellular targets, transfection experiments	[83], [84],
C 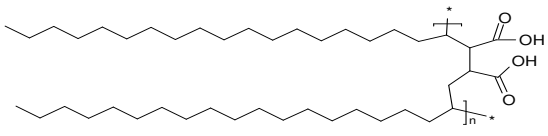 Poly(maleic acid-alt-1-olefin) derivative	transfection experiments	[87]
D 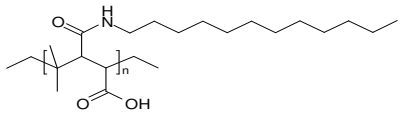 Poly(isobutylene-alt-1-maleic acid) derivative	FRET experiments	[88]

Micelles

An often-used alternative to coating with amphiphilic polymers is the encapsulation of quantum dots in micelles, e.g. composed of polymer modified surfactants (table 5). The advantage of this method is the applicability of a wide variety of surfactants/lipids with different functionally terminated groups. As micelle building compounds mostly PEG derivatisized phospholipids are applied due to their improved solubilization capability [89-91]. Also many other suitable surfactants, like lipids containing paramagnetic gadolinium complexes, can be used for nanocrystal encapsulation [92,93], providing the possibility for luminescence imaging as well as for MRI (magnetic resonance imaging). The QD containing micelles preserve the optical properties of the encapsulated quantum dots and additionally offer a high biocompatibility. The drawback of this method is that only nanocrystals of predefined diameters and consequently emission wavelength can be encapsulated by certain micelle building surfactants or lipids. This fact is founded in a given micellar size of a particular surfactant, defining the inner free space available for the incorporated quantum dots [89].

Table 5: Examples of surfactant used for quantum dot capping with their application.

Capping polymers	**Applications**	**References**
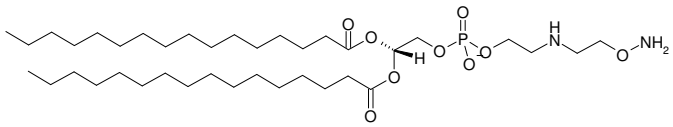 Phospholipid	tracking of plasmid DNA, in-vivo imaging, cell detection	[89],[90], [92]

Heterocyclic amphiphiles

A coating method aiming at the sensoric application of quantum dots is the use of different cyclodextrines, where an interaction of the coating with the core is still desirable [94,95]. Here, the hydrophobic pockets of the saccharide oligomers interact with the aliphatic chains of the TOPO present on the nanoparticle surface. Nevertheless, the immobilized cyclodextrines retain their capability of engaging molecular recognition. Due to this fact and the observation of fluorescence changes while analyte binding, this modification method is very promising for possible sensing applications [95]. Another benefit of this capping strategy

is the resulting small diameter of the QDs, which is achieved due to the small space requirements of the cyclodextrines. A related approach to small water-soluble quantum dots without a ligand exchange is the use of calixarenes, similarly structural organic polycyclic systems [96,97]. This coating also preserves the emission intensity of the quantum dots and their small diameter. Calixarenes are cyclic oligomers based on a hydroxyalkylation product of phenol and an aldehyde. It was also shown that calixarenes could be derivatisized with sugars or peptides to allow biological applications of these systems [96]. However, also derivatization with aliphatic and sulfonato groups was achieved for optical detection of small molecular weight molecules, like acetylcholine [97] (table 6).

Table 6: Examples of heterocyclic amphiphiles used for quantum dot capping with their application.

Capping polymers	**Applications**	**References**
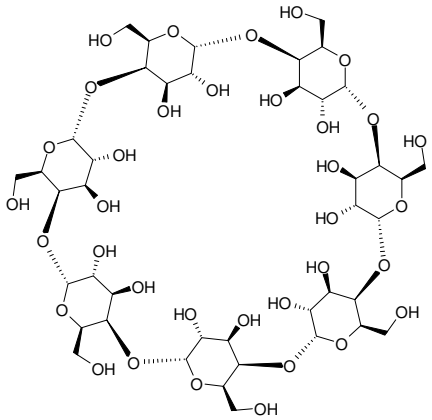 β-Cyclodextrin	molecular recognition	[79]
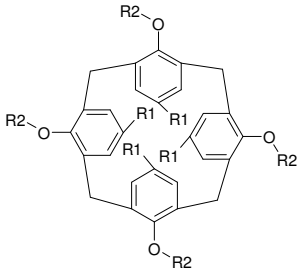 Calix[4]arene	acetylcholine detection	[81]

2.3.4. Application of surface coatings

The various coating methods, substances and the different characteristics of the resulting nanoparticles open a wide range of application areas, particularly the field of sensorics and diagnostics. For sensorical approaches, it is important to have a surface coating that allows an interaction of the analytes or the reporter molecules with the quantum dot. In contrast the diagnostic applications rely on biocompatibility, especially concerning the cytotoxicity and the undesirable adsorption of proteins and possible subsequent particle aggregation.

Sensoric applications

The basis for sensoric applications of quantum dots is, in most cases, the interaction of the analyte molecule or ion with the nanocrystal surface, leading to a change in the apparent fluorescent properties of the particle. Following this approach, quantum dots were coated with cystein, thioglycolic acid or related ligands for the detection of metal ions like Ag^+ [89], Cu^{2+} [99], Zn^{2+} [100] and also small toxic anions, for example cyanide [101]. Additionally, coated quantum dots were applied to optical temperature detection [102-104]. The conjugation of selective reagents or reporter molecules to the surface of luminescent nanocrystrals is also utilized for quantum dot probes. Particularly dihydrolipoic acid can be modified with functional moieties for selective K^+[11] or even glucose [12] sensing. Nevertheless, these approaches seem to be restricted to a small number of analytes interacting with the surface coatings and the underlying quantum dots. Additionally they possess only a low stability in biological systems and limited applicability in realistic sample arrangements due to many possible interactions with similar ions present in solution.

The potential of QDs to be used in much more analyte specific FRET (Förster resonance energy transfer) based sensors can expand the applicability of semiconductor nanocrystals in sensorics. Here, the tunable wavelengths and the high quantum yields of the nanocrystals theoretically enable efficient energy transfer with a wide number of conventional dyes. Indeed it should be mentioned, that FRET efficiencies obtained with QDs as donor species today are still low compared to efficiencies of common dyes, which is mainly founded in the comparatively large size of even thin-coated quantum dots, making it very complicated to bring the acceptor into close proximity to the donor for efficient FRET. Nevertheless, a variety of quantum dot FRET applications were yet developed and strategies arose to improve the energy transfer. Protein binding-sites were studied by FRET investigations, whereas the acceptor dyes are bound to a protein affording FRET when the assembly is adsorbed on the

QD surface [105]. Therefore, even inside of cells different sensing applications can be achieved, as pH, nuclear cleavage or protease activity detection [106-109]. In addition, immunoassays for specific cancer marker detection are developed [110]. Not only conventional fluorescent dyes are utilized as acceptors, also several so-called dark quenchers, molecules or nanocrystals only absorbing and not re-emitting the light, were bound to QDs for FRET applications. This consequently results in a detectable decrease of the fluorescence signal upon increasing FRET events. Examples for these systems are the use of functionalized gold nanocrystals for DNA hybridization investigations [111,112], inhibition assays [113], glucose sensing [114] or alternatively, the application of an organic dark quencher dye for pH sensing [115] or maltose binding assays [116].

Diagnostic applications

The diagnostic approaches of modified quantum dots, on the other hand, are more dependent on impermeable polymer shells and efficient physical and biological shielding of the quantum dot to prevent unspecific adsorption of proteins and fast degradation leading to fluorescence loss. This can mainly be achieved with densely packed polymer shells and subsequent PEGylation. On the one hand these water soluble and often targeted quantum dots can be used for in-vitro cellular imaging, e.g. histology, on the other hand for in-vivo imaging of tumors, e.g. in small animals. The applied in-vivo imaging here is a non-invasive possibility to detect highly sensitive and in a high contrast deep tissue regions in mice and even larger species without the use of radioactive radiation or larger instrumental setups, like computed tomography. The intravenous injection of biocompatible quantum dots was performed for blood vessel imaging [84], targeting of tissue specific vascular markers [68], or lymph node mapping [117]. A promising application is also the targeting of tumor cells in-vivo using specific antibodies against Her2 markers [83]. Another improvement in the field of in vivo imaging are self-illuminating quantum dots, these polymer coated and luciferase modified nanocrystals need no external light for excitation. In this system the chemical energy of the substrate coelenterazine is converted into photon energy by the enzyme luciferase. This photon energy excites the quantum dot through bioluminescence resonance energy transfer (BRET). With this excitation mechanism the autofluorescence is virtually eliminated, however the emitted photons are still absorbed or scattered in the surrounding tissuemaking sensitive detection necessary [118-121].

In the area of cellular imaging, quantum dot probes are as well used for the tagging of whole cells as for the investigation of single intracellular processes. Many studies here are focused

on membrane specific markers due to the easy access form the outside of the cells and the unnecessary passage through the cell membrane. Additionally, also several attempts for the internalization of quantum dots in live cells have been performed. One approach to internalize the nanoparticles is the use of membrane translocation peptides [122], also attempts utilizing electroporation or established transfection reagents [123] were preformed. The latter strategy to internalize QDs allows then the targeting of sub-cellular compartments as for example mitochondria or the nucleolus using specific targeting peptides allowing for the labeling of the small compartments in living cells for subsequent studies of cellular biology [68,124,125]. Recently, quantum dot conjugates for combined cancer imaging and therapy were developed. An apamer, which is able to target cancer cells and simultaneously bind a cancer drug was immobilized on the surface of the quantum dot. The fluorescent properties of the drug quench the luminescence of the quantum dot by a FRET mechanism, and by the release of the drug the luminescence of the nanocrystal is restored. Therfore, a targeted QD imaging system that is capable of differential uptake, imaging and therapy of prostate cancer cells was build [126].

2.4. Conclusion

A great variety of polymeric surface coatings for quantum dots is currently applied for a wide range of different applications. All applications require distinct characteristics of the quantum dots, which are adjustable by the used surface coating polymer. The size and photostability of water-soluble quantum dots here strongly depend on the used capping strategy and the resulting particle architecture.

Ligand exchange on the one hand can produce small particles, but often lacks the long-term stability and photoluminescence intensity. Their resistance against acids or bases and, in some cases, against chemical oxidation is only very week. Nevertheless, FRET experiments, for example, urgently require small hydrodynamic radii, and also other sensoric applications depend on the accessibility of the nanocrystal surface, which can only be achieved by the attachment of short ligands. For ligand exchange procedures the recent adaptation of phosphine groups is very beneficial due to the improved stabilization of the nanocrystal surface and the additional surface passivation against oxidation, while mere PEGylation mainly provides protection against unspecific protein absorption. For transfection experiments, substitution with cationic polymers, like branched PEI or PAMAM dendrimers, is suggestive.

On the other hand, the ligand capping strategies with their effective shielding of the nanocrystal surface, their subsequently low cytotoxicity and high stability in biological

environments are ideal for cellular and even in-vivo experiments. These studies rely on a sustained fluorescence in the presence of oxidizing agents and low cytotoxicity. Also in assays conducted in high salt buffers, uncharged and sterically stabilized nanocrystals, like PEG coated QDs, can be of avail. Therefore, protection of the quantum dots with an amphiphilic bilayer, e.g. using phospholipids or amphiphilic polymers is very useful. The amphiphilic capping then can be easily modified with targeting sequences or proteins using carbodiiminde chemistry. Subsuming the different strategies, none of the encapsulation methods can be universally optimal for several biological and sensorical applications at once.

2.5. Future Outlook

The different polymeric surface coatings developed in the last decade combining biological materials with inorganic nanocrystals have not only been crucial for the successful use of quantum dots in cell and tissue imaging. Additionally, they have afforded new systems in materials science for the controlled assembly of nanomaterials used in the biological environment. As research continues to produce different nanomaterials with novel unique properties, it will become possible to gather new multimodal imaging agents. Combining QDs for fluorescence imaging with magnetic resonance imaging (MRI) or computed tomography (CT) contrast agents, like Fe_2O_3 [127], FePt [128] or Gd complexes [92] allows deep tissue imaging and fluorescence tracking of one system for sophisticated diagnostic applications. In the area of sensorics, QDs can moreover function as effective protein carriers and exciton donors for prototype self-assembled FRET nanosensors for the detection of many relevant signal molecules, like acetylcholine [82] or others. Furthermore, they could even drive more biosensors through a two-step FRET mechanism overcoming inherent donor-acceptor distance limitations, already realized with the FRET maltose-binding sensor [102]. To this time, mostly intensity-based measurements with quantum dots have been employed in the fields of sensing and imaging. Indeed, lifetime-based methods will draw more and more attention due to their superior resolution, independence from fluorescence intensity and concentration at the detection point and, finally, the possibility to out-gate the tissue autofluorescence present in all living biological systems, like cell cultures or whole animals. For these developments QDs are an especially powerful tool due to their long excited state lifetimes compared to the common organic dyes and the interfering tissue autofluorescence.
However, for all that semiconductor nanocrystals will not overcome the use of conventional organic dyes in biological and sensorical applications. They could complement dye deficiencies in particular approaches such as in vivo imaging and break up to new

applications as long-term imaging and lifetime measurements. Moreover, adapting QD nanoparticles for biological use will teach us important lessons about creating future inorganic-organic hybrids for many other applications.

2.6. References

[1] C.M. Niemeyer, Nanoparticles, proteins, and nucleic acids: biotechnology meets materials science, Angew. Chem. Int. Ed. Engl. 40 (2001) 4128--4158.

[2] S.R. Whaley, D.S. English, E.L. Hu, P.F. Barbara, A.M. Belcher, Selection of peptides with semiconductor binding specificity for directed nanocrystal assembly, Nature 405 (2000) 665--668.

[3] M. Bruchez Jr, M. Moronne, P. Gin, S. Weiss, A.P. Alivisatos, Semiconductor nanocrystals as fluorescent biological labels, Science 281 (1998) 2013--2015.

[4] W.C.W. Chan, S.M. Nie, quantum dot bioconjugates for ultrasensitive nonisotopic detection, Science 281 (1998) 2016--2018.

[5] H. Mattoussi, J.M. Mauro, E.R. Goldman, G.P. Anderson, V.C. Sundar, F.V. Mikulec, M.G. Bawendi, Self-assembly of CdSe–ZnS quantum dots bioconjugates using an engineered recombinant protein, J. Am. Chem. Soc. 122 (2000) 12142--12150.

[6] G.P. Mitchell, C.A. Mirkin, R.L. Letsinger, Programmed assembly of DNA functionalized quantum dots, J. Am. Chem. Soc. 121 (1999) 8122--8123.

[7] S. Pathak, S.K. Choi, N. Arnheim, M.E. Thompson, Hydroxylated quantum dots as luminescent probes for in situ hybridization, J. Am. Chem. Soc. 123 (2001) 4103--4104.

[8] M.Y. Han, X.H. Gao, J.Z. Su, S. Nie, quantum-dot-tagged microbeads for multiplexed optical coding of biomolecules, Nat. Biotechnol. 19 (2001) 631--635.

[9] X. Michalet, F.F. Pinaud, L.A. Bentolila, J.M. Tsay, J.J. Li, G. Sundaresan, A.M. Wu, S.S. Gambhir, S. Weiss, quantum dots for Live Cells, in Vivo Imaging and Diagnostics, Science 307 (2005) 538--544.

[10] I.L. Mednitz, H.T. Uyeda, E.R. Goldman, H. Mattoussi, quantum dot bioconjugates for imaging, labeling and sensing, Nat. Mater. 4 (2005) 435--446.

[11] C.-Y. Chen, C.-T. Cheng, C.-W. Lai, P.-W. Wu, K.-C. Wu, P.-T. Chou, Y.-H. Chou, H.-T. Chiu, Potassium ion recognition by 15-crown-5 functionalized CdSe/ZnS quantum dots in H2O, Chem. Commun. (2006) 263--365.

[12] D.B. Cordes, S. Gamsey, B. Singaram, Fluorescent quantum dots with Boronic Acid Substituted Viologens To Sense Glucose in Aqueous Solution, Angew. Chem. Int. Ed. 45 (2006) 3829--3832.

[13] T.M. Jovin, quantum dots finally come of age, Nat. Biotechnol. 12 (2003) 32--33.

[14] C.B. Murray, D.J. Norris, M.G. Bawendi, Synthesis and Characterisation of Nearly Monodisperse CdE (E = S, Se, Te) Semiconductor Nanocrystallites, J. Am. Chem. Soc. 115 (1993) 8706--8715.

[15] M.A. Hines, P. Guynot-Sionest, Synthesis and Characterisation of Strongly Luminescing ZnS-Capped CdSe Nanocrystals, J. Phys. Chem. 100 (1996) 468--471.

[16] L.H. Qu, X. G. Peng, Control of photoluminescence properties of CdSe nanocrystals in growth, J. Am. Chem. Soc. 124 (2002) 2049--2055.

[17] X.H. Zhong, Y.Y. Feng, W. Knoll, M.Y. Han, Alloyed ZnxCd1-xS nanocrystals with highly narrow luminescence spectral width, J. Am. Chem. Soc. 125 (2003) 13559--13563.

[18] R.E. Bailey, S.M. Nie, Alloyed semiconductor quantum dots: tuning the optical properties without changing the particle size, J. Am. Chem. Soc. 125 (2003) 7100--7106.

[19] S. Kim, B. Fisher, H.J. Eisler, M. Bawendi, Type-II quantum dots: CdTe/CdSe(core/shell) and CdSe/ZnTe(core/shell) heterostructures, J. Am. Chem. Soc. 125 (2003) 11466--11467.

[20] B.L Wehrenberg, C.J. Wang, P. Guyot-Sionnest, Interband and intraband optical studies of PbSe colloidal quantum dots, J. Phys. Chem. B 106 (2002) 10634--10640.

[21] D. Gerion, F. Pinaud, S.C. Williams, W.J. PArak, D. Zanchet, S. Weiss, P.A. Alivisatos, Synthesis and Properties of Biocompartible Water-Soluble Silica-Coated CdSe/ZnS Semiconductor quantum dots, J. Phys. Che. B 105 (2001) 8861--8871.

[22] B. Balluo, B.C. Lagerholm, L.A. Ernst, M.P. Bruchez, A.S. Waggoner, Noninvasive imaging of quantum dots in mice, Bioconjug. Chem. 15, (2004) 79--86.

[23] W.C. Chan, D.J. Maxwell, X. Gao, R.E. Bailey, M. Han, S. Nie, Luminescent quantum dots for multiplexed biological imaging, Curr. Opin. Biotechnol. 13 (2002) 40--46.

[24] H.E. Grecco, K.A. Lidke, R. Heintzmann, D.S. Lidke, C. Spagnuolo, O.E. Martinez, E.A. Jares-Erijman, T.M. Jovin, Ensemble and single particle photophysical proper-ties (Two-Photon excitation, anisotropy, FRET, lifetime, spectral conversion) of commercial quantum dots in solution and in live cells, Microsc. Res. Tech. 65 (2004) 169--179.

[25] M. Dahan, T. Laurence, A. Schumacher, D.S. Chemla, A.P. Alivisatos, M. Sauer, S. Weiss, Fluorescence lifetime study of single qdots, Biophys. J. 78 (2000) 2270.

[26] M. Dahan, T. Laurence, F. Pinaud, D.S. Chemla, A.P. Alivisatos, M. Sauer, S. Weiss, Time-gated biological imaging by use of colloidal quantum dots, Opt. Lett. 26 (2001) 825--827.

[27] A.P. Alivisatos, Semiconductor clusters, nanocrystals, and quantum dots, Science 271 (1996) 933--937.

[28] A.P. Alivisatos, Perspectives on the Physical Chemistry of Semiconductor Nanocrystals, J. Phys. Chem. 100 (1996) 13227—13239.

[29] D. Crouch, S. Norager, P. O'Brien, J.-H. Park, N. Pickett, New synthetic routes for quantum dots, Phil. Trans. R. Soc. Lond. A 361 (2003) 297--310.

[30] Z.A. Peng, X.G. Peng, Formation of high-quality CdTe, CdSe, and CdS nanocrystals using CdO as precursor, J. Am. Chem. Soc. 123 (2001) 183--184.

[31] D.V. Talapin, A.L. Rogach, A. Kornowski, M. Haase, H. Weller, Highly Luminescent Monodisperse CdSe and CdSe/ZnS Nanocrystals Synthesized in a Hexadeclyamine-Trioctylphosphine Oxide-Trioctylphosphine Mixture, Nano Lett. 1 (2001) 207--211.

[32] I. Mekis, D.V. Talapin, A. Koronowski, M. Haase, H. Weller, One-Pot Synthesis of Highly Luminescent CdSe/CdS Core-Shell Nanocrystals via Organometallic and "Greener" Chemical Approaches, J. Phys. Chem. 107 (2003) 7454--7462.

[33] G.G. Yordanov, C.D. Dushkin, G.D. Gicheva, B.H. Bochev, E. Adachi, Synthesis of high-quality semiconductor nanoparticles in a composite hot-matrix, Colloid Polym. Sci. 284, (2005) 229--232.

[34] W.W. Yu, X. Peng, Formation of High-Quality CdS and Other II-VI Semiconductor Nanocrystals in Noncoordinating Solvents: Tunable Reactivity of Monomers, Angew. Chem. Int. Ed. 41 (2002) 2368--2371.

[35] G.-W. Huang, C.-Y. Chen, K.-C. Wu, M.O. Ahmed, P.-T. Chou, One-pot synthesis and characterisation of high-quality CdSe/ZnX (X = S, Se) nanocrystals via the CdO precursor, J. Cryst. Growth. 265 (2004) 250--259.

[36] X. Liu, Y. Lin, Y. Chen, L. An, X. Ji, B. Jiang, New Organometallic Approach to Synthesize High-quality CdSe Quantum Dots, Chem. Lett. 34 (2005) 1284--1285.

[37] P. Reiss, S. Carayon, J. Bleuse, Large fluorescence quantum yield and low size dispersion from CdSe/ZnSe core/shell nanocrystals, Physica E 17 (2003) 95--96.

[38] P. Reiss, J. Bleuse, A. Pron, Highly Luminescent CdSe/ZnSe Core/Shell Nanocrystals of Low Size Dispersion, Nano Lett. 2 (2002) 781--784.

[39] A. Schroedter, H. Weller, Biofunctionalization of Silica-Coated CdTe and Gold Nanocrystals, Nan. Lett. 2 (2002) 1363--1367.

[40] T. Nann, P. Mulvaney, Single quantum dots in Spherical Silica Particles, Angew. Chem. Int. Ed 43 (2004) 5393--5396.

[41] M.A. Petruska, A.P. Bartko, V.I. Klimov, An Amphiphilic Appoach to Nanocrystal quantum dot-Titania Nanocomposites, J. Am. Chem. Soc 126 (2004) 714--715.

[42] S.T. Selvan, T.T. Tan, J.Y. Ying, Robust, Non-Cytotoxic, Silica-Coated CdSe quantum dots with Efficient Photoluminescence, Adv. Mater. 17 (2005) 1620--1625.

[43] Y. Yang, M. Gao, Preparation of Fluorescent SiO2 Particles with Single CdTe Nanocrystal Cores by the Reverse Microemulsion Method, Adv. Mater. 17 (2005) 2354--2357.

[44] M. Darbandi, R. Thomann, T. Nann, Single quantum dots in Silica Spheres by Microemulsion Synthesis, Chem Mater 17 (2005) 5720--5725.

[45] R. Bakalova, Z. Zhelev, I. Aoki, H.Ohba, Y. Imai, I. Kanno, Silica-Shelled Single quantum dot Micelles as Imaging Probes with Dual or Multimodality, Anal. Chem. 78 (2006) 5925--5932.

[46] Z. Zehlev, H. Ohba, R. Bakalova, Single quantum dot-Micelles with Silica Shell as Potentially Non-Cytotoxic Fluorescent Cell Tracers, J. Am. Chem. Soc. 128 (2006) 6234--6235.

[47] A. Wolcott, D. Gerion, Micah Visconte, J. Sun, A. Schwartzberg, S. Chen,J.Z. Zhang, Silica-Coated CdTe quantum dots Functionalized with Thiols for Bioconjugation to IgG Proteins, J. Phys. Chem. B 110 (2006) 5779--5789.

[48] T. Zhang, J.L. Stilwell, D. Gerion, L. Ding, O. Elboudwarej, P.A. Cook, J.W. Gray, A.P. Alivisatos, F.F. Chen, Cellular Effect of High Doses of Silica-Coated quantum

dot Profiled with High Throughput Gene Expression Analysis and High Content Cellomics Measurements, Nan. Lett 6 (2006) 800--808.

[49] S.T. Selvan, P.K. Prata, C.Y. Ang, J.Y. Ying, Synthesis of Silica-Coated Semiconductor and Magnetic quantum Dos and their Use in the Imaging of Live Cells, Angew. Chem. Int. Ed. 46 (2007) 248--2452.

[50] W.G.J.H.M. van Sark, P.L.T.M. Frederix, A.A. Bol, H.C. Gerritsen, A. Meijerink, Bluening, Bleaching, and Blinking of Single CdSe/ZnS quantum dots, Chem. Phys. Chem. 3 (2002) 871--879.

[51] L. Sanhel, M. Haase, H. Weller, A. Henglein, Photochemistry of Colloidal Semiconductors. 20. Surface Modification and Stability of Strong Luminescing CdS Particles, J. Am. Chem. Soc 109 (1987) 5649--5655.

[52] J.E.B. Katari, V.L. Colvin, A.P. Alivisatos, X-ray Spectroscopy of CdSe Nanocrystals with Applications to Studies of the Nanocrystal Surface, J. Phys. Chem. 98 (1994) 4109--4117.

[53] A.P. Alivisatos, Perspectives on the Physical Chemistry of Semiconductor Nanocrystals, J. Phys. Chem. 100 (1996) 13226--13239.

[54] W.G.J.H.M. van Sark, P.L.T.M. Frederix, D.J. van den Heuvel, H.C. Gerritsen, Photooxidation and Photobleaching of Single CdSe/ZnS quantum dots Probed by Room-Temperature Time-Resolved Spectroscopy, J. Phys. Chem. B 105, (2001) 8281--8284.

[55] W.G.J.H.M. van Sark, P.L.T.M. Frederix, D.J. van den Heuvel, A.A. Bol, J.N.J. van Lingen, C. de Mello Donea, H.C. Gerritsen, A. Meijerink, Time-Resolved Fluorescence Spectroscopy Study on the Photophysical Behavior of quantum dots, J. .Fluoresc. 12 (2002) 69--75.

[56] H. Ron, A toxicological review of quantum dots: Toxicity depends on physico-chemical and environmental factors, Environ. Health Perspect. 114 (2006) 165--172.

[57] A.M. Derfus, W.C.W. Chan, S.N. Bhatia, Probing the cytotoxicity of semiconductor quantum dots, Nano Lett. 4 (2004) 11--18.

[58] C. Kirchner, T. Liedl, S. Kudera, T. Pellegrino, A.M. Javier, H.E. Gaub, S. Stölzle, N. Fertig, W.J. Parak, Cytotoxicity of colloidal CdSe and CdSe/ZnS nanoparticles, Nano Lett. 5 (2005) 331--338.

[59] A.M. Smith, H. Duan, M.N. Rhyner, G. Ruan, S. Nie, A systematic examination of surface coatings an the optical and chemical properties of semiconductor quantum dots, Phys. Chem. Chem. Phys. 8 (2006) 3895--3903.

[60] E.L. Bentzen, I.D. Tomlinson, J. Manson, P. Gresch, M.R. Warnement, D. Wright, E. Sanders-Bush, R. Blakely, S.J. Rosenthal, Surface Modification To Reduce Nonspecific Binding of quantum dots in Live Cell Assays, Bioconj. Chem. 16 (2005), 1488--1494.

[61] J.K. Jaiswal, H. Mattoussi, J.M. Mauro, S.M. Simon, Long-term multiple color imaging of live cells using quantum dot bioconjugates, Nat. Biotechnol. 21 (2003) 47--51.

[62] I. Potapova, R. Mruk, S. Prehl, R. Zentel, T. Basche, A. Mews, Semiconductor nanocrystals with Multifunctional Polymer Ligands, J. Am. Chem. Soc. 125 (2003) 320--321.

[63] H.T. Uyeda, I. L. Mednitz, J.K. Jaiswal, S.M. Simon, H. Mattoussi, Synthesis of Compact Multidentate Ligands to Prepare Stable Hydrophilic quantum dot Fluorophores, J. Am. Chem. Soc. 127 (2005) 3870--3878.

[64] E.-C. Kang, a. Ogura, K. Kataoka, Y. Nagasaki, Preparation of Water-soluble PEGylated Semiconductor Nanocrystals, Chem. Lett. 33 (2004) 840--841.

[65] S.K. Dixit, N.L. Goicochea, M.-C. Daniel, A. Murali, L. Bronstein, M. De, B. Stein, V.M. Rotello, C.C. Kao, B. Dragnea, quantum dot Encapsulation in Viral Capsids, Nano Lett. 6 (2006) 1993--1999.

[66] A.M. Derfus, W.C.W. Chan, S.N. Bhatia, Intracellular Delivery of quantum dots for Live Cell Labelling and Organelle Tracking, Adv. Mater. 16 (2004) 961--966.

[67] F. Hu, Y. Ran, Z. Zhou, M. Gao, Preparation of bioconjugates of CdTe nanocrystals for cancer marker detection, Nanotechnology 17 (2006) 2972--2977.

[68] S.-Y. Ding, G. Rumbles, M. Lones, M.P. Tucker, J. Nedeljkovic, M.N. Simon, J.S. Wall, M.E. Himmel, Bioconjugation of (CdSe)ZnS quantum dots Using a Genetically engineered Multiple Polyhistidine Tagged Cohesin/Dockerin Protein Polymer, Macromol. Mater. Eng. 289 (2004) 622--628.

[69] M.E. Akerman, W.C.W. Chan, P. Laakkonen, S.N. Bhatia, E. Ruoslahti, Nanocrystal targeting in vivo, PNAS 99 (2002) 12617--12621.

[70] W. Cai, D.-W. Shin, K. Chen, O. Gheysens, Q. Cao, S.X. Wang, S.S. Gambhir, X. Chen, Peptide-Labeled Near-Infrared quantum dots for Imaging Tumour Vasculature in Living Subjects, Nano Lett. 6 (2006) 669--676.

[71] M.J. Cloninger, Biological applications of denrimers, Curr. Opin. Chem. Biol. 6 (2002) 742-748.

[72] B. Huang, D.A. Tomalia, Dendronisation of gold and CdSe/CdS (core-shell) quantum dots with tomalia type, thiol core, functionalized Poly(amidoamine) (PAMAM) dendrons, J. Luminesc.111 (2005) 215--223

[73] B. Pan, F. Gao, R. He, D. Cui, Y. Zhang, Study on interaction between poly(amidoamine) dendrimer and CdSe nanocrystal in chloroform, J. Colloid Interface Sci. 297 (2006) 151--156.

[74] A.C. Wisher, I. Bronstein, V. Chechik, Thiolated PAMAM dendriner-coated CdSe/ZnS nanoparticles as protein transfection agents, Chem. Commun. (2006) 1637--1639.

[75] A.M. Smith, S. Nie, Minimizing the Hydrodynamic Size of quantum dots with Multifunctional Multidentate Polymer Ligands, J. Am. Chem. Soc. 130 (2008) 11278--11279.

[76] T. Nann, Phase-transfer of CdSe@ZnS quantum dots using amphiphilic hyperbranched polyethyleneimine, Chem. Commun. (2005) 1735--1736.

[77] M. Wang, J.K. Oh, T.E. Dykstra, X. Lou, G.D. Scholes, M.A. Winnik, Surface Modification of CdSe and CdSe/ZnS Semiconductor Nanocrystals with Poly(N,N-dimethylaminoethyl methacrylate), Macromolecules 39 (2006) 3664--3672.

[78] M. Wang, J.K. Oh, T.E. Dykstra, X. Lou, M.R. Salvador, G.D. Scholes, M.A. Winnik, Colloidal CdSe Nanocrystals Passivated by a Dye-Labeled Multidentate Polymer: Quantitaitve Ananlysis by Size-Exclusion Chromatography, Angew. Chem. Int. Ed. 45 (2006) 2221--2224.

[79] M. Wang, J.K. Oh, T.E. Dykstra, X. Lou, G.D. Scholes, M.A. Winnik, Surface Modification of CdSe and CdSe/ZnS Semiconductor Nanocrystals with Poly(N,N-dimethylaminoethyl methacrylate), Macromolecules 39 (2006) 3664--3672.

[80] S. Kim, M.G. Bawendi, Oligomeric Ligands for Luminescent and Stable Nanocrystal quantum dots, J. Am. Chem. Soc. 125 (2003) 14652--14653.

[81] S.-W. Kim, S. Kim, J.B. Tracy, A. Jasanoff, M.G. Bawendi, Phosphine Oxide Polymer for Water-Soluble Nanoparticles, J. Am. Chem. Soc. 127 (2005) 4556--4557.

[82] B. Huang, D.A. Tomalia, Poly(ether) dendrons possessing phosphine focal points for stabilisation and reduced quenching of luminescent quantum dots, Inorg. Chim. Act. 359 (2006) 1951--1966.

[83] C. Luccardini, C. Tribet, F. Vial, V. Marchi-Artzner, M. Dahan, Size, Ccharge, and Interactions with Giant Lipid Vesikles of quantum dots Coated with an Amphiphilic Macromolecule, Langmuir 22 (2006) 2304--2310.

[84] X. Wu, H. Liu, J. Liu, K.N. Haley, J.A. Treadway, J.P. Larson, N. Ge, F. Peale, M.P. Bruchez, Immunofluorescent labelling of cancer marker Her2 and other cellular targets with semiconductor quantum dots, Nat. Biotechnol. 21 (2003) 41--46.

[85] D.R. Larson, W.R. Zipfel, R.M. Willams, S.W. Clark, M.P. Bruchez, F.W. Wise, W.W. Web, Water-Soluble quantum dots for Multiphoton Fluorescence Imaging in Vivo, Science 300 (2003) 1434--1436.

[86] T. Pellegrino, L. Manna, S. Kudera, T. Liedl, D. Koktysh, A.L. Rogach, S. Keller, J. Rädler, G. Natile, W.J. Parak, Hydrophobic nanocrystals Coated with an Amphiphilic Polymer Shell: A General Route to Water Soluble Nanocrystals, Nano Lett. 4 (2004) 703--707.

[87] W.W. Yu, E. Chang, J.C. Falkner, J. Zhang, A.M. Al-Solmali, C.M. Sayes, J. Johns, R. drezek, V.L. Colvin, Forming Biocompatible and Nonaggegated Nanocrystals in Water Using Amphiphilic Polymers, J. Am. Chem. Soc. 129 (2007) 2871--2879.

[88] L. Qi, X. Gao, quantum dot-Amphilpol Nanocomplex for Intracellular Delivery and Real-Time Imaging of siRNA, ACS Nano 2 (2008) 1403-1410.

[89] M.T. Fernandez-Arguelles, A. Yakovlev, R.A. Sperling, C. Luccardini, S. Gaillard, A. Sanz Medel, J.-M. Mallet, J.-C. Brochon, A. Feltz, M. Oheim, W.J. Parak, Synthesis and Characterization of Polymer-Coated quantum dots with Integrated Acceptor Dyes as FRET-Based Nanoprobes, Nano Lett. 7 (2007) 2613--2617.

[90] B. Dubertret, P. Skourides, D.J. Norris, V. Noireaux, A.H. Brivanlou, A. Libchaber, In Vivo Imaging of quantum dots Encapsulated in Phospholipid Micelles, Science 298 (2002) 1759--1762.

[91] C. Srinivasan, J. Lee, F. Papadimitrakopoulos, L.K. Silbart, M. Zhao, D.J. Burgess, labelling and Intracellular Tracking of functionally Active Plasmid DNA with Semiconductor quantum dots, Mol. Therapy 14 (2006) 192--200.

[92] H. Fan, E.W. Leve, C. Scullin, J. Gabaldon, D. Tallant, S. Bunge, T. Boyle, M.C. Wilson, C.J. Brinker, Surfactant-Assisted Synthesis of Water-Soluble and Biocompatible Semiconductor quantum dot Micelles, Nano Lett. 5 (2005) 645--648.

[93] F. Boulmedais, P. Bauchat, M.J. Brienne, I. Arnal, F. Artzner, T. Gaocin, M. Dahan, V. Marchi-Artzner, Water-Soluble Pegylated quantum dots: From a Composite Hexagonal Phase to Isolated Micelles, Langmuir 22 (2006) 9797--9803.

[94] G.A.F. van Tilborg, W.J.M. Mulder, P.T.K. Chin, G. Strom, C.P. Reutelingsperger, K. Nicolay, G.J. Strijkers, Annexin A5-Conjugated quantum dots with a Paramagnetic Lipidic Coating for the Multimodal Detection of Apoptotic Cells, Bioconjug. Chem. 17 (2006) 865--868.

[95] J. Feng, S.-Y. Ding, M.P. Tucker, M.E. Himmel, Y.-H. Kim, S.B. Zhang, B.M. Keyes, G. Rumbles, Cyclodextrine driven hydrophobic/hydrophilic transformation of semiconductor nanoparticles, Appl. Phys. Lett. 86 (2005) 033108.

[96] K. Palaniappan, S.A. Hackney, J. Liu, Supramolecular control of complexation-induced fluorescence change of water-soluble, β-cyclodextrin-modified CdS quantum dots, Chem. Commun. (2004) 2704--2705.

[97] T. Jin, F. Fujii, H. Sakata, M. Tamura, M. Kinjo, Calixarene-coated water-soluble CdSe-ZnS semiconductor quantum dots that are highly fluorescent and stable in aqueous solution, Chem. Commun. (2005) 2829--2831.

[98] T. Jin, F. Fujii, H. Sakata, M. Tamura, M. Kinjo, Amphiphilic p-sulfonatocalix[4]arene-coated quantum dots for the optical detection of the neurotransmitter acetylcholine, Chem. Commun. (2005) 4300--4302.

[99] J.-L. Chen, C.-Q. Zhu, Functionalized cadmium sulphide quantum dots as fluorescence probe for silver ion determination, Anal. Chim. Act. 546 (2005) 147--153.

[100] M.T. Fernandez-Argülles, W.J. Jin, J.M. Costa-Fernandez, R. Pereiro, A. Sanz-Medel, Surface-modified CdSe quantum dots for the sensitive and selective determination of Cu(II) in aqueous solutions by luminescent measurements, Anal. Chim. Act. 549 (2005) 20--25.

[101] Y. Chen, Z. Rosenzweig, Luminescent CdS quantum dots as Selective Ion Probes, Anal. Chem. 74 (2002) 5132--5138.

[102] W.J. Jin, M.T. Fernandez-Argueelles, J.M. Costa-Fernandez, R. Pereiro, A. Sanz-Medel, Photoactivated luminescent CdSe quantum dots as sensitive cyanide probes in aqueous solutions. Chem. Commun. (2005) 883--885.

[103] T.-C. Liu, Z.-L. Huang, H.-Q. Wang, J.-H. Wang, X.-Q Li, Y.-D. Zhao, Q.-M. Luo, Temperature-dependent photoluminescence of water-soluble quantum dots for a bioprobe, Anal. Chim. Act. 559 (2006) 120--123.

[104] S.F. Wuister, A. van Houselt, C. de Mello Donega, D. Vanmaekelbergh, A. Meijerink, Temperature Antiquenching of the Luminescence from Capped CdSe quantum dots, Angew. Chem. Int. Ed. 43 (2004) 3029--3033.

[105] P.A.S. Jorge, M. Mayeh, R. Benrashid, P. Cadas, J.L. Santos, F. Farahi, quantum dots as self-referenced optical fibre temperature probes for luminescent chemical sensors, Meas. Sci. Technol. 17 (2006) 1032--1038.

[106] A.R. Clapp, I.L. Medintz, J.M. Mauro, B.R. Fisher, M.G. Bawendi, H. Mattoussi, Fluorescence Resonance Energy Transfer Between quantum dot Donors and Dye-Labeled Protein Acceptors, J. Am. Chem. Soc. 126 (2004) 301--110.

[107] M. Susuki, Y. Yuzuru, H. Komatsu, K. Suzuki, K.T. Douglas, quantum dot FRET Biosensors that Respond to pH, to Proteolytic or Nucleolytic Cleavage, to

DNA Synthesis, or to a Multiplexing Combination, J. Am. Chem. Soc. 130(2008) 5720--5725.

[108] [D. Zhou, L. Ying, X. Hong, E.A. Hall, C. Abell, D.Klenerman, A Compact Functional quantum dot-DNA Conjugate: Preparation, Hybridization, And Specific Label-Free DNA Detection. Langmuir 24 (2008) 1659--1664.

[109] Y.S. Liu, Y.Sun, P.T. Vernier, C.-H. Liang, S.Y.C.Chong, M.A. Gundersen, pH-Sensitive photpluminescence of CdSe/ZnSe/ZnS quantum dots in human ovarian cancer cells, J. Phys. Chem. C 111 (2007) 2872--2878.

[110] L. Shi, V. de Paoli, N. Rosenzweig, Z. Rosenzweig, Synthesis and Application of quantum dots FRET-Based Protease Sensors, J. Am. Chem. Soc. 128 (2006) 10378--10379.

[111] . Kerman, T. Endo, M. Tsukamoto, M. Chikae, Y. Takamura, E. Tamiya, quantum dot-based immunosensor for the detection of prostate-specific antigen using Fluorescence microscopy, Talanta 71 (2007) 1494--1499.

[112] L. Dyadyusha, H. Yin, S. Jaiswal, T. Brown, J.J. Baumberg, F.P. Booy, T. Melvin, Quenching of CdSe quantum dot emission, a new approach for biosensing, Chem. Commun. (2005) 3201--3203.

[113] D. Zhou, J.D. Piper, C. Abell, D. Klenerman, D.-j. Kang, L. Ying, Fluorescence resonance energy transfer between a quantum dot donor and a dye acceptor attached to DNA, Chem. Commun. (2005) 4807--4809.

[114] E. Oh, M.-Y. Hong, D. Lee, S.-H. Man, H.C. Yoon, H.-S. Kim, Inhibition Assay of Biomolecules based on Fluorescence Resonance Energy Transfer (FRET) between quantum dots and Gold Nanoparticles, J. Am. Chem. Soc. 127, (2005) 3270--3271.

[115] B. Tang, L. Cao, K. Xu, L. Zhuo, J. Ge, Q. Li, L. Yu, A new nanobiosensor for glucose with high sensivity and selectivity in serum based on fluorescence resonance energy transfer (FRET) between CdTe quantum dots and Au nanoparticles, Chem. Eur. J. 14 (2008) 3637--3644.

[116] M. Tomasulo, I. Yildiz, F.M. Raymo, pH-Sensitive quantum dots, J. Phys. Chem. B 110 (2006) 3853--3855.

[117] I.L. Medintz, A.R. Clapp, H. Mattoussi, E.R. Goldman, B. Fisher, J.M. Mauro, Self-assembled nanoscale biosensors based on quantum dot FRET donors, Nat. Mater. 2 (2003) 630--638.

[118] S. Kim, Y.T. Lim, E.G. Soltesz, A.M. De Grand, J. Lee, A. Nakayama, Near-infrared fluorescent type II quantum dots for sentinel lymph node mapping, Nat. Biotechnol. 22(2004) 93--97.

[119] J.V. Frangioni, Self-illuminating quantum dots light the way, Nat. Biotechnol. 24 (2006) 326--328.

[120] M.-K. So, C. Xu, A.M. Loening, S.S. Gambhir, J. Rao, Self-illuminating quanum dot conjugates for in vivo imaging, Nat. Biotechnol. 24 (2006) 339--343.

[121] Y. Zhang, M.-K. So, A.M. Loening, H.Yao, S.S. Gambhir, J. Rao, HaloTag Protein-Mediated Site-Specific Conjugation of Bioluminescent Proteins to quantum dots, Angew. Chem. Int. Ed. 45 (2006) 4936--4940.

[122] Y. Gao, Y. Cui, R.M. Levenson, L.W.K. Chung, S. Nie, In vivo cancer targeting and imaging with semiconductor quantum dots, Nat. Biotechnol. 22 (2004) 969--976.

[123] A. Hoshino, K. Fujioka, T. Oku, S. Nakamura, M. Suga, Y. Yamaguchi, quantum dots targeted to the assigned organelle in living cells, Microbiol. Immunol. 48 (2004) 985--994.

[124] A.M. Derfus, W.C.W. Chan, S.N. Bhatia, Intracellular delivery of quantum dots for live cell labelling and organelle tracking, Adv. Mater. 16 (2004) 961.

[125] F. Pinaud, X. Michalet, L.A.Bentonlila, J.M. Tsay, S. Doose, J.J. Li, G. Iyer, S. Weiss, Advances in fluorescence imagigng with quantum dot bio-probes, Biomater. 27 (2006) 1679--1687.

[126] F.Q. Chen, D. Gerion, Fluorescent CdSe/ZnS nanocrystal-peptide conjugates for long-term, nontoxic imaging and nuclear targeting in living cells, Nano Lett. 4 (2004) 1827--1832.

[127] V. Bagalkot, L.Zhang, E. Levy-Nissenbaum, S. Jon, P.W. Kantoff, R. Langer, O.C. Farokhzad, quantum dot-Apamer Conjugates for Synchonous Cancer Imaging, Therapy, and Sensing of Drug Delivery Based on Bi-Fluorescence Resonace Energy Transfer, Nano. Lett. 7 (2007) 3065--3070.

[128] D.S Wang, J.B. He, N. Rosenzweig, Z. Rosenzweig, Superparamagnetic Fe_2O_3 beads-CdSe/ZnS quantum dots core-shell nanocomposite particles for cell separation, Nano Lett. 4 (2004) 409--413.

[129] H.W. Gu, R.K. Zheng, X.X. Zhang, B. Xu, Facile one-pot synthesis of bifunctional heterodimers of nanoparticles: a conjugate of quantum dot and magnetic nanoparticles, J. Am. Chem. Soc. 126 (2004) 5664--5665.

Chapter 3

Quantum Dots - Materials and Methods

3. Materials and Methods

3.1. Quantum dots

Cadmiumoxide (99.99+%), elemental selenium (99.5%, 100 mesh) and tellurium (99.997%, 30 mesh), zinc stearate (techn.), oleic acid (techn.), tributylphosphine (techn.), trioctylphosphine (techn.), trioctylphosphine oxide (techn.), octadecene (techn.), hexadecylamine (techn.) for synthesis were obtained from Sigma-Aldrich (Sigma-Aldrich Chemie GmbH, Munich, Germany). Sulfur (sulfur praecipitatum Ph.Eur.) was purchased at Caelo (Ceasar&Lorenz GmbH, Hilden, Germany). Lauric acid was purchased at Henkel (Henkel&Cie GmbH, Düsseldorf, Germany). Methanol (p.a.), ethanol (p.a), nitric acid, fuming (p.a) were purchased at Merck (Merck KGaA, Darmstadt, Germany). Acetone (p.a) methylenechloride (p.a.), hexane (p.a.) were obtained from Acros (Acros organics, Fischer scientific GmbH, Nidderau, Germany)

3.2. Dihydrolipoic acid

The used lipoic acid (>89%) was obtained from Sigma-Aldrich (Sigma-Aldrich Chemie GmbH, Munich, Germany), sodium borohydride (p.a.), and sodium hydrogen carbonate (p.a.) were purchased at Merck (Merck KGaA, Darmstadt, Germany)

3.3. Synthesis of amino Poly(ethylene glycol)mercaptoundecyl ether

Ethylene oxide (purum), potassium bis(trimethylsilyl) amid (0.5 M in toluene), di(tert-butyl)dicarbonate (purum), 11-bromoundecen (p.a.), thioacetic acid (p.a.), α,α´azoisobutyronitrile (p.a.) were obtained from Sigma-Aldrich (Sigma-Aldrich Chemie GmbH, Munich, Germany). Potassium hydroxide (p.a.) and sodium hydride (p.a.) were purchased at Merck (Merck KGaA, Darmstadt, Germany). Dioxane p.a. was obtained from Acros (Acros Organics, Fischer scientific GmbH, Nidderau, Germany) hydrochloric acid in methanol

3.4. Coating of Quantum Dots

The hexa(ethylene glycol)mercaptoundecyl ether and tri(ethylene glycol) mercaptoundecly ether and mercaptouncedanol (purum), were provided from Sigma-Aldrich (Sigma-Aldrich Chemie GmbH, Munich, Germany). Amino poly(ethylene glycol)$_{2000}$ mercaptodecyl ether

was custom made in the Department of Pharmaceutical Technology, University of Regensburg, according to an established procedure [1].

3.5. Fluram assay

The sodium tetraborat decahydrat (p.a.) was obtained from Merck (Merck KGaA, Darmstadt, Germany). Fluram ® (>99%) and 6-aminohexanoic acid (98%) were provided from Sigma-Aldrich (Sigma-Aldrich Chemie GmbH, Munich, Germany).

3.6. Cytotoxicity Test

Fetal Bovine Serum (FBS) was purchased from Biochrom (Biochrom KG, Berlin, Germany), 0.25% Trypsin-EDTA was obtained from Invitrogen (Invitrogen GmbH, Karlsruhe, Germany). 3-[4,5-Dimethylthiazol-2-yl]-2,5- diphenyltetrazolium bromide (MTT) was purchased from AppliChem (AppliChem GmbH Darmstadt, Germany). Dulbecco´s modified Eagle´s medium (EMEM) and nutrient mixture F-12 HAM were obtained from Sigma-Aldrich (Sigma-Aldrich Chemie GmbH, Munich, Germany). Titriplex® III (ethylendinitrilotetraacetic acid disodium salt dihydrate) (p.a.) was obtained from Merck (Merck KGaA, Darmstadt, Germany).

3.7. Syntheses of Quantum Dots

Due to the fact, that quantum dot synthesis is highly susceptible to water and oxygen, all syntheses were carried out under nitrogen atmosphere using a combined stock /schlenck technique. The nitrogen as well as all reactants and experimental setup were dried before use. For heating either a metal bath (wood´s alloy) in combination with a heated stirrer (Heidolph 3001 K, 800W), or a heating mantle with controller (Isopad TD 2000) was applied. Furthermore, the use of silicone-free grease for all glassware was necessary. All quantum dot syntheses are based on the procedures developed by Wang et al. for the CdSe cores, Huang et al. for the ZnS coating, and Yu et al for the CdTe cores [2-4].

3.7.1. Synthesis of Cadmium selenide Quantum Dots

For the synthesis of cadmium selenide quantum dots, 0.1 mmol cadmium oxide (12.7 mg, 1eq) and 0.8 mmol lauric acid (160 mg, 8eq) were heated up to 220 °C until the cadmium oxide was completely dissolved. Subsequently, 5 mmol of trioctylphosphine oxide (1.94 g)

and 8 mmol of hexadecylamine were added under nitrogen atmosphere, and the temperature was raised to 280 °C. In parallel 1.0 mmol of elemental selenium (80 mg, 10eq) dissolved in 8.0 mmol trioctyphosphine (2 mL, 80eq) and this as-obtained trioctylphosphine selenide precursor solution was quickly injected to the cadmium laureate precursor solution afterwards. The heating bath was removed and the as synthesized quantum dots were precipitated with anhydrous methanol [2].

The precipitated quantum dots were centrifuged (8000 g, 10 min, 18 °C) for purification. Then, the methanolic supernatant was removed and the precipitate was dispersed in hexane. Afterwards, the dispersed quantum dots were again precipitated with methanol and the procedure was repeated for another two times.

3.7.2. Synthesis of Cadmium selenide/Zinc sulfide Core/Shell Quantum Dots

The zinc sulfide shell precursor was prepared by dissolving 1.3 mmol (43.0 mg, 13 eq) of elemental sulfur and 10 mmol zinc stearate (613 mg, 100eq) in 10 mmol trioctylphosphine (5 mL, 100 eq). The cadmium selenide quantum dots for the core were synthesized in analogy to 2.1.1. After injection of the trioctyphosphine precursor to the cadmium precursor solution, the temperature was lowered to 200 °C and kept constant for 3 min. Afterwards, the zinc sulfide precursor was slowly injected to the cadmium selenide quantum dot solution. The temperature was kept constant at 180 °C for one hour, and subsequently, the reaction was cooled to 50 °C and quenched with methanol [3]. The purification was done analogue to 3.7.1.

3.7.3. Synthesis of Cadmium telluride Quantum Dots

For the cadmium telluride quantum dots 0.1 mmol elemental tellurium (12.8 mg, 1eq) and 0.6 mmol trioctylphosphine or tributhylphosphine (267 or 149 µL, 6eq) were combined in 5 mL octadecen. The tellurium was dissolved under slight warming (approx. 50 °C). In parallel, 0.2 mmol cadmium oxide (25.6 mg, 2eq) and 0.8 mmol oleic acid (253 µL, 8eq) dispersed in 10 mL octadecene were heated up to 300 °C, until all cadmium oxide was dissolved. Subsequently, the tellurium precursor was quickly injected into the cadmium precursor solution. The reaction was cooled to 260 °C and kept constant for 5 min. Afterwards, the quantum dot solution was cooled down to room temperature and was purified [4].

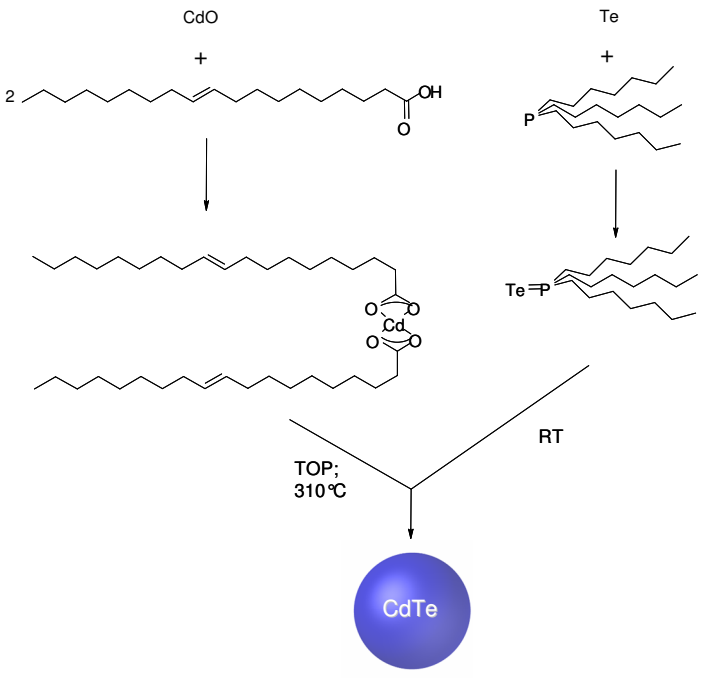

Figure 1: Reaction scheme of CdTe synthesis

For purification, the quantum dots were precipitated with ethanol and centrifuged (8000 g, 10 min, 18 °C). Subsequently, the ethanolic supernatant was removed. The precipitate was dispersed in methylenechloride and the quantum dots were again precipitated with ethanol. This procedure was repeated two times. A reaction scheme of the CdTe quantum dot synthesis is shown in figure1.

3.7.4. Synthesis of Cadmium telluride/Cadmium selenide Core/Shell Quantum Dots

The cadmium telluride/cadmium selenide quantum dots were synthesized following a related procedure as for the cadmium telluride quantum dots. For the cadmium telluride core 0.2 mmol (25.7 mg, 2eq) cadmium oxide were dissolved in 3 mmol trioctylphosphine (1.33 mL, 7.5eq) at 320 °C. Thereafter, the precursor solution was cooled down to 280 °C. Simultaneously, 0.1 mmol elemental tellurium (12.8 mg, 1 eq) were reacted with 2.15 mmol trioctyphosphine (962 µL, 21.5eq) under slight heating (50 °C), giving a clear solution. The cadmium selenide shell precursor was prepared by first synthesizing a cadmium precursor analogue to the cadmium precursor for the core. Therefore, 0.1 mmol (7.9 mg, 1eq) cadmium oxide was dissolved in 0.46 mmol trioctylphosphine (204 µL, 4.6 eq) and cooled to 50 °C. Then the selenium precursor was produced, whereas 0.1 mmol selenium (12.9 mg, 1eq) dissolved in 4.0 mmol trioctylphosphine (1.80 mL, 40eq). These two precursor solutions were then combined at room temperature.

The tellurium precursor solution for the core was quickly injected to the cadmium precursor for the core. The temperature was lowered to 250 °C and was held for 2 min. For shell growth, the temperature was lowered to 120 °C and the shell precursor was injected. The temperature was kept constant for 20 h, to obtain shell growth. The purification was performed according to 3.7.3 [5].

3.7.5. Synthesis of Cadmium telluride/Cadmium zinc sulfide Core/Shell Quantum Dots

The core of the cadmium telluride/cadmium zinc sulfide quantum dots was synthesized in an analogue procedure as 2.1.3. For the cadmium zinc sulfide shell a precursor was prepared. Therefore, 0.5 mmol elemental sulfur (16 mg, 5eq) and 0.36 mmol zinc stearate (228 mg, 3.6 eq) were dissolved in 2 mL trioctylphosphine at 120 °C. This zinc sulfide precursor solution was injected into the cadmium telluride quantum dot solution at 180 °C and the temperature was kept constant for 15 min, allowing the shell growth [3,4]. The purification was achieved according to 3.7.3. The reaction sheme of the shell synthesis is displayed in figure 2.

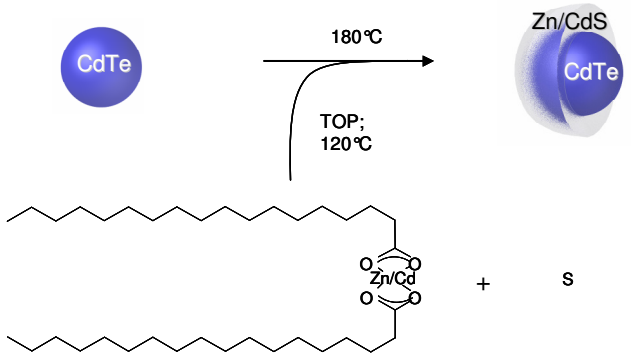

Figure 2: Reaction scheme of Zn/CdS shell synthesis

3.8. Syntheses of Ligands

3.8.1. Synthesis of Dihydrolipoic acid

For the coating of quantum dots with dihydrolipoic acid, the cleaving of the disulfide bond of lipoic acid was necessary. This reaction was carried out in aqueous solution. 0.5 mmol of lipoic acid (0.103 g, 1 eq) were dissolved in 25 mL of 0.25 M $NaHCO_3$ solution and was cooled to 0°C in an ice bath. Subsequently, 2 mmol sodium borohydride (76 mg, 4eq) were added slowly to the reaction solution and the temperature was kept below 4°C. After stirring for 2 h, the mixture was acidified with 6 M hydrochloric acid to pH 1 and extracted three

times with toluene. The organic phase was dried using magnesium carbonate. After evaporation of the product remained as a clear colorless oil [6]. The product was applied as obtained after purification.

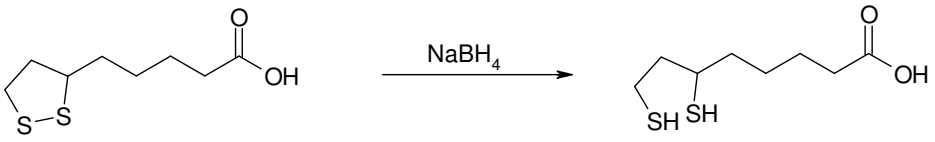

Figure1: Reaction scheme of the disulfide cleaving of lipoic acid.

3.8.2. Synthesis of amino Poly(ethylene glycol)$_{750}$mercaptoundecyl ether

The synthesis of the amino poly(ethylene glycol)$_{750}$mercaptoundecyl ether was carried out according to the route developed by Knerr [1].

Synthesis of Poly(ethylene glycol)$_{750}$ monoamine

For the synthesis of poly(ethylene glycol)$_{750}$monoamine, 0.45 mol (20 g, 360 eq) of ethylene oxide gas were condensed in 150 mL of dried THF at -79°C, cooled by a dry ice – methanol bath. Subsequently, 40 mL of 0.5% potassium bis(trimethylsilyl) amide (1.25 mmol, 1eq) in toluene were added and the solution was stirred for 36 h at room temperature, according to figure 3. The solvent was evaporated and the oily raw product was dissolved in methylene chloride. For purification, the solution was centrifuged, removing unsoluble impurities, and washed with ice cooled ether. The unsoluble product was collected from the ether solution by means of centrifugation (-10°C, 8000g, 5 min).

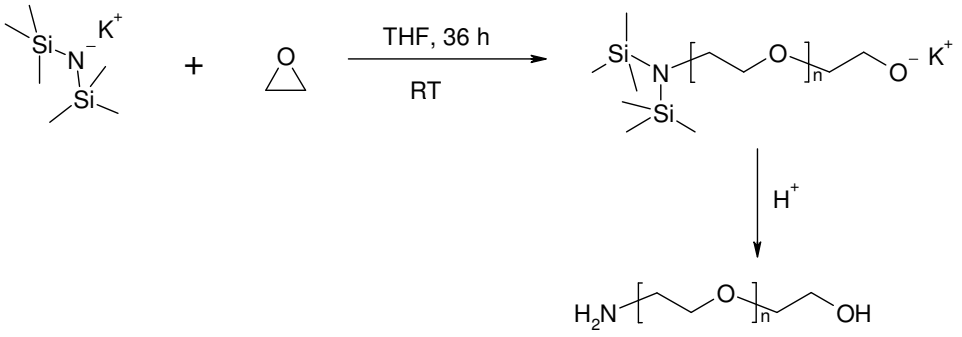

Figure3: Synthesis of poly(ethylene glycol) monoamine.

Protection of the primary amine group

To avoid the alkylation of the amine group during Williamson ether synthesis, this group has to be protected as shown in figure 4. Therefore, 2.5 mmol (1.8 g, 1 eq) of the poly(ehtlyene glycol)$_{750}$ monoamine and 10 mmol (0.6 g, 4eq) of potassium hydroxide were dissolved in 15 mL of water at 0°C. In parallel, 7.5 mmol (1.64 g, 3 eq) of di(tert-butly)dicarbonate were dissolved in 15 mL of dioxane. Subsequently, the dioxane solution was added dropwise to the aqueous solution of the poly(ehtlyene glycol)$_{750}$ monoamine. The reaction mixture was stirred for four hours at 0°C, followed by warming to room temperature over night. Afterwards, the product containing solution was concentrated and again dissolved in acetone, filtrated to remove insoluble salt, and washed with ice cold ether. The reaction product was obtained after centrifugation of the etheric solution (-10°C, 8000 g, 5 min).

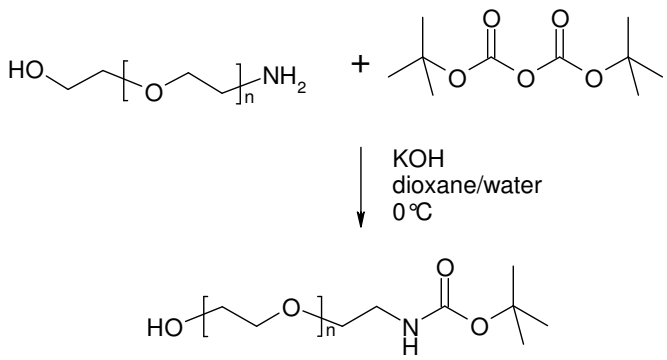

Figure 4: Synthesis of BOC-protected poly(ethylene glycol) monoamine.

Synthesis of BOC-protected Amino poly(ethylene glycol)$_{750}$-1-undecene

For the synthesis of BOC-protected amino poly(ethylene glycol)-1-undecene (see figure 5), 2 mmol (1.8 g, 1 eq) of BOC-protected amino poly(ethylene glycol) were mixed with 6 mmol (0.144 g, 3eq) of sodium hydride and allowed to react at 110°C for 30 min. After the reaction has stopped, observable from the stopping hydrogen development, 10 mmol (2.18 mL, 5 eq) of 11-bromoundecen were added and the reaction was stirred for another 24 hours. Subsequently, the reaction was quenched with methanol and the excess solvent was evaporated. Finally, the same purification procedure as for the BOC-protected amino poly(ethylene glycol) was applied.

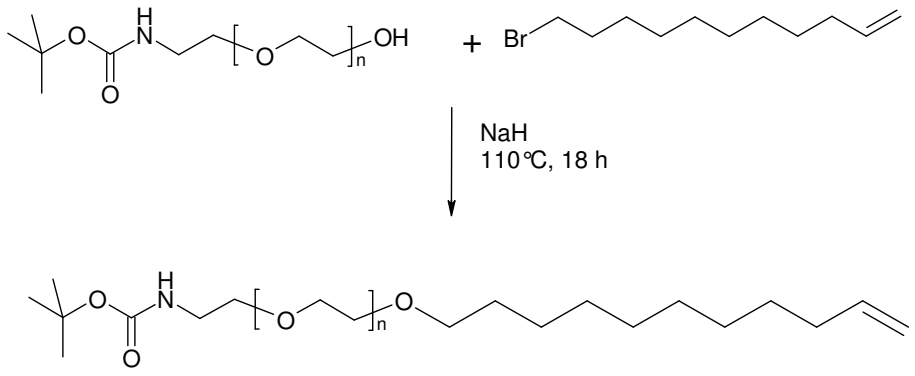

Figure 5: Synthesis of BOC-protected amino poly(ethylene glycol)-1-undecene.

Addition of thioacetic acid to BOC-protected Amino poly(ethylene glycol)$_{750}$-1-undecene

The addition of the thiol functionality was carried out by a radicalic reaction of amino poly(ethylene glycol)$_{750}$-1-undecene with thioacetic acid as displayed in figure 6. 1.5 mmol (1.6 g, 1eq) of amino poly(ethylene glycol)$_{750}$-1-undecene was dissolved in dry methanol, 2.25 mmol (0.369 g, 1.5 eq) α,α´azoisobutyronitril (AIBN) and 18 mmol (1.3 mL, 12 eq) thioacetic acid were added and the reaction solution was refluxed under nitrogen atmosphere for 72 hours.

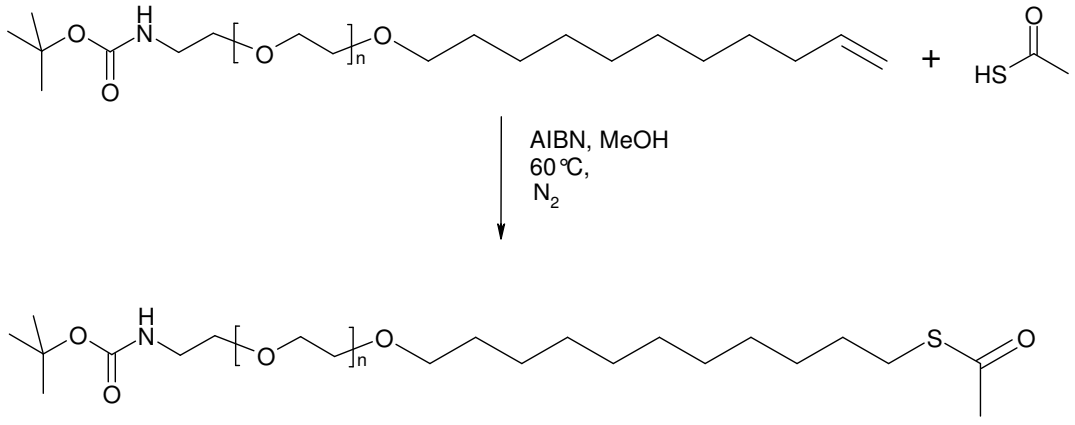

Figure 6: Synthesis of BOC-protected amino poly(ethylene glycol)-1-undecane thioester.

Hydrolysis of BOC-protected Amino poly(ethylene glycol)$_{750}$-1-undecane thioester

The BOC-protected amino poly(ethylene glycol)-1-undecane thioester was hydrolyzed to yield the free thiol and the unprotected amine group as showed in figure 7. For this reaction,

20 mL of hydrochloric acid in methanol was added to the reaction mixture and refluxed overnight. After evaporation of the solvent, the poly(ethylene glycol)mercaptoundecyl ether was purified by repeating the procedure described for the synthesis of BOC-protected poly(ethylene glycol) monoamine several times. The resulting reaction product was analyzed by HPLC and ^{1}H NMR, and used as obtained after purification.

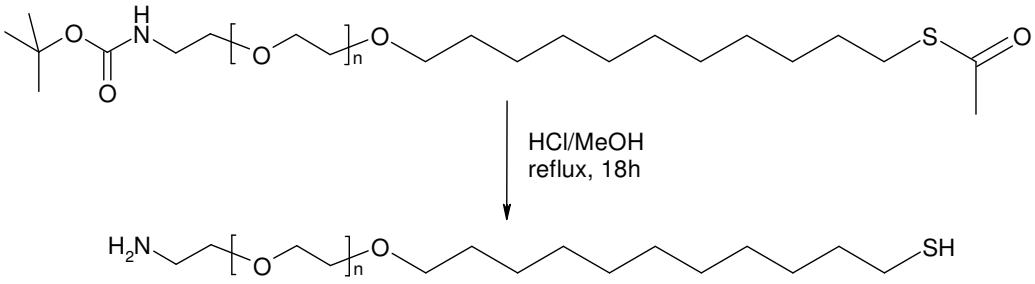

Figure7: Hydrolysis of BOC-protected amino poly(ethylene glycol)-1-undecane thioester to amino poly(ethylene glycol)mercaptoundecyl ether.

3.9. Coating of Quantum Dots

3.9.1. Coating of Quantum Dots with dihydrolipoic acid

The coating of the quantum dots with dihydrolipoic acid was achieved by combining 500 µL raw quantum dot solution with 100µL of the pure dihydrolipoic acid. The mixture was stirred for 30 min, and afterwards 2 mL of purified water were added. The dispersion was stirred for another 30 min. Meanwhile a phase transfer occurs. The aqueous phase containing the coated quantum dots was separated and purified. For the purification, the quantum dots were centrifuged (15000 g, 30 min, 18 °C) 3 times and the aqueous supernatant was removed. Finally, the coated quantum dots were dispersed in purified water. A reaction scheme of the ligand exchange on the quant um dot surface is depicted in figure 8.

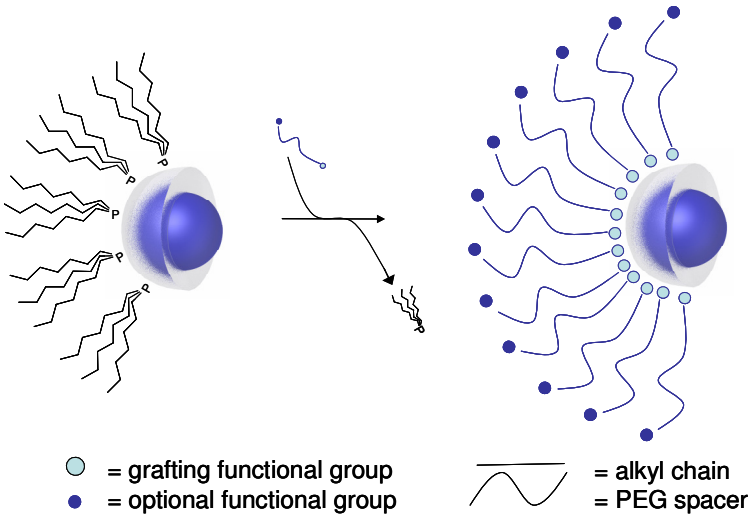

Figure 8: Reaction scheme of ligand exchange

3.9.2. Coating of Quantum Dots with Poly(ethylene glycol)mono-11-mercaptouncedyl ether derivatives

For the coating of quantum dots with poly(ethylene glycol)mono-11-mercaptouncedyl ether derivatives, unpurified quantum dot reaction solution was used. 250 µL of this dispersion were precipitated with ethanol and centrifuged (12000 g, 10 min, 18 °C). The precipitate was dispersed in 400 µL solution of the respective ligand, or a mixture of different ligands in mehtylenechloride (10-15 mg/mL). Subsequently, 2 mL of ethanol were added and the methylenechloride was evaporated. This ethanolic solution of the now coated quantum dots was transferred into an ultrafiltration spin column (Vivaspin 2, Satorius; MWCO 5000 Da), centrifuged and diluted with water (12000g, 30 min, 18°C) three times, to achieve a solvent exchange and purification. Afterwards, the purified quantum dots were transferred into another ultrafiltration spin coloum (Vivaspin 2, Satorius; MWCO 300000) and centrifuged (8000 g, 30 min, 18 °C) to accomplish a separation of bigger particles aggregates and precipitated byproducts.

3.10. Analysis of particles

3.10.1. Spectroscopic analysis

The absorbance spectra of the quantum dots were measured with a UVIKON 941 two-beam spectrophotometer (Kontron Instruments). The excitation and emission spectra were measured with a Perkin-Elmer LS 55 (Prekin-Elmer) equipped with a R928 red-sensitive

photomultiplier and the FL WinLab V4.00.03 software. 1 cm quartz cuvettes were used for all measurements.

The quantum yields ($\mathbf{\Phi_F}$) of the quantum dots were measured in methylenechloride. The quantum yields of the coated quantum dots were determined in purified water. For the identification a reference fluorophore with a known quantum yield and appropriate absorption and emission spectra was used (see table 1)[7].

Table 1: Quantum yield standards

Standard fluorophore	**quantum yield**	**Solvent**	**Applied spectral range**
Fluorecein	0.9	0.1 N sodium hydoxide	400 – 590 nm
Rhodamin 6G	0.94	Ethanol	580 – 640 nm
Oxazin 127	0.6	Ethanol	630 – 820 nm

The absorbance spectra of sample and reference solution were measured. Therefore the absorbance of the solutions have to be lower than 0.1 for avoiding an inner filter effect. After that, the emission spectra of sample and reference solution were determined. The excitation wavelength of the quantum dots used herein was 400 nm. Subsequently, the emission spectra were corrected using the spectrum correction file of the fluorimeter and the areas under the corrected spectra were determined via integration, using the integration function of the software.

For the calculation of the quantum yields, following formula was used:

$$\Phi_S = \Phi_R \cdot \frac{E_R \cdot A_s \cdot n_s^2}{E_s \cdot A_R \cdot n_R^2} \quad (1)$$

Φ_S quantum yield of the substance to be determined

Φ_R quantum yield of the reference

E_S absorbance at the excitation wavelength of the tested substance

E_R absorbance at the excitation wavelength of reference fluorophore

A_S integrated area under the corrected fluorescence spectrum of the tested substance

A_R integrated area under the corrected fluorescence spectrum of the reference fluorophore

n^2_S square of the refractive index of the solvent for the tested substance

n^2_R square of the refractive index of the solvent for the reference fluorophore

3.10.2. Analysis of composition

The composition of the quantum dots was analyzed using a Jobin Yvon 70 P (S+S) (Horiba Yovin Ivon GmbH) inductively coupled plasma optical emission spectrometer (ICP-OES) in a sequential analysis mode. The standard stock solution for calibration was composed of cadmium, selenium, tellurium and zinc in 3% nitric acid solution. The concentration of each element was 1000 ppb, respectively.

The quantum dot samples for the ICP-OES measurement were prepared from the unpurified reaction solution. First, 0.5 mL of the reaction solution was purified 3 times according to the method described in 2.1.3. Afterwards the precipitated quantum dots were disintegrated with 0.3 mL concentrated nitric acid and diluted with purified water to a volume of 10 mL and a nitric acid concentration of 3%, using a 10 mL volumetric flask.

3.10.3. Size analysis with photon correlation spectroscopy

The solvodynamic or hydrodynamic diameter of the quantum dots were measured with a ZetaSizer 3000 A (Malvern Insruments Inc.) photon correlation spectrometer (PCS). Purified water was used as solvent for coated quantum dots. Furthermore, all water-soluble samples were filtrated through a 0.22 µm PES syringe filter before measurement. The uncoated quantum dots were measured in methlyenechloride, and filtrated through a 1.0 µm glass fiber syringe filter. All measurements were carried out at 20 °C.

3.10.4. Size and concentration calculation

The size, size distribution, and resulting absorbance coefficients of the quantum dot solutions were calculated according to following, empirically determined, equations [4], based on the first absorbance peak and it respective broadness.

For CdSe based quantum dots

$$D = 161.22 \cdot 10^{-11} \cdot \lambda_{max}^4 - 265.75 \cdot 10^{-8} \cdot \lambda_{max}^3 + 162.42 \cdot 10^{-5} \cdot \lambda_{max}^2 - 14.77 \cdot 10^{-2} \cdot \lambda_{max} + 41.57 \quad (2)$$

$$D\pm = (161.22 \cdot 10^{-11} \cdot (\lambda_{max}^4 + fwhm) - 265.75 \cdot 10^{-8} \cdot (\lambda_{max}^3 + fwhm) + 162.42 \cdot (\lambda_{max}^2 + fwhm) - 14.77 \cdot 10^{-2} \cdot (\lambda_{max} + fwhm) + 41.57) - (161.22 \cdot 10^{-11} \cdot (\lambda_{max}^4 - fwhm) - 265.75 \cdot 10^{-8} \cdot (\lambda_{max}^3 - fwhm) + 162.42 \cdot 10^{-5} \cdot (\lambda_{max}^2 - fwhm) - 14.77 \cdot 10^{-2} \cdot (\lambda_{max} - fwhm) + 41.57) \quad (3)$$

$$\varepsilon = 5857 \cdot D^{2,56} \quad (4)$$

D diameter of the nanaoparticles [nm]

D± size distribution of the diameter of the nanoparticles [nm]

λ_{max} wavelength of the first absorbance maximum [nm]

ε = decadic molar absorbance coefficient [L/mol*cm]

For CdTe based quantum dots

$$D = 981.27 \cdot 10^{-9} \cdot \lambda_{max}^3 - 171.47 \cdot 10^{-5} \cdot \lambda_{max}^2 + 100.46 \cdot 10^{-2} \cdot \lambda_{max} - 194.47 \tag{5}$$

$$\begin{aligned} D\pm = & (981.27 \cdot 10^{-9} \cdot (\lambda_{max}^3 + fwhm) - 171.47 \cdot 10^{-5} \cdot (\lambda_{max}^2 + fwhm) + \\ & 100.46 \cdot 10^{-2} \cdot (\lambda_{max} + fwhm) - 194.47) - \\ & (981.27 \cdot 10^{-9} \cdot (\lambda_{max}^3 - fwhm) - 171.47 \cdot 10^{-5} \cdot (\lambda_{max}^2 - fwhm) + \\ & 100.46 \cdot 10^{-2} \cdot (\lambda_{max} - fwhm) - 194.47 \end{aligned} \tag{6}$$

$$\varepsilon = 10043 \cdot D^{2.12} \tag{7}$$

D diameter of the nanaoparticles [nm]

D± size distribution of the diameter of the nanoparticles [nm]

λ_{max} wavelength of the first absorbance maximum [nm]

ε = decadic molar absorbance coefficient [l/mol*cm]

The concentration can be calculated from the determined absorbance coefficient and the measured absorbance according to Lambert Beer´s law:

Lambert Beer´s law

$$A = \varepsilon \cdot c \cdot d \tag{8}$$

A absorbance of sample

c concentration of sample [mol/L]

d length of penetratured medium [cm]

ε decadic molar absorbance coefficient [L/mol*cm]

3.10.5. Morphologic analysis with transmission electron microscopy/Cryo-transmission electron microscopy

For the morphologic analysis a Zeiss EM 10 C/CR (Carl Zeiss AG) transmission electron microscope (TEM) with 60 kV operating voltage was used. The specimen were prepared on 3.05 mm formvar/carbon coated copper grids (300 mesh). They were dropped on the grids in methylenechloride or water and dried using a vacuum pump.

The Cryo-TEM measurements were carried out on a Zeiss 922 Omega (Carl Zeiss AG) transmission electron microscope in the cryo mode. The samples were prepared by spreading

of a diluted (ca 1 Vol%) aqueous solution of quantum dots on a 3.05 mm formvar/carbon coated copper grid (300 mesh), followed by a fast freezing of the specimen in liquid nitrogen.

3.10.6. Amino group determination with a modified Fluram® assay

The amount of free amino groups on the surface of coated quantum dots was determined using a fluorescamin (Fluram®) assay. The fluorimetric Fluram® (4-Phenylspiro-[furan-2(3*H*),1-phthalan]-3,3′-dione) assay is based on the reaction of the non-fluorescent reagent, which converts with primary amines to a stable, highly fluorescent compound (see figure 9).

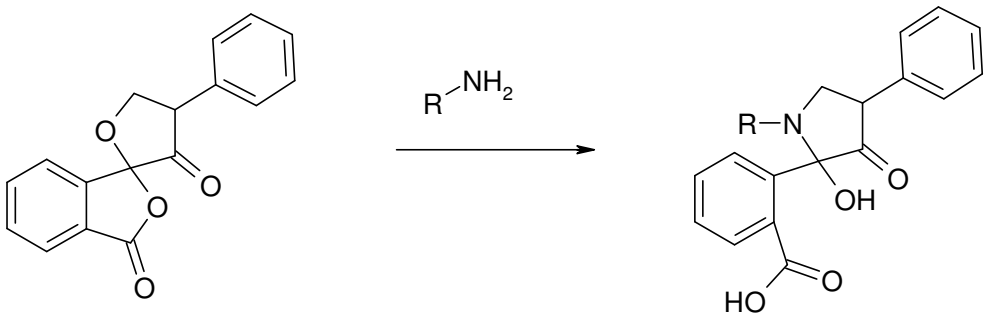

Figure 9: Reaction scheme of fluorescamin with primary amine

For the borate buffer (50 mM, pH 8.5) 19,06 g sodium tetraborat decahydrat was dissolved in approx. 900 mL purified water and thesolution was adjusted to pH 8.5 with 3 M hydrochloric acid or 3 M sodium hydroxide. The solution was transferred into a 1 L volumetric flask and filled up to 1000 mL. The fluorescamin stock solution (0.3 mg/mL) was prepared by dissolving 15 mg Fluram® in a 50 mL volumetric flask using acetone as solvent. For the stock solution of 6-aminohexanoic acid (0.01 mg/mL), 5 mg 6-aminohexanoic acid were dissolved in borate buffer using a 500 mL volumetric flask. Subsequently, the stock solution was diluted to a standard solution (0.005 mg/mL). 5.0 mL of the 6-aminohexanoic acid stock solution were diluted to 10 mL with borate buffer using a 10 mL volumetric flask.

First, a calibration curve for the Fluram® assay was recorded with the 6-aminohexanoic acid standard solution as reference. Due to the strong absorbance of the quantum dots, it was necessary to substitute the Fluram® stock solution for the calibration with the same amount of a solution of poly(ethylene glycol) coated quantum dots. These reference quantum dot solutions were adjusted to the same optical density as the measured samples. For the measurement, all samples of the amino poly(ethylene glycol) coated quantum dot were

adjusted to the same optical density ranging from 0.05 - 0.1. Subsequently, Fluram® solution was added and the samples were diluted with borate buffer to the same volume as the samples for the calibration. Afterwards, the micoplate with the calibration samples and the quantum dot samples was incubated for 10 min at room temperature in the dark. The assay was carried out in a 96-well plate utilizing the well-plate-reader accessory of the Perkin-Elmer LS 55 fluorimeter with 390 nm as exaction and 480 nm as emission wavelength, additionally a 390 nm cut-off filter was used.

3.10.7. Cytotoxicity Test

The cell lines used for the cytotoxicity test were L929 and CHO cells. The L929 cells were grown in T-75 cell culture flasks containing 20 mL EMEM supplemented with 10% FBS. The CHO cells were grown in T-75 cell culture flasks containing 20 mL of HAM supplemented with 10% FBS. Both cell lines were cultured at standard cell culture conditions (37°C, 95% relative humidity, and 5% CO_2). The growth medium was changed every third day. The cells were harvested at 90% confluence by exposure to a 0.25% trypsin-EDTA solution (3 mL/flask) and resuspended at a density of 50000 cells/mL for the MTT assay.
The colorimetric cytotoxicity assay is based on the conversion of yellow, water-soluble MTT [3-(4,5-dimethylthiazol-2-yl)-2,5-diphenyl tetrazolium bromide] by the mitochondrial dehydrogenases of viable cells, to the purple, water insoluble end-product formazan (see figure 10).

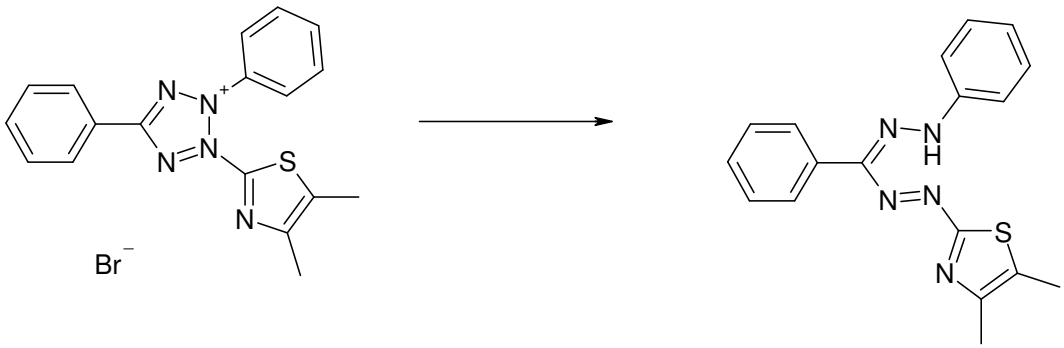

Figure 10: Reaction scheme of MTT to MTT formazan

All MTT assays were carried out in 96-well plates. The cells were seeded at a density of 10,000 cells/well and the solution of MTT was prepared by dissolving 2.5 g MTT/mL in sterile PBS. The L929 cells were grown for 24 h in 200 µL EMEM supplemented with 10% FBS at standard cell culture conditions; the CHO cells were grown for 24 h in 200 µL HAM

supplemented with 10% FBS at standard cell culture conditions. 200 µL of nanoparticle dispersions of different concentrations in the respective medium containing 10% FBS were added to the cells and were incubated for 4 h at standard cell culture conditions. After incubation, the nanoparicles were removed and the cells were washed with 200 µL sterile PBS. The MTT stock solution was diluted to a concentration of 0.625 mg/mL with the according medium, was added to the cells and incubated for 4 h at standard cell culture conditions. Afterwards, the MTT solution was removed carefully. Finally, 200 µL of 10% SDS in PBS were added to each well and incubated additional 24 h [9-11]. The absorbance of each well was determined on a TitertekPlus Microplate Reader (Friedrich S. Bartolomey) with 550 nm as probe wavelength and 630 nm as reference wavelength.

3.11. References

[1] R. Knerr, S. Drotleff, C. Steinem, A. Goepferich, Self-assembling of PEG derivatives for protein-repellent biomimetic model surfaces on gold, Biomaterialien 7 (1) (2006) 12--20.

[2] D.S Wang, J.B. He, N. Rosenzweig, Z. Rosenzweig, Superparamagnetic Fe_2O_3 beads-CdSe/ZnS quantum dots core-shell nanocomposite particles for cell separation, Nano Lett. 4 (2004) 409--413.

[3] G.-W. Huang, C.-Y. Chen, K.-C. Wu, M.O. Ahmed, P.-T. Chou, One-pot synthesis and characterisation of high-quality CdSe/ZnX (X = S, Se) nanocrystals via the CdO precursor, J. Cryst. Growth. 265 (2004) 250--259.

[4] W.W. Yu, L.H. Qu, W.Zh. Guo, X.G. Peng, Experimental Determination of the Extinction Coefficient of CdTe, CdSe, and CdS Nanocrystals, Chem. Mater. 15 (2003) 2854—2860

[5] S.F. Wuister, I. Swart, F. van Driel, S.G. Hickey, C. de Mello Donegá, Highly Luminescent Water-Soluble CdTe Quantum Dots, Nano Lett. 3 (4) (2003), 503—507.

[6] H.T. Uyeda, I. L. Mednitz, J.K. Jaiswal, S.M. Simon, H. Mattoussi, Synthesis of Compact Multidentate Ligands to Prepare Stable Hydrophilic quantum dot Fluorophores, J. Am. Chem. Soc. 127 (2005) 3870--3878.

[7] J.R. Lakowicz, Principles of Fluorescence Spectroscopy, 2th Edition, Kluwer Academic/Plenum Publishers, New York (1999).

[8] C.Y. Lai, Detection of peptides by fluorescence methods, Methods Enzymol. 47 (1977) 236—243.

[9] S. Udenfriend, S. Stein, P. Bohien, W. Dainnan, W. Leimgruber, M.Welgele, Fluorescamine: a reagent for assay of amino acids, peptides, proteins, and primary amines in the picomole range, Science 178 1(972) 871--872.

[10] T. Mosmann, Rapid Colorimetric Assay for Cellular Growth and Survival: Application to Proliferation and Cytotoxicity Assays, J. lmmunol. Methods 65 (1983) 55--63.

[11] J.A Plumb, R. Milroy, S.B Kaye, Effects of the pH Dependence of 3-[4,5 Dimethylthiazol-2-yl]-2,5-diphenyltetrazolium bromide – Formazan. Absorption on Chemosensitivity Determined by a Novel Tetrazolium-based Assay. Cancer Res. 49 (1989) 4435--4440.

[11] M. Shiau, H. Chiou, Y. Lee, T. Kuo, Y. Chang, Establishment of a consistent L929 bioassay system for TNF- α quantitation to evaluate the effect of lipopolysaccharide, phytomitogens and cytodifferentiation agents on cytotoxicity of TNF-α secreted by adherent human mononuclear cells. Mediat. Inflamm. 10 (2001) 199--208.

Chapter 4

Quantum dots - Results

Synthesis and optimization of Quantum Dots

The objective of the quantum dot syntheses was the preparation of stable, highly luminescent, NIR-emitting, and non-toxic nanoparticles. For the optimization of these properties, quantum dots of different compositions, and sizes were synthesized and coated with different inorganic and organic materials, respectively.

The emission wavelength of quantum dots depends on the one hand on the size of the quantum dot core , and on the other hand on the chemical composition [1-4]. The elements used herein belong to the II and IV elemental group, namely cadmium, zinc, tellurium, selenide and sulfur. Futhermore, varying synthesis methods based on the “hot injection method” were utilized.

4.1. Cadmium Selenide based Quantum Dots

The CdSe and CdSe/ZnS quantum dots were synthesized according to the method described in 3.7.1 and 3.7.2. In figure 1, the absorbance and emission spectra of both quantum dot species are displayed. The CdSe nanoparticles show an emission maximum of 561 nm and a full width at half maximum (fwhm) of 26 nm. Upon the shell growth according to the coating with ZnS, the emission maximum is shifted to 572 nm. Nevertheless, the fwhm (27 nm) does not broaden significantly.

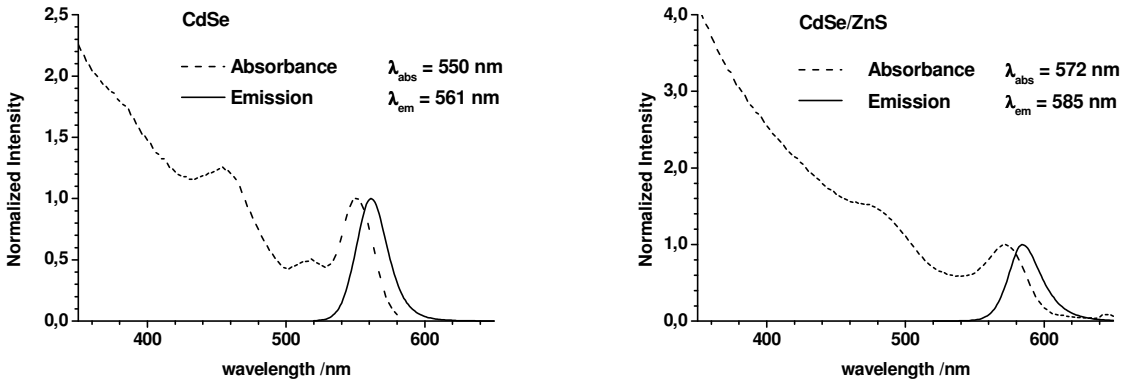

Figure 1: Absorbance and emission spectra of CdSe and CdSe/ZnS quantum dots.

However, it is not possible to synthesize CdSe/ZnS quantum dots exceeding an emission wavelength of approx. 635 nm. Therefore, the composition of the quantum dots was changed to CdTe as core material, providing the opporiunity of longer emission wavelengths.

4.2. Cadmium Telluride based Quantum Dots

4.2.1. CdTe Quantum Dots

The CdTe quantum dots were synthesized according to the method described in 3.7.3. In figure 2 on the left side, representative absorbance and emission spectra of CdTe quantum dots are displayed. On the right side, the evolution of the emission wavelength as well as the fwhm of the quantum dots with reaction time of the synthesis is depicted. The maximum emission wavelength achieved applying this method was about 720 nm. Nevertheless, the fwhm broadens significantly upon quantum dot growth, too. Until a reaction time of 30 min, the wavelength increases almost linear and the fwhm is quite low for CdTe quantum dots [6]. After 30 min, the emission maximum barely increases, whereas the fwhm strongly increases. This can be ascribed to a rising Ostwald ripening [7].

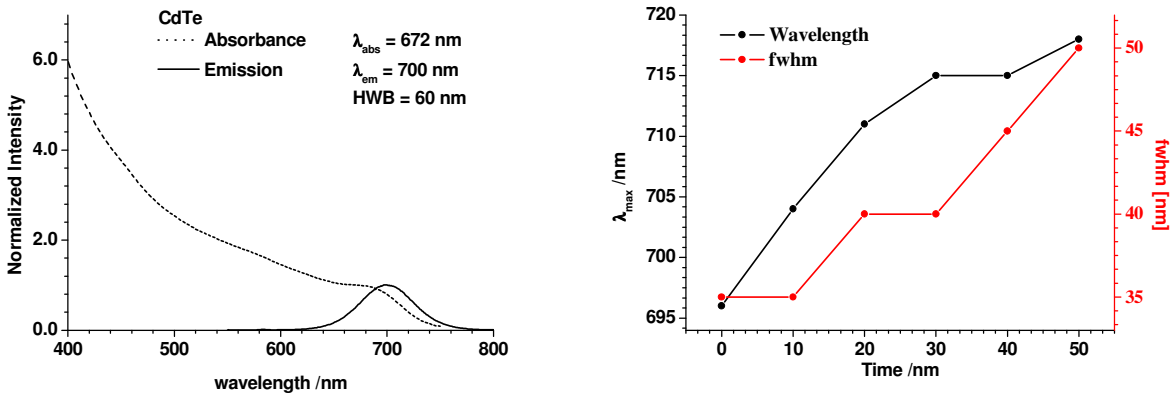

Figure 2: Absorbance and emission spectrum of CdTe quantum dots; development of the emission wavelength and fwhm with reaction time.

Unfortunately, blank CdTe quantum dots are not very stable against oxidation, and they therefore loose luminescence intensity, upon coating with water-soluble polymers. Accordingly, a further shell growth with a more stable inorganic material is needed. It seems to be most promising to use CdSe as a shell for CdTe quantum dots, because the lattice parameters of these two materials match quite well [8], which is a prerequisite for satisfying shell growth.

4.2.2. CdTe/CdSe Quantum Dots

The CdTe/CdSe quantum dots were prepared according to the method presented in chapter 3.7.4. A characteristically absorbance and emission spectrum is presented in figure 3. The

maximum emission wavelength of this kind of quantum dots is not altered compared to blank CdTe quantum dots.

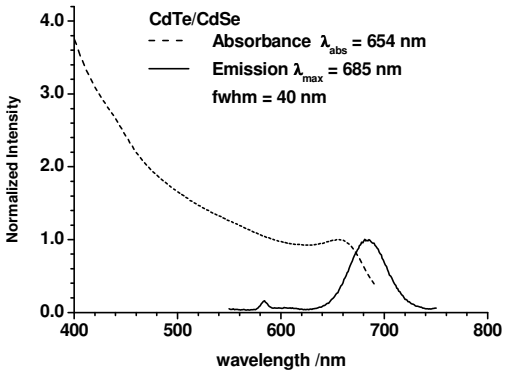

Figure 3: Emission and absorbance spectrum of CdTe/CdSe quantum dots.

This quantum dot core/shell system is suitable in terms of emission wavelengths and stability. However, the remaining toxicity of the Cd in the CdSe shell is likely to be too high for application (see chapter 2.5.1). Another material with appropriate lattice parameters of CdTe is CdS [8]. However, this does not solve the toxicity problem. Another common material for shell growth is ZnS. Unfortunately, its lattice parameters do not fit with those of CdTe [9]. Nonetheless, this problem can be avoided by the growth of a mixed CdZnS shell. This minimizes the toxicity and alters the lattice constants to an adequate extent.

4.2.3. CdTe/CdZnS Quantum Dots

The CdTe/CdZnS quantum dots were synthesized following the method described in chapter 3.7.5. In figure 4 the dependence of the quantum dot size and the corresponding emission wavelength on the growth temperature is presented. The addition of the ZnS shell precursor to the CdTe reaction solution induces no additional wavelength shift. Therefore, the ZnS shell does not contribute to the maximum emission wavelength. This finding is in contrast to the shell growth in CdSe/ZnS quantum dots (chapter 4.1), where a wavelength shift of up to 30 nm can be observed.

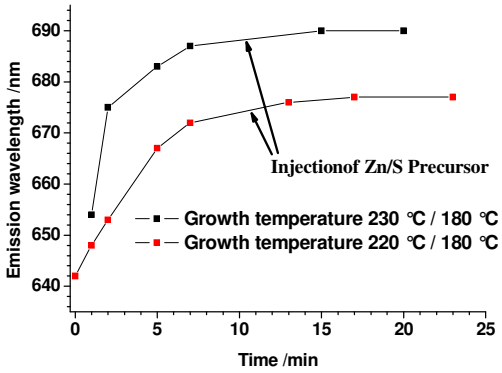

Figure 4: Development of the emission wavelength with reaction time for two different growth temperatures.

Due to the fact that the CdTe/CdZnS quantum dots have the most promising characteristics concerning emission wavelength, stability, and toxicity, the synthesis procedure of these nanoparticles was optimized and fine-tuned in terms of wavelength, quantum yield and stability.

A quite interesting finding was the formation of tetrapod-shaped nanoparticles under the same conditions, if silicon grease instead of silicon free grease for the glassware in synthesis is used. A cryo-TEM picture of these irregularly shaped quantum dots in hexane is shown in figure 5. The photophysical characteristics only differ in terms of quantum yield, which is quite low for these quantum tetra-pods compared to quantum dots.

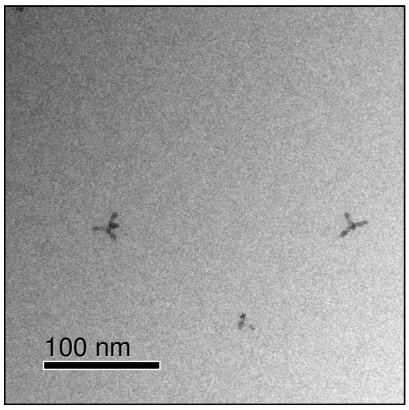

Figure 5: Cryo-TEM picture of tetra-pod shaped CdTe/CdZnS nanoparticles in hexane

The ICP-OES analysis gave a ratio of core:shell of 1:14, thus indicating that the “arms” of the tetrapods are composed of the shell material.

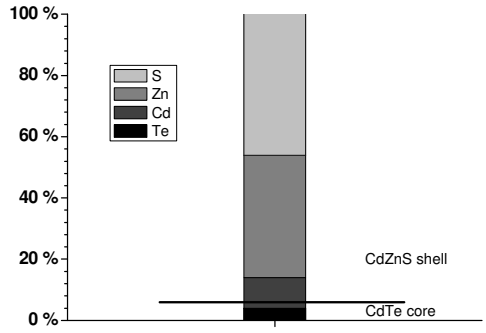

Figure 6: Elemental composition of CdTe/CdZnS quantum tetra pods.

This formation of tetra-pods by addition of mediators, which intensify the growth of certain crystal facets, is described in literature [10]. Nevertheless, the influence of silicon grease is not yet described.

4.2.4. Optimisation of CdTe/CdZnS Quantum Dot synthesis

For further optimization of the synthesis, all variables were altered based on the "standard conditions", namely 0.076 mmol/mL Te-precursor, 0.152 mmol/mL Cd-precursor, 300°C injection temperature, 180°C growth temperature, the use of oleic acid for Cd-precursor, 5 min growth time for CdTe, and 15 min shell growth time for CdTe/CdZnS quantum dots according to the synthesis described in 3.7.5.

Effects of Tellurium precursor

First of all, the effects of the type of tellurium precursor on the reaction speed and the corresponding emission wavelength were investigated. Hence, two different tellurium precursors were synthesized, one with the short-chained tributylphosphine (TBP) reactant, the other one with the longer-chained trioctylphosphine (TOP) reactant. The two reactions were carried out under standard conditions. The emission spectra of quantum dots prepared with these two different Te-precursors, respectively, are displayed in figure 7.

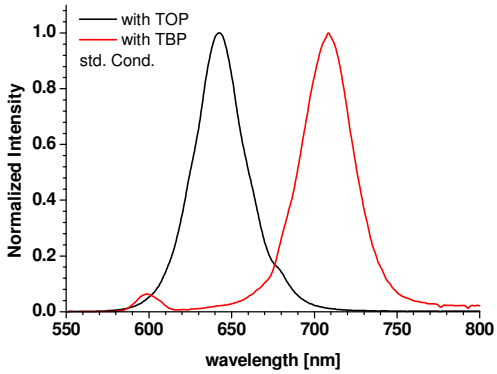

Figure 7: Emission spectra of CdTe/CdZnS quantum dots synthesized with TBP or TOP Te-precursor

The use of the TBP based Te-precursor yields in quantum dots of approx. 80 nm longer emission wavelength, compared to those synthesized applying the TOP based precursor. This is due to the faster reaction speed of this short chained reactant. Nevertheless, the quantum yields of the as synthesized nanoparticles are approx. 15% lower. This is on the one hand founded in the longer emission wavelength, which results in lower quantum yields, and on the other hand maybe in a more imperfect surface of the quantum dots (see chapter 2.5.1).

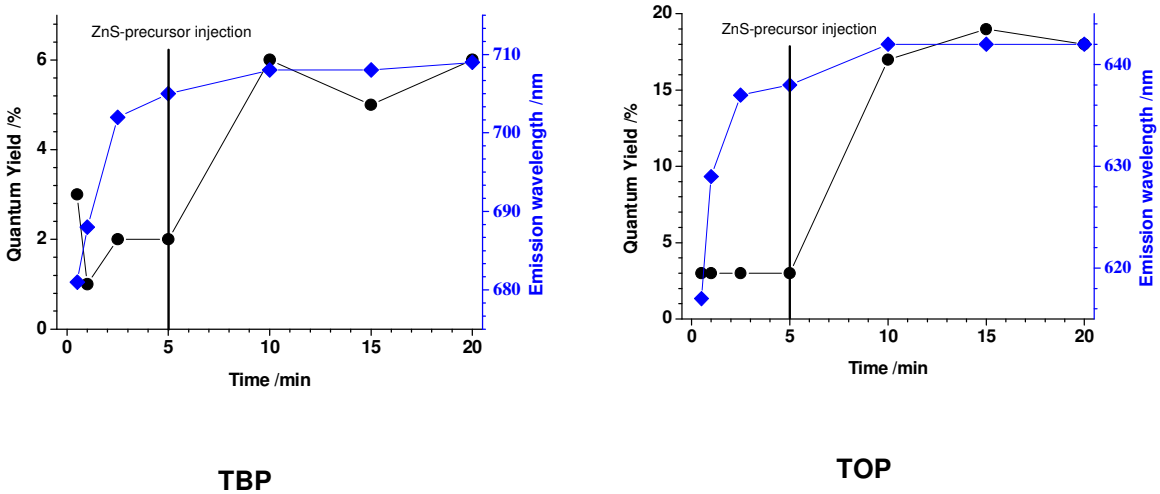

Figure 8: Development of the emission wavelength and quantum yield with time, for TBP and TOP precursors

In both reactions, the addition of the Zn/S-precursor (after 5 min) leads to a strong increase of the quantum yield, which, however, is independent of the emission wavelength. The quantum yield increase is caused by the overgrowth of the ZnS shell and the resulting stabilization of the CdTe core surface [11].

The composition and the overall yield of the quantum dots synthesized with the two different Te-precursors were investigated with ICP-OES. The yield of the synthesis using the TOP precursor is 11%. 16% are reached with the TBP precursor. This result supports the assumption of different reactivities of the precursors. Concerning the composition of the quantum dots, a higher amount of Cd in the shell was achieved applying the TOP precursor compared to the TBP precursor, as can be seen in figure 9. All following syntheses were performed with both Te-precursors, due to the fact that the TOP precursor results in higher quantum yields and the TBP precursor leads to higher emission wavelengths.

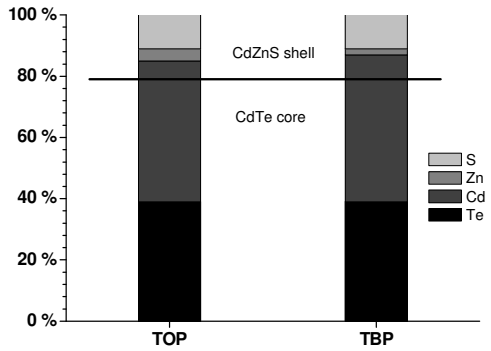

Figure 9: Composition of quantum dots synthesized with TBP and TOP precursors.

Effects of Reaction Temperatures

The influence of the two reaction temperatures used was investigated in the next step. The temperature for the core growth was varied between 270°C to 300°C, whereas the temperature for the shell growth was phased in a range from 180°C to 230°C. The nucleation heat was lowered in order to study the influence on the emission wavelength, which should lower with decreasing temperature. The shell growth heat was increased in order to examine the effect on the core growth rate, and therefore the quantum yield. This increase was supposed to result in a quantum yield increase, due to a bigger shell and thus a better protection of the core. In figure 10, the emission wavelengths and quantum yields for the synthesis with TOP and TBP Te-precursor at different nucleation and shell growth heats is shown.

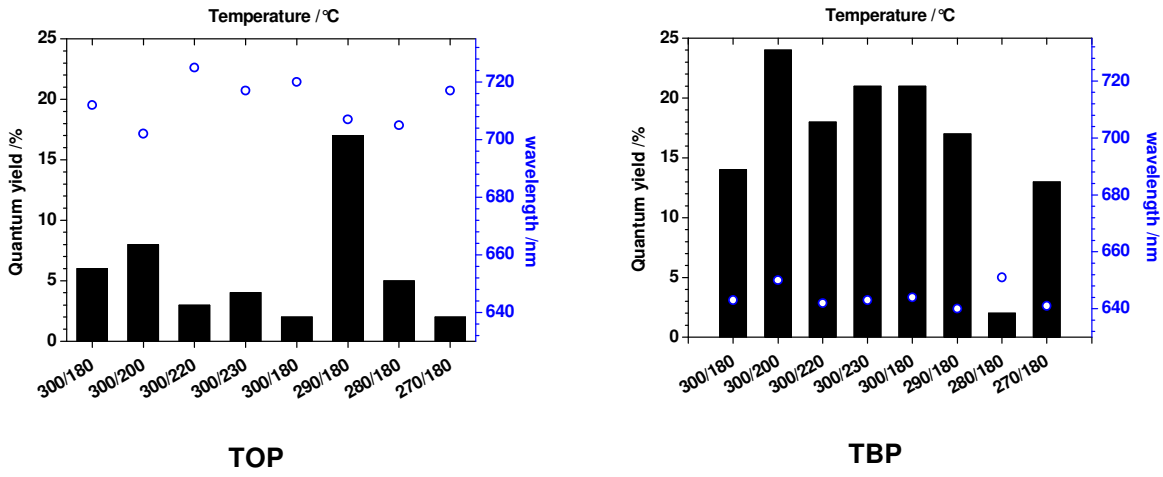

Figure 10: Influence of the reaction temperatures (nucleation temperature/shell growth temperature) on emission wavelength and quantum yield.

In both cases the variation of the temperatures does not result in the expected dependence of the emission wavelength and quantum yield. This effect can be ascribed to the lack of sufficient temperature control of the chosen experimental setup and the comparable large volumes to be thermostatted. Nevertheless, a better temperature control could not be achieved without a complete change of the experimental setup.

Effects of cadmium precursor

By the reason that the Te-precursor effects the formation and growth of the nanoparticles quite strong, different Cd-precursors were tested as well. For this experiment, elemental Cd was reacted with different fatty acids of the same chain length, but increasing amounts of double bonds (stearic acid, oleic acid, linoleic acid). The dependence of the emission wavelength and quantum yield on the Cd-precursor used is displayed in figure 11.

With both Te-precursors, the same results for the varying Cd-precursors were achieved. The highest emission wavelengths, but lowest quantum yields, are reached with linoleic acid, whereas the lowest emission maxima and highest quantum yields are obtained with the use of olecic acid as Cd-precursor.

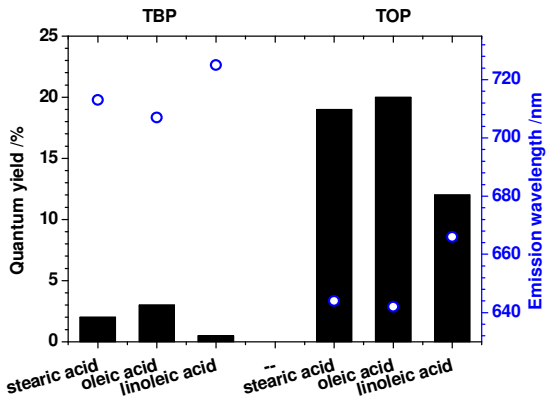

Figure 11: Influence of the Cd-precursor on emission wavelength and quantum yield.

These outcomes suggest that the oleic acid stabilizes the quantum dots during the synthesis to a bigger extent than the other fatty acids investigated, whereas the linoleic acid exhibits a higher reaction rate.

Effects of precursor concentration and reaction scale

The effect of precursor concentration and reaction scale was investigated, since these parameters also influence both growth speed and nucleation of the quantum dots.

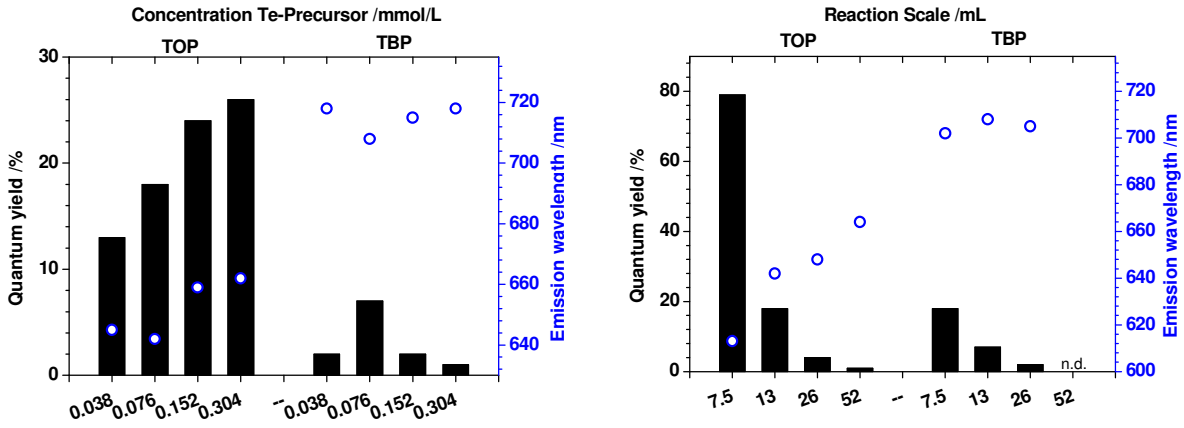

Figure 12: Influence of precursor concentration and reaction scale on emission wavelength and quantum yield.

As can be seen from figure 12, an increased concentration of the TOP Te-precursor yields an increased emission wavelength and quantum yield. Applying the TBP precursor, a maximum in the quantum yield is reached at a concentration of 0.076 mmol/L, whereas the emission wavelength shows the same dependence as using the TOP precursor. The results of this experiment can be explained with the ascending amount of reactable Te in the reaction

solution, which increases the reaction speed, and thus resulting in a higher emission wavelength. The higher quantum yields may also depend on the Te concentration, because the phosphine precursors also act as surface ligands for the nanoparticle, and preferably bind to Te atoms at the surface. This results in an enclosed Te shell around the quantum dot, thus protecting the CdTe core more efficiently [12]. Accordingly, a bigger amount of Te results in a more effective protection of the core. The investigation of the influence of the reaction scale clearly indicates, that upscaling results in increased emission wavelength but decreased quantum yield for both the TOP and the TBP precursors. This may be, again, founded in the experimental setup. By increasing the reaction scale, an inferior mixing, and a worse thermostatting are given. Therefore, the reaction conditions in the flask are inhomogeneous, resulting in a lowered quality of the synthesized quantum dots.

Comparison of differently synthesized CdTe/CdZnS Quantum Dots

The determination of the quantum dot stability against aggregation and of the shape of the synthesized quantum dots was carried out with TEM and PCS analysis. For a comparison of the different syntheses three conditions for the two Te-precursors were chosen (standard conditions, linoleic acid as Cd-precursor, 0.304 mmol/L precursor concentration). In figure 13 a1-a3, TEM images of different quantum dots using the TOP Te-precursor are displayed. The as synthesized quantum dots show spherical shapes and only a low extent of aggregation. In figure 13 b1-b3, TEM images of different nanoparticles using the TBP Te-precursor are shown. The images of the quantum dots prepared under standard conditions and with linoleic acid Cd-precursor show spherically shaped quantum dots, whereas the nanoparticles synthesized with 0.304 mmol/L precursor exhibit tetra-pod shape. Nevertheless, the tetrapods are not that pronounced as in figure 5, synthesized with silicon grease. This irregular shape growth may be due to the high precursor concentration and fast reaction speed of the TBP Te-precursor.

In image b2, the aggregation of quantum dots is displayed, observable by the particles clustering and lying on top of each other. This finding is supported by the determination of the solvodynamic radii of the quantum dots in methylene chloride, where the aggregation tendency is even more pronounced as shown in the TEM picture. The calculated and measured radii are compared in table 1. The differences between these two values are founded in the fact that the calculated radius of the CdTe/CdZnS quantum dots only considers the CdTe core.

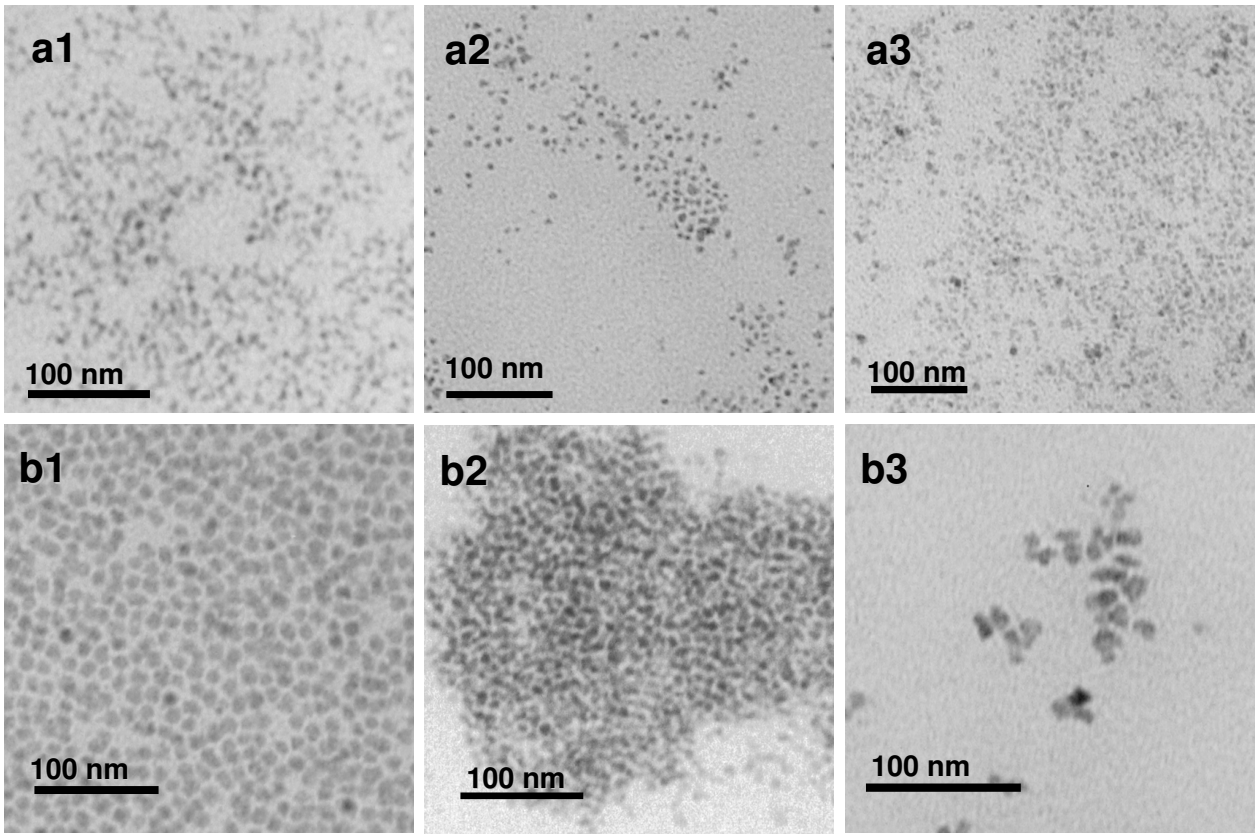

Figure 13: TEM pictures of quantum dots synthesized with TOP (a1)Std. cond., (a2) linoleic acid, (a3) 0.304 mmol/mL; TBP (b1) Std. Cond., (b2) linoleic acid, (b3) 0.304 mmol/mL

Furthermore, the measured diameter is a solvodynamic diameter which takes the size of the bound ligand shell and the associated methylene chloride molecules into account. Therefore, the contribution of the inorganic and the organic shell adds to about 4 nm.

Table 1: Comparison of the calculated and the measured sizes of quantum dots synthesized under different conditions

	Reaction conditions	**Calculated radius**	**Particle size distribution**	**Solvatodynanic radius**	**Polydisperisty Index**
TOP	Std. cond.	4.11	0.45	12.40	0.12
	Linoleic acid	4.47	0.53	8.70	0.16
	0.304 mmol/L	4.22	0.63	8.90	0.3
TBP	Std. cond.	5.82	1.99	12.40	0.13
	Linoleic acid	5.96	1.86	550.00	0.16
	0.304 mmol/L	5.96	0.39	341.00	0.13

Overall there are no “perfect” reaction conditions for preparation CdTe/CdZnS quantum dots. However, there are different variables that enable for the tailoring of quantum dots for different applications. The choice of the type of Te-precursor and its respective concentration in the reaction solution is a crucial factor. The reaction scale has great influence on the quality of the synthesized quantum dots, which unfortunately limits the fabrication of bigger batches. In contrast the effect of the Cd-precursor is quite low, and the influence of the temperature was not observable in this experiments. Nevertheless, for the TOP precursor, the use of a high precursor concentration, low reaction scale and the oleic acid cadmium precursor gives the best results. The TBP precursor based synthesis, on the other hand, yields the best particles with a comparably low precursor concentration.

Coating of Quantum Dots

The ligand syntheses and coating procedures of the quantum dots aimed to produce water-soluble, stable, and non-toxic particles. Therefore, different water-soluble ligands and coating procedures were applied (see chapter 3.9). The molecules used herein provide a thiol group for grafting on the quantum dot surface, an alkyl chain as a spacer and a hydrophilic end group or chain to introduce water-solubility.

4.3. Dihydroliponic acid coated CdTe/CdZnS Quantum Dots

The dihydroliponic acid coating was performed according to method 3.9.1, using the CdTe/CdZnS quantum dots described in chapter 3.7.5. and the ligand synthesized according to chapter 3.8.1., The photophysical characteristics shown in figure 14 were recorded after phase transfer and purification of the nanoparticles. Nevertheless the absorbance and emission spectra are not significantly altered compared to the uncoated quantum dots. The cryo-TEM analysis illustrates slightly aggregated quantum dots in aqueous dispersion (figure 14), which also correlates with the hydrodynamic diameter of approx. 50 nm measured with PCS.

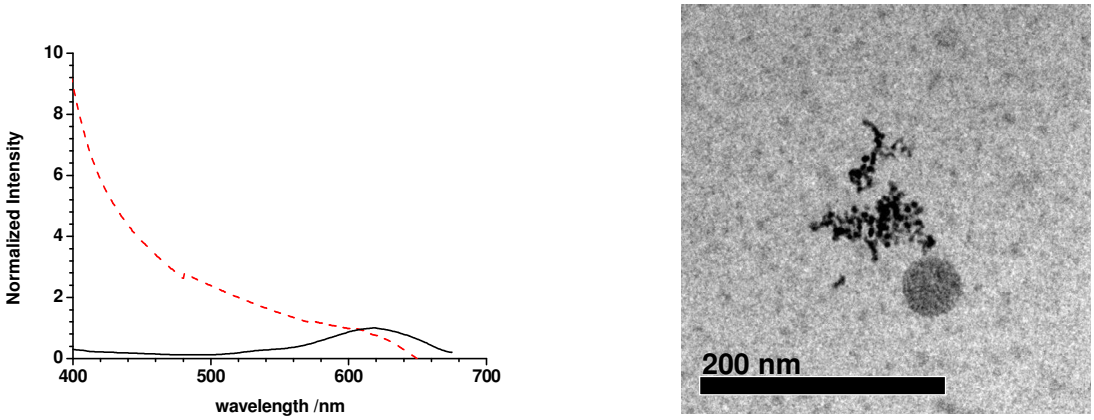

Figure 14: Absorbance and emission spectra of dihydrolipoic acid coated quantum dots; cryo-TEM image of dihydrolipoic acid coated quantum dots in water.

The TEM images and PCS data indicate an aggregation tendency of the coated nanoparticles, which can be ascribed to a poor stabilization capability of the dihydrolipoic acid. The single carboxy group of this molecule provides not enough hydrophilicity to keep the nanoparticles dispersed in aqueous solution. Therefore, a more hydrophilic ligand for the preparation of stable, water-soluble quantum dots has to be applied. A molecule group which provides

promising characteristics for the application as coating material are poly(ethyleneglycol) mercaptoundecyl ether (see chapter 2.5.2). These molecules are widely used to coat gold surfaces and nanoparticles [13,14].

4.4. Poly(ethyleneglycol)mercaptoundecylether coated CdTe/CdZnS Quantum Dots

All coating procedures were conducted according to the method described in chapter 3.9.2. Three different non-functionalized ligands, namely mercaptouncdecanol (UD), tri(ethylene glycol) mercaptoundecyl ether (PEG3), hexa(ethylene glycol) mercaptoundecyl ether (PEG 6), and two amino-functionalized ligands namely, amino poly(ethylene glycol)$_{750}$ mercaptoundecyl ether (PEG750-NH_2) and amino poly(ethylene glycol)$_{2000}$ mercaptoundecyl ether (PEG2000-NH_2) were used for coating experiments.

4.4.1. Non functionalized Quantum Dots

First of all, quantum dots with ligands of varying chain length were produced (see figure 15), in order to investigate the influence of hydrophilicity on the photophysical and physicochemical characteristics.

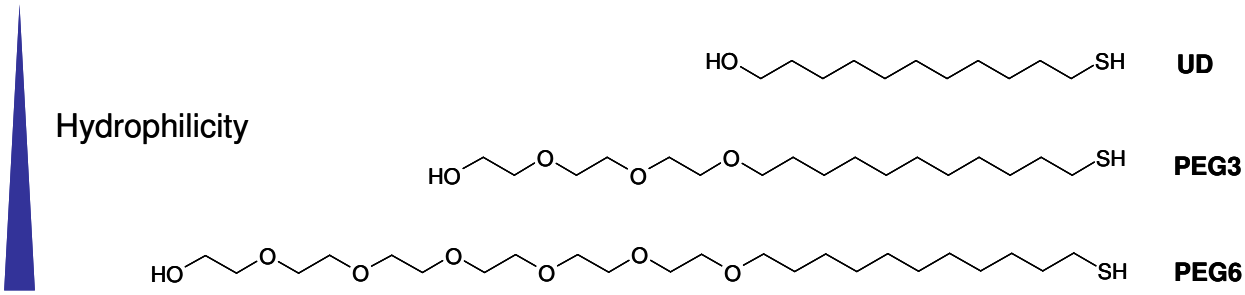

Figure 15: Ligands of increasing hydrophilicity used for the quantum dot coating

Upon coating of the quantum dots, all emission spectra exhibit a slight hypsochromic shift of the maximum. By replacing of the lipophilic phosphine ligands from synthesis with more hydrophilic molecules, the surface of the quantum dot is harmed, resulting in a loss of material. In fact, this causes a decrease in quantum dot size, and a smaller emission wavelength. This assumption is supported by the observation of the coated quantum dots taking about one week to restore their fluorescence (see figure 16). This time is presumably needed to “heal” the defects of the surface by dissolution processes [15].

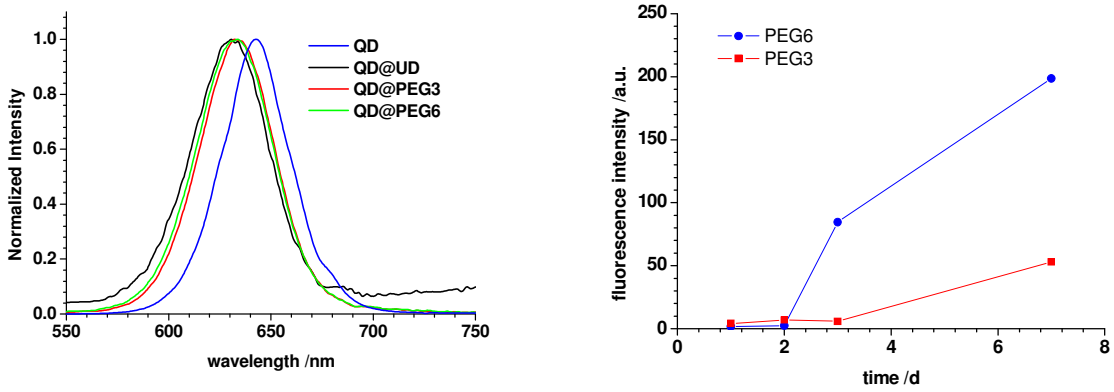

Figure 16: Emission spectra of differently coated CdTe/CdZnS quantum dots; development of fluorescence intensity over time after coating of quantum dots.

Furthermore, the quantum yields of the coated nanoparticles show highly solvent dependent quantum yields (see figure 17). Nanoparticles measured in ethanol exhibit a higher fluorescence as the respective particles measured in water. The quantum yield appears to be dependent on the lipophilicity of the surrounding solvent and, accordingly, on the degree of surface shielding achieved by the ligand. The higher the degree of protection is, the higher the quantum yields are, and the more hydrophilic the solvent is, the lower the quantum yields are. The short mercaptoundecanol ligand protects the surface less good than the molecules with the oligo(ethylene glycol) chains. Furthermore, this lipophilic ligand, with only a hydroxyl group, is not even able to render the quantum dots soluble in water.

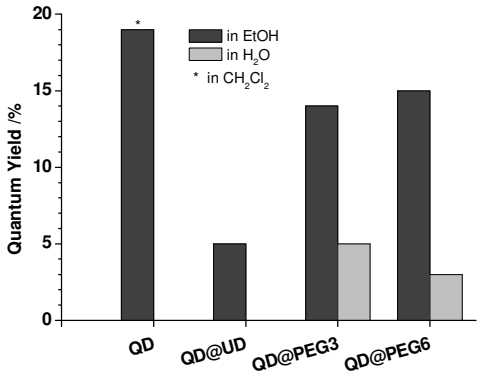

Figure 17: quantum yields of differently coated quantum dots in different solvents.

In figure 18 TEM images of quantum dots coated with the oligo(ehtlyene glycol) ligands in water are shown. There is no tendency of aggregation visible, indicated by particles lying in

one layer, not clustering. The appearance of quantum dots “sticking” together is an artifact caused by the drying process of the sample on the TEM grid.

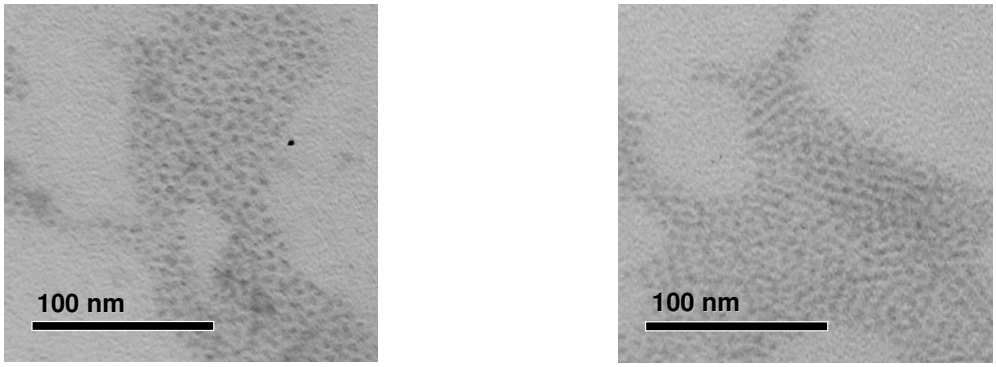

Figure 18: TEM images of oligo(ehtlyene glycol) coated quantum dots.

The PCS analysis of the particles confirms these results (see figure 19). Whereas the oligo(ehtlyene glycol) coated particles display a very small hydrodynamic diameter of under 10 nm, the mercaptoundecanol functionalized quantum dots exhibit strong aggregation in water. The small diameters of the stable nanoparticles are in the same range as the solvodynamic diameter of the non coated quantum dots, indicating that the organic shell and the associated water molecules sum up to about 4 nm only.

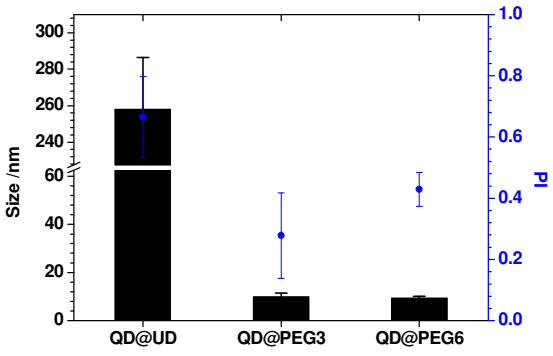

Figure 19: Hydrodynamic radii of differently coated quantum dots.

Therefore, the coating with oligo(ethylene glycol) mercaptoundecyl ethers seem to be likely to fabricate small, stable, and luminescent quantum dots. Nevertheless, these quantum dots lack the possibility of linking them to other molecules of interest in order to allow for

targeting or receptor mediated uptake in cells. To establish a reactive moiety, the introduction of amino groups was evident.

4.4.2. Amino-functionalized Quantum Dots

The amino groups on the surface were introduced by larger amino functionalized poly(ethylene glycol) mercaptoundecyl ether of two different chain lengths (750 : n = 17; 2000 : n = 45). The longer chain length compared to the non functionalized ligands was chosen to assure a good availability of the functional group on top of the particles with mixed surface, as shown in figure 20.

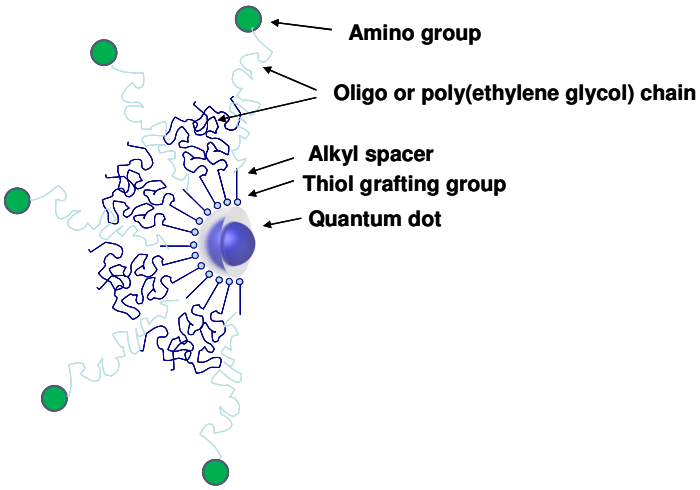

Figure 20: Schematic drawing of amino-functionalized quantum dot structure

The coating procedure was the same as for non functionalized ligands. For the “mixed” functionalized - non functionalized nanoparticles, hexa(ethylene glycol)mercaptoundeyl ether and one of the amine group carrying ligands were mixed in the molar ratios 1:0, 1:3, 2:2, 3:1, 0:1. Subsequently, the amount of amino groups per quantum dot was determined with the adapted fluorescamine assay described in chapter 3.10.6.

In figure 21, the increasing amount of amino groups per quantum dot is displayed for both amine containing ligands. If a part of the added ligands is non-functionalized, only few amino groups per nanoparticle can be detected for both types of amine containing ligands. The development of the detectable groups per quantum dot is quite similar for both types of ligand, whereas the detectable amount for the nanoparticles with mere amino ligands differs by the factor 3.3.

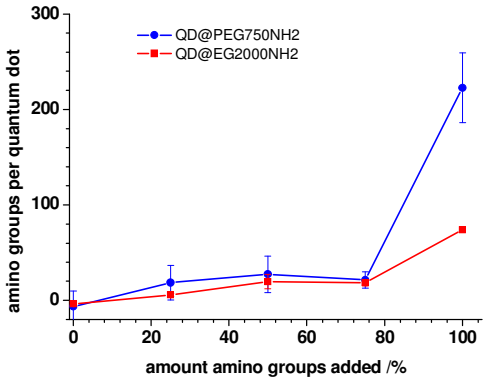

Figure 21: Detected amino groups per quantum dot with increasing amount of added amino groups.

These findings can be explained by the affinity of the different ligands to the quantum dot surface. It seems that the shorter non functionalized ligands have a higher affinity the nanoparticulate surface than the long-chained amino ligands. This may be due to the lower hydrophilicity of the shorter ligands. On the other hand, the difference for the two mere amino group carrying ligands is founded in a difference in assembling on the surface. The longer the chain is, the more space is needed and the less ligands can bind to the dot.
Therefore, the fabrication of quantum dots with different amounts of available amino groups on the surface was successful.

4.4.3. Cytotoxicological investigation of water-soluble Quantum Dots

The cytotoxicity of the quantum dots, the mere ligands and free cadmium ions was investigated using the MTT assay described in chapter 3.10.7. For the assay, freshly prepared dispersions of samples in medium with two different concentrations were used (see table 2). The chosen dilutions of the quantum dot samples are based on known cytotoxic concentrations of mercaptopropionic acid coated CdTe quantum dots (10µg/mL) and uncoated CdTe quantum dots (1µg/mL) [16]. For the ligands, the amount of the coating molecules in the corresponding quantum dot sample was used as standard. The cadmium ion concentrations conform to the known toxic cadmium amount (400 - 100 µM) [17]. Nevertheless, the investigated range of cadmium concentration also covers the theoretical amount of cadmium present in the quantum dot samples (100 – 60 µM). The slight variations in the quantum dot amounts result from the preparation procedure.

Table 2: Concentrations of quantum dot, ligand and cadmium ion samples and their respective cytotoxicity

Composition of sample	**Concentration** [a]		**Cytotoxicity /%**	
	/µmol/L	**/µg/mL**	**L929**	**CHO**
QD@PEG750NH_2	0.29 (64.9)	15.6 (7.29)	98	65
	0.03 (6.5)	1.6 (0.73)	81	44
QD@PEG2000NH_2	0.40 (87.7)	21.1 (9.82)	71	36
	0.04 (8.8)	2.1 (0.98)	52	42
QD@PEG6	0.48 (105.4)	25.3 (11.80)	86	67
	0.05 (10.5)	2.5 (1.18)	54	62
PEG750NH_2	$15.7 \cdot 10^3$	$14.1 \cdot 10^3$	69	58
	$1.6 \cdot 10^3$	$1.5 \cdot 10^3$	65	73
PEG2000NH_2	$5.7 \cdot 10^3$	$12.5 \cdot 10^3$	86	67
	570.0	$1.3 \cdot 10^3$	54	62
PEG6	$8.5 \cdot 10^3$	$5.1 \cdot 10^3$	100	98
	850.0	500	100	97
Cd^{2+}	389.0	44.7	82	70
	38.9	4.5	23	22

[a] (corresponding cadmium concentration)

The investigated quantum dot samples show, as expected, an observable cytotoxicity in the investigated concentration ranges (see figure 22). Nevertheless a significant concentration effect can be seen upon 1:10 dilution of the samples with the L929 cell line. The analysis of the control experiments with ligands and cadmium ions indicate that the bigger part of the toxic effect can be ascribed to the coating molecules. Regarding the ligands, the smaller ones (hexa(ethylene glycol)mercaptoundecyl ether and amino poly(ethylene $glycol)_{750}$mercaptoundecyl ether) are highly toxic, whereas the longer chained ligand ($poly(ethylene\ glycol)_{2000}$mercaptoundecyl ether) is less harmful. This is mainly caused by the amphiphilic nature of these molecules and the adsorbtion-desorbtion equilibrium of the ligands from the quantum dot surface. The significant lower cytotoxicity of the longer amine-containing ligand may be ascribed to the higher likeliness of these molecules to form micelles, due to their longer hydrophilic chain. This also can explain the constant toxicity upon dilution of the samples, because the ligands should be non-toxic when bound in micelles, nevertheless, always the same amount of free, toxic ligand is present in solution due to the critical micellar concentration.

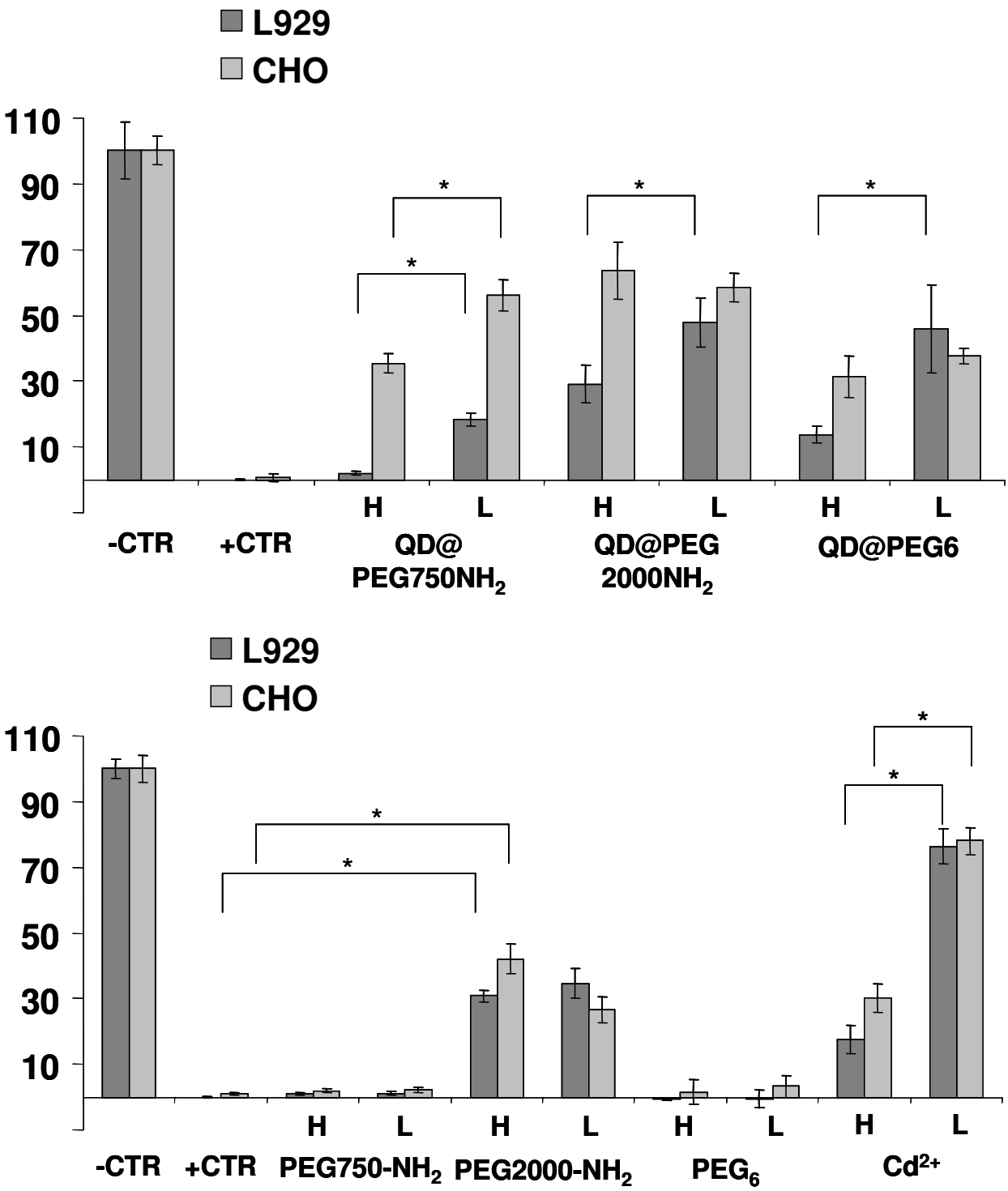

Figure 22: Viability two different cell lines under treatment with quantum dots, ligands and cadmium ions; H marks the higher, L the lower concentration; * significantly different $p < 0.01$.

The investigated cadmium concentrations display middle toxicity and a significant lowering upon dilution, implying that the free cadmium concentration in the quantum dot samples, which should be even lower, can not cause the observed cytotoxicity. Nevertheless, taking into account that the necessary quantum dot concentration for cell experiments covers a range

of 10 – 40 nM [18], which is about 10^3 lower than the concentrations used herein, it can be assumed that, within this scope, the investigated quantum dots are not cytotoxic.

4.5. References

[1] L.H. Qu, X. G. Peng, Control of photoluminescence properties of CdSe nanocrystals in growth, J. Am. Chem. Soc. 124 (2002) 2049--2055.

[2] X.H. Zhong, Y.Y. Feng, W. Knoll, M.Y. Han, Alloyed ZnxCd1-xS nanocrystals with highly narrow luminescence spectral width, J. Am. Chem. Soc. 125 (2003) 13559--13563.

[3] R.E. Bailey, S.M. Nie, Alloyed semiconductor quantum dots: tuning the optical properties without changing the particle size, J. Am. Chem. Soc. 125 (2003) 7100--7106.

[4] S. Kim, B. Fisher, H.J. Eisler, M. Bawendi, Type-II quantum dots: CdTe/CdSe(core/shell) and CdSe/ZnTe(core/shell) heterostructures, J. Am. Chem. Soc. 125 (2003) 11466--11467.

[5] B.L Wehrenberg, C.J. Wang, P. Guyot-Sionnest, Interband and intraband optical studies of PbSe colloidal quantum dots, J. Phys. Chem. B 106 (2002) 10634--10640.

[6] R. Jose, V. Biju, Y. Yamaoka, T. Nagase, Y. Makita, Y. Shinohara, Y. Baba, M. Ishikawa, Synthesis of CdTe quantum dots using a heterogeneous process at low temperature and their optical and structural properties, Appl. Phys. A 79 (2004) 1833--1838.

[7] R.D. Vengrenovich, Yu.V. Gudyma, S.V. Yarema, Ostwald ripening of quantum-dot nanostructures, Semiconductors 35(12) (2001) 1378--1382.

[8] J.-Y. Chang, S.-R.Wang, C.-H. Yang, Synthesis and characterization of CdTe/CdS and CdTe/CdSe core/shell type-II quantum dots in a noncoordinating solvent, Nanotechnol. 18 (2007) 345602--34608.

[9] Y. He, H.-T. Lu, L.-M. Sai, Y.-Y. Su, M. Hu, C.-H. Fan, W. Huang, L.-H. Wang, Microwave Synthesis of Water-Dispersed CdTe/CdS/ZnS Core-Shell-Shell Quantum Dots with Excellent Photostability and Biocompatibility, Adv. Mater. 20 (2008) 3416--3421.

[10] W.W. Yu, Y.A. Wang, X. Peng, Formation and stability of size-, shape-, and structure-controlled CdTe nanocrystals: ligand effects on monomers and nanocrystals, Chem. Mater. 15 (2003) 4300--4308.

[11] M.A. Hines, P. Guynot-Sionest, Synthesis and Characterisation of Strongly Luminescing ZnS-Capped CdSe Nanocrystals, J. Phys. Chem. 100 (1996) 468--471.

[12] I. Moreels, B. Fritzinger, J.C. Martins, Z. Hens*, Surface Chemistry of Colloidal PbSe Nanocrystals, J. Am. Chem. Soc. 130 (2008) 15081--15086.

[13] R. Knerr, B. Weiser, S. Drotleff, C. Steinem, A. Göpferich, Measuring Cell Adhesion on RGD-Modified, Self-Assembled PEG Monolayers Using the Quartz Crystal Microbalance Technique, Macromol. Biosci. 6 (10) (2006) 827--838.

[14] http://www.sigmaaldrich.com/catalog/ProductDetail.do?N4=687863|ALDRICH&N5=SEARCH_CONCAT_PNO|BRAND_KEY&F=SPEC&lang=en_US%3E

[15] R. Jose, Z. Zhelev, T. Nagase, R. Bakalova, Y. Baba, M. Ishikawa, Self-Surface Passivation of CdX (X = Se, Te) Quantum Dots, J. Nanosci. Nanotechnol. 6 (2006) 618--623.

[16] R. Hardman, A Toxicologic Review of Quantum Dots: Toxicity Depends on Physicochemical and Environmental Factors, Environ. Health Perspect. 114(2) (2006) 165--172.

[17] A.M. Derfus, W.C.W. Chan, S.N. Bhatia, Probing the cytotoxicity of semiconductor quantum dots, Nano Lett. 4 (2004) 11--18.

[18] http://probes.invitrogen.com/media/pis/mp10198.pdf

Chapter 5

Quantum Dots - Discussion

5.1. Discussion

For the synthesis of the quantum dots the applied “hot injection” route was chosen due to their numerous advantages. It is quite easy to adapt this technique to the different requirements fabricating a wide range of different quantum dots. Additionally, these nanoparticles exhibit low size dispersity and very good optical properties. On the other hand, there is one big handicap, the necessity to detach the lipophilic ligands and replace them by hydrophilic ones (see chapter 2.3.2). There are also other possibilities to synthesize quantum dots, like the synthesis in aqueous medium, providing the water-dispersability as inherent property of the nanoparticles [1,2]. Nevertheless, these strategies have their drawbacks as well. The fabrication of quantum dots in aqueous environment needs for example the use of hydrogen selenide or telluride, which is highly toxic and difficult to handle. Moreover, it is quite challenging to fabricate nanoparticles of low size dispersity and high quantum yields, and finally, the need for ligand exchange is also given for these dots. They may be water dispersable after synthesis, but to add the required biocompatible and targeting features a modification or exchange of the surface ligands is a prerequisite for application in biological environment. Summarizing, the synthesis in organic solvents seemed the best possible way the reach the goal of water-soluble, long-wavelength emitting, and functionizable quantum dots.

To initially test the quantum dot properties and the adaptability of the synthesis route, the “easiest” quantum dot system, cadmium selenide particles, was chosen. These nanoparticles with high quantum yields and emission wavelengths up to 600 nm turned out to be the optimal system for establishing the synthesis techniques and the respective analytics. Moreover, the method for shell growth could be optimized for cadmium selenide/zinc sulfide nanoparticles. Nevertheless, CdSe/ZnS quantum dots do not allow to fabricate long-wavelength emitting particles, exceeding an emission maximum of 635 nm [3]. Therefore, applying the improved synthesis setup, the switch to other more complex quantum dot systems could be achieved. The cadmium telluride based nanoparticles provide the required optical properties, and hence an optimization of this nanoparticulate system was carried out. Comparing the different cadmium telluride based systems, blank CdTe, CdTe/CdSe and CdTe/CdZnS nanoparticles, the latter offer the most promising characteristics, not only in terms of emission wavelength but also in terms of stability against oxidation under ligand exchange. The coating of the CdTe particles with a ZnS shell was only possible with admixing Cd, to alter the lattice parameters of the shell material to match the lattice parameters of the core [4]. This was necessary to achieve a satisfactory shell growth, and

therefore an adequate stability and non-toxicity. The reduced toxicity of the stabilized quantum dots is based on a protection of the CdTe core from reaction with oxygen, and therefore the suppression of reactive oxygen species and the dissolution of the toxic core components [5]. Furthermore, the ZnS shell provides a better grafting of the thiol groups bound to the water-soluble ligands and hence a better stability of the polymeric shell. The reaction parameters of the quantum dot synthesis were investigated to optimize the nanoparticles in terms of quantum yield and emission wavelength. Herein, the biggest influence on has the tellurium precursor, as well on the emission wavelength as on the quantum yield. By only changing this precursor, and keeping all other parameters constant, a tuning of the emission wavelength in the range of 50 nm is possible. This big difference in the use of the tellurium precursors derives from a considerable discrepancy in the reactivities of both investigated types. The tributylphosphine reactant is much more instable, and therefore more reactive as the trioctylphosphine based one. This fact can be easily seen in the high sensitity of TBP against ambient air oxygen compared to TOP. This difference in reactivity leads to a higher reaction speed and therefore to the formation of bigger particles, which, of course, gives higher emission wavelengths. The loss of quantum yield with the use of the TBP precursor, is, as already mentioned in chapter 4.2.4, based on the longer emission wavelength and maybe also the less perfect surface of the dots. This insufficient surface is caused, again, by the higher reaction speed. Concerning the other investigated parameters, cadmium precursor, precursor concentration and reaction scale, optimal conditions for highly luminescent nanoparticles could be found.

The importance of the ligands used for the exchange, and hence for the water-dispersability, was also proved in an experiment with coating molecules of different hydrophilicity. A clearly visible trend connecting the quantum yield and the ligand and also the solvent hydophilicity could be seen. The more lipophilic the ligands and solvents are, the higher the quantum yield is. This is, of course a not very satisfying result, keeping the application of the quantum dots in aqueous medium in mind, nevertheless it was an expected one. As already mentioned, the quantum dot surface is very susceptible to oxidation and degradation (see chapter 1.5.1), and the better this surface is protected by lipophilic ligands, the less oxygen or water may diffuse to the surface. The problem with the disintegration of the surface is not only a toxicological, but also an optical one. Under oxidation of the surface, defects can arise, acting as “traps” for the absorbed energy and opening a non radiative pathway for energy loss [6,7]. This mainly affects the quantum yield of the particles, but also can lead to a loss in maximum wavelength. A very good example for this purpose is the “recovery time” the

quantum dots need after ligand exchange. Due to the defects arising from ripping off the "native" phosphine ligands, the quantum dots loose all luminescence. It takes about one week of slow adsorption-desorption and dissolution processes to restore their optical characteristics to some degree. Nevertheless, a considerable shift of the emission wavelength can be observed. In figure 1 an overview of all synthesized quantum dot species, their stability and hydrophilicity is depicted.

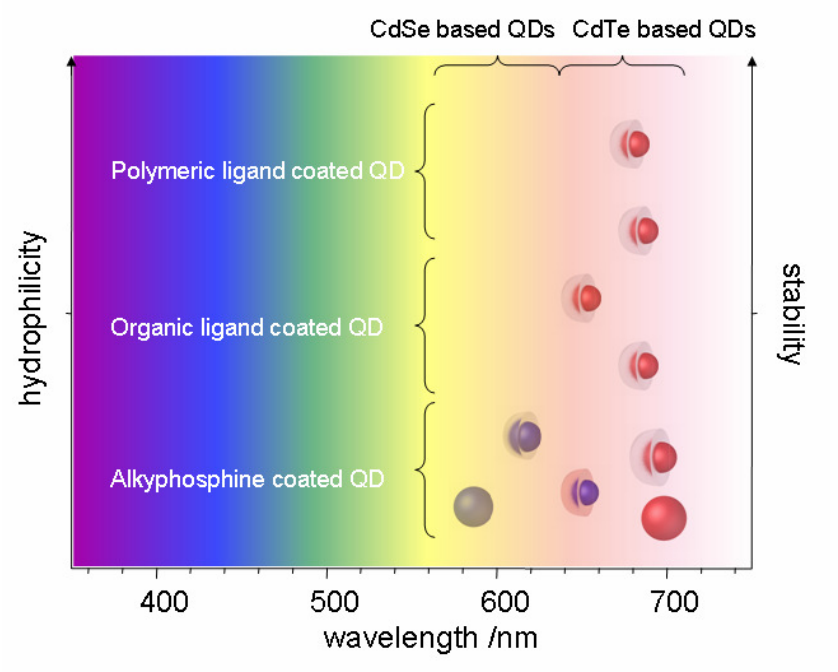

Figure 1: Overview of all synthesized quantum dot species, their stability and hydrophilicity.

To "bolster" the hydrophilic effect on the quantum dots, a ligand architecture with an alkyl spacer was chosen. This molecule part can retain a more lipophilic environment around the quantum dot surface and therefore provide a better protection. For the hydrophilic part poly(ethylene glycol) chains of various length were employed. The poly(ethylene glycol) is known for its biocompatible properties, stabilizing nanoparticles very well in biological environment and preventing unspecific adsorption of proteins [8]. Moreover, the use of short pol(ethylene glycol) ligands gave the possibility to fabricated very small, under 10 nm, stable water-dispersable semiconductor particles. To add functionality, and therefore provide the possibility to attach targeting molecules, ligands with a terminal amino group were applied. The amount of terminal amino groups was adjusted by mixing non-functionalized and functionalized ligands together. Moreover, the accessibility of the amino groups was ensured by using longer chained amino ligands. Subsequently, the amount of bound amino

functionalities, with two different amino ligands, was detected by a modified fluorescamine assay. The quantum dots show a strong absorption in the emission range of the reacted fluorescamine, and therefore the results can be falsified. Hence, the modification of this assay was necessary, to guarantee an accurate and reliable result. To avoid the problem, all samples, including the calibration samples, contained the same amount of quantum dots, adjusted by their optical density. The obtained results of the amino group amounts indicate that there are only three possibilities of polymeric surface composition, (1) no amino groups, (2) about 20 amino groups per quantum dot and (3) only amino groups on the surface. In the third case the overall amount of amino groups depends on the used polymeric ligand. This non-linear composition of the functionalized and non-functionalized ligands may be based on the different affinities of the ligands towards the surface. The “small” unfunctionalized PEG ligand seems to have a higher likeliness to bind to the surface due to its lower hydrophilicity. Hence, independent of the added concentration only a small amount of amino ligands can attach. The difference in the amount of bound amino ligands with the pure amino surface is due to the differing length, resulting in an unequal space demand of both molecules. Therefore, applying the “shorter” ligand, a higher amount of amino groups on the surface is realizable.

The tested cytotoxicity of the coated quantum dots is significant. Hence, the experiments demonstrated that this toxicity can be mainly ascribed to the coating ligands and not, as normally assumed to the cadmium ions. Nevertheless, this toxic effect occurs in a concentration range much higher than the normally applied dilutions used for cell tests [9]. Therefore, it can be supposed that the quantum dots are not toxic under normal cell culture conditions. However, they are certainly not suitable for diagnostic applications. Summarizing, the synthesis and functionalization of long wavelength emitting, stable, very small, biocompatible quantum dots was successfully achieved. Moreover, a way to adjust the amount of functionalizable groups on the surface could have been developed.

5.2. References

[1] H. Zhang, D. Wang, H. Moehwald, Ligand-selective aqueous synthesis of one-dimensional CdTe nanostructures, Angew. Chem. Int. Ed. 45(5) (2006) 748--751.

[2] N. aponik, D.V. Talapin, A.L. Rogach, K. Hoppe, E.V. Shevchenko, A. Kornowski, A. Eichmueller, H. Weller, Thiol-capping of CdTe Nanocrystals: An Alternative to Organometallic Synthetic Routes, J. Phys. Chem. B 106(29) (2002) 7177--7185.

[3] G.-W. Huang, C.-Y. Chen, K.-C. Wu, M.O. Ahmed, P.-T. Chou, One-pot synthesis and characterisation of high-quality CdSe/ZnX (X = S, Se) nanocrystals via the CdO precursor, J. Cryst. Growth. 265 (2004) 250--259.

[4] Y. He, H.-T. Lu, L.-M. Sai, Y.-Y. Su, M. Hu, C.-H. Fan, W. Huang, L.-H. wang, Microwave synthesis of Water-Dispersed CdTe/CdS/ZnS Core-Shell-Shell Quantum Dots with Excellent Photostability and Biocompatibility, Adv. Mater. 20 (2008) 3416--3421.

[5] J.M. Tsaya, X. Michalet, New Light on Quantum Dot Cytotoxicity, Chem. Biol. 12 (2005) 1159--1161.

[6] W.G.J.H.M. van Sark, P.L.T.M. Frederix, A.A. Bol, H.C. Gerritsen, A. Meijerink, Bluening, Bleaching, and Blinking of Single CdSe/ZnS quantum dots, Chem. Phys. Chem. 3 (2002) 871--879.

[7] L. Sanhel, M. Haase, H. Weller, A. Henglein, Photochemistry of Colloidal Semiconductors. 20. Surface Modification and Stability of Strong Luminescing CdS Particles, J. Am. Chem. Soc 109 (1987) 5649--5655.

[8] A.M. Smith, H. Duan, M.N. Rhyner, G. Ruan, S. Nie, A systematic examination of surface coatings an the optical and chemical properties of semiconductor quantum dots, Phys. Chem. Chem. Phys. 8 (2006) 3895--3903.

[9] http://probes.invitrogen.com/media/pis/mp10198.pdf

Chapter 6

Gadolinium Oxide Nanoparticles-Introduction and General Aspects

6.1. Introduction

For a long time, especially gadolinium ions are widely used as active cores in chelate-based MRI contrast agents [1-20]. Moreover, the gadolinium complexes also seem to be adaptive for contrast enhancement in CT imaging, due to their heavy metal nature [20-25]. They therefore open up the way to alternative detection methods in vivo. In the course of developing more potent and non-toxic MRI and CT contrast agents, the step towards inorganic nanoparticulate systems is quite short.

Nevertheless, the research on gadolinium containing inorganic particles was dominated by their application as optical materials due to their luminescent properties upon doping with different ions. They are called “phosphors” and normally used for trichromatic lamps, cathode ray tubes, or color television [26-30]. These phosphors are composed of an inert host lattice and an optically excited activator, typically a 3d or 4f electron material. Especially rare earth ions are good activators for luminescent materials, and oxide phosphors have recently gained much attention not only as optical or electronic materials, but also in the field of molecular imaging [31-34]. The unique optical properties are the reason why these nanopartilces have significant advantages over common organic dyes and genetically engineered fluorescent proteins in many biological and biomedical applications. Compared to organic dyes they offer possibilities like multiplexed imaging and long-term investigations, e.g. for cell uptake studies and in-vivo imaging [35,31]. They have been investigated as emerging materials for fluorescent labeling due to their large stokes´ shift, sharp emission peaks, long luminescence lifetime, flexibility of excitation wavelength, suitability for multiphoton excitation, luminescence up-conversion excitation and reduced photobleaching [36-40]. In rare earth doped nanophosphors, the lanthanide ions´ 4f electronic states are spatially localized to dimensions much smaller than the size of the nanoparticles and thus are not affected by the nanostructure. Therefore, the wavelength of the rare earth doped nanoparticles is independent of the particle size, in contrast to quantum dots, as the Bohr exciton radius in such materials is very small [41]. Hence, particles of user-defined size for various applications and size-independent emission wavelengths can be obtained by controlled doping of lanthanide ions into the host material. Therefore, the combination of both research areas and the application of doped gadolinium oxide nanoparticles for multimodal imaging was obvious. Moreover, these gadolinium oxide nanoparticles open up the way for combined imaging and therapy, due to their high neutron capture cross section, making neutron capture therapy possible [42-45].

These luminescent materials in nanosize crystal form have been fabricated by sol-lyophilization, emulsion, precipitation, combustion, polyol mediated and spray-pyrolytic methods.

6.2. Synthesis of doped Gadolinium Oxide Nanoparticles

As already mentioned above, the quite contrarian applications of the particles lead to a lot of different ways for synthesizing luminescent rare earth oxides. Nevertheless, most of the utilized synthesis routes are based on the same principles, as doping is achieved by mixing host and activator educts in the respective ratio. Two main techniques can be identified. One method originates from the "phosphor" fabrication, where the monodispersity, morphology, and surface characteristics of the particles are less important than the luminescent properties. High temperature annealing is used as last step, leading to particles in the size range of 60 – 300 nm. The other method was developed in the imaging research area, where high value is set on small size, dispersability in aqueous medium, and monodispersity. These are approaches using organic solvents as medium, yielding very small particles from 4 – 30 nm. Nevertheless, it has to be considered that the different syntheses methods lead to particles of not only different size, but size distribution, morphology, and surface. For that, the synthesis method should be chosen with respect to the application, as normally the "polyol" routes are utilized to produce ultra small, dispersable particles for imaging and the annealing routes to fabricate sub-micron powder "phosphors" for optical devices. However, the imaging applications can also benefit from the characteristics of particle syntheses normally used for "phosphor" production.

The majority of the organic solvent mediated syntheses are so called "polyol" routes. Herefore, the starting materials are dissolved in a high boiling medium, mostly diethylene glycol, followed by an addition of sodium hydroxide and heating to temperatures between 180-260°C for several hours. Bazzi et al. developed this "polyol" route in 2003 [46], based on syntheses for sub-micrometer transition metal particles [47]. They dissolved lanthanide chlorides in diethylene glycol at evelated temperatures, added sodium hydroxide in diethylene glycolic solution, and stirred the mixture for 4h at 180°C. As a result, sub-5 nm lanthanide oxide particles could be detected. During the following years, some changes in the mediator used [48], the temperature [49], or the heating device [50] were introduced. However, the concept of the polyol route is still the same. Nevertheless, also some other organic solvent based routes are applied, using different lanthanide precursors as reactants. One of the underlying reaction concepts is the degradation of a fatty acid based precursor in a high

boiling solvent, supported by surface-active molecules, in analogy to “hot injection” quantum dot syntheses [51].

The diversity of annealing-based synthesis routes is much bigger. There are different methods of producing gadolinium containing nanoparticles, which are converted to gadolinium oxide by means of high temperature annealing (500 – 1300 °C) under oxygen containing atmosphere. The two most prominent ways of fabricating the precursor particles are the so called “combustion” synthesis and a homogeneous precipitation method. For the combustion synthesis rare earth nitrates and a reaction partner, mostly glycine, are mixed in aqueous solution, followed by heating the mixture to dryness. After further overheating of the precipitate, combustion occurs, yielding a pure fluffy white powder of lanthanide containing nanoparticles [52-54]. The homogeneous precipitation synthesis is founded in a reaction of a reducing agent, e.g. urea, with rare earth chlorides in boiling water. The emerging nanoprecipitate can be separated by centrifugation. In both cases gadolinium oxide carbonate is formed [55]. Nevertheless there are also precipitation methods producing gadolinium hydroxide precursor particles, as the sol-lyophilisation technique [56]. Another related method for the fabrication of rare earth nanoparticles is the spray-pyrolysis or hydrogen flame pryolysis technique. It is a more technological way of preparation, where the solution of lanthanide nitrates is sprayed via carrier gas jet in a combustion chamber for pyrolysis. Afterwards the particles annealed in a high temperature furnace, carried by the combustion flow [57,40].

6.3. Physical and toxicological properties of Gadolinium Oxide Nanoparticles

Within the lanthanide containing nanoparticles, the doped gadolinium oxide has the most versatile properties. It is not only possible to fabricate luminescent nanoparticles, but they also exhibit highly MRI active properties. Moreover, the good accordance oft their X-ray absorbance edges with common tungsten tube emission make them ideal candidates for CT imaging applications. A fascinating characteristic of gadolinium is the high neutron capture cross section, giving them great potential for neutron capture therapy, perhaps even exceeding those of normally applied boron compounds.

6.3.1. Optical properties

The luminescence phenomena described for doped gadolinium oxides or oxyhalides are, as already mentioned in chapter 1.1.1, that the transitions involve a change in electronic state or

a change in electronic and vibrational states of the system. Furthermore, the luminescence emissions originate from point defects, foreign ions substituting normal constituents of the crystalline lattice. If these are present in sufficiently low concentrations, the point defects or impurity centers can be regarded as independent of each other, as shown in figure 1. It can be assumed that the ground and lower excited states of the impurity centers do not enter into compositions of the electronic band states of the host lattice. In other words, the energies of the relevant vibronic transitions for luminescence in the impurity center are below the absorption edge of the host lattice. Normally, the spectra of point defects such as transition metal ions or rare earth ions in host lattices can be best described with the crystal field approximation.

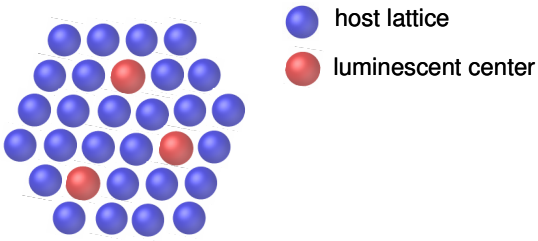

Figure 1: Luminescent centers in a host nanocrystal lattice

This theory accounts for the symmetry and strength of the crystal field imposed by the surrounding ions on the impurity ion energy levels. Nevertheless, lanthanide ions with partly filled and screened $4f^n$ orbitals are much less sensitive to the crystal field. Since the crystal field effect is so small, the energy levels of the rare earth ions resemble strongly those of the free ion [58].

This is caused by the electronic structure of the lanthanide ion, consisting, in the most common trivalent state, of a regular xenon core and a $4f^n$ shell, which is progressively filled through the series. Imperfect shielding of $4f^n$ electrons results in them being drawn inside of the $5s^25p^6$ closed shells of the xenon core, leading to the effect known as lanthanide contraction. Consequently, such $4f^n$ electrons interact weakly with any external environment, and only a small crystalline Stark splitting of 4f levels takes place. As a result, absorption and emission spectra of rare earth(III) ions appear as sharp, narrow bands, whose positions are barely dependent on the environment or crystal fields. Additionally, the f – f transitions are partially forbidden and many of them are spin forbidden, too. Therefore the optical transitions are generally very slow. The fine structure of these bands can provide important information about the crystallography and position of lanthanide ions in crystal structures [59].

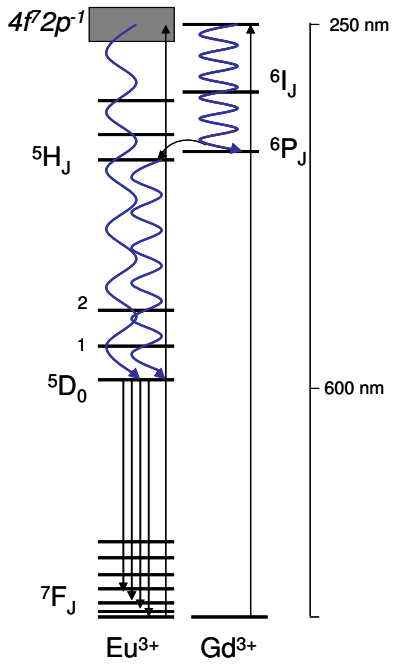

Figure 2: Jablonski diagram with energy transfer pathways of a europium doped gadolinium oxide nanocrystal.

As an example, figure x displays the typical energy transfers of the lanthanides occurring in a europium doped gadolinium oxide or oxyhalide crystal. The excitation of this system is dominated by the energy uptake of europium and gadolinium ions in the UV range, completed by energy charge transfer from the oxide ions to the lanthanide ions in the VUV region (not shown). Additionally, an energy transfer from the gadolinium excited states to the europium takes place. Therefore, the absorbance spectra of the nanocrystals are very broad, whereas the emission characteristics of these nanocrystals only depend on the $^5D_0 \rightarrow {}^7F_n$ transfers of europium [60,61], resulting in sharp emission lines. The same transfer pathways are given for terbium and erbium doped crystals [62,63].

6.3.2. MRI and CT active properties

As already mentioned, the gadolinium oxide nanoparticles provide also alternative possibilities of detection. Magnetic resonance imaging has a high spatial resolution; however, its use as a tool for the investigation of cellular molecular events in normal and pathological processes is hampered by its low sensitivity. Therefore, a relatively large local concentration of contrast agent is required to achieve the desired contrast enhancement [64]. The technique relies upon the relaxation of water protons depending on the magnetic fields, on the pulse sequence, and on the heterogeneous distribution and environment of water in an organism. Nowadays, gadolinium complexes are used in MRI examinations of patients, where the

function of the contrast agent in the human body is to reduce the ^{1}H spin relaxation times of water. This is accomplished by the paramagnetic properties of the gadolinium(III) ion, stemming from its seven unpaired electrons. The close contact of water with positive contrast agents as gadolinium-based ones, is revealed by a brightness which reflects the shortening of the longitudinal relaxation time T_1 [65].

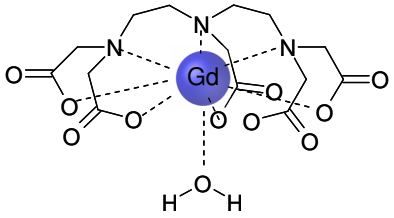

Figure 3: Structure of $[Gd(DTPA)(H_2O)]^{2-}$ (Magnevist ®)

These relaxivities depend on the number of bound water molecules. The higher the hydration number, the higher are the relaxivities. In commercially available chelate-based contrast agents, the hydration number is normally one, as displayed in figure 3. With nanoparticulate gadolinium oxide, an enhancement of the positive contrast can be induced [66]. There are two possible reasons for that fact. The first is the higher concentration of gadolinium ions at the site of interest, and the second is the higher possible hydration number of the gadolinium ions. The CT active properties of gadolinium depend, as already mentioned in chapter 1.2.2, on their heavy metal nature and the good accordance of their X-ray absorbance with the tungsten X-ray tube emission. Herein, the intensity of the filtered energy spectrum for a commonly used scanner set, for 100-140 kV, is 50-70 keV. This is actually a better match to gadolinium having a K-edge of 50 keV, than to iodine having a K-absorbance-edge of 30 keV [67]. In this energy range gadolinium attenuates photons roughly twice as well as iodine. Nevertheless, until today the use of gadolinium compounds in CT imaging is limited by the lack of concentrating enough of the gadolinium chelate used at the site of interest. Herein, the maximal approved gadolinium concentration per kilogram in humans is too low to achieve sufficient contrast in deeper tissues [68]. Therefore, the application of nanoparticles with higher on-site concentration of lanthanide ions, and additional targeting moieties is a promising way to overcome this problem.

6.3.3. Neutron capture properties

Moreover, therapy is also possible with gadolinium containing nanoparticles. The neutron capture therapy is a promising radiation therapy for treating cancers. This cancer therapy utilizes, in the case of gadolinium, γ-rays and electrons emitted by the ^{157}Gd (n, γ)^{158}Gd reaction in order to kill tumor cells, as shown in figure 4. The ^{157}Gd as a neutron capture element has some advantages over the ^{10}B, which has been widely used. First, neutron capture cross section of ^{157}Gd is 66 times larger than that of ^{10}B. Secondly, the emitted γ-rays have a long range (> 100 µm), so that considerable tumor killing effects can be expected even if gadolinium is only in the vicinity of cells. Thirdly, emitted Auger electrons may additionally lead to an efficient destruction of DNA because of their high linear energy transfer and short range [42-45].

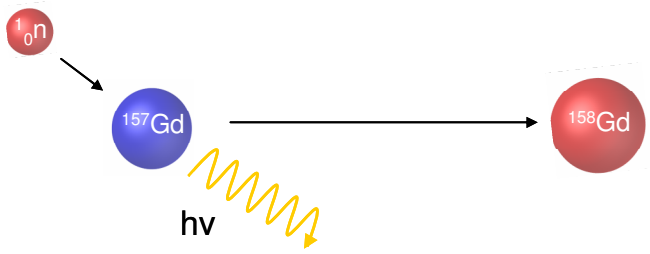

Figure 4: Scheme of neutron capture process of ^{157}Gd.

The prerequisite for Auger emission is a vacant inner shell orbital. Processes other than photoionisation, such as electron capture and internal conversion, also result in Auger electron cascades. The connection between Auger electrons and ^{157}Gd neutron capture resides in the fact that internal conversion is associated with (n,γ) reactions. In particular, the conversion electron spectrum of the ^{157}Gd(n, γ)^{158}Gd reaction yields 0.8 conversion electrons per neutron capture event. Moreover, the vacancies left by the conversion electrons would be expected to result in Auger electron emission [45]. Herein, the higher on-site concentration of gadolinium in targeted nanoparticles leads to higher γ-ray and Auger electron emissions, and therefore a better therapeutic effect [70].

6.3.4. Toxicological properties

Despite the fact that gadolinium is known as a heavy metal toxin, the intravenous gadolinium chelates, approved for human use, have been shown to be remarkably stable and safe pharmaceutical agents, due to the high stability and fast clearing of the used complexes in

vivo. On the other hand, free gadolinium ions are known to block the reticuloendothelial system, and their intravenous administration inhibits the phagocytic activity of Kuppfer cells (liver macrophages) [71]. Nevertheless, the full impact of gadolinium toxicity in vivo is not completely enlightened. Therefore, the cytotoxic effects of gadolinium nanoparticles were investigated by some research groups. They found satisfactory biocompatibility in all tested dosages for different cell lines and differently prepared and composed particles, and moreover, very low leaking of toxic gadolinium ions over time from the particles [72]. However, the toxicity depends not only on the inorganic composition, but also on the size and the coating stability of the particles, as for all nanoparticulate species. For a successful application of new nanoparticulate contrast agents, detailed toxicological investigations are necessary.

6.4. Coating of Gadolinium Oxide Nanoparticles

Reduced toxicity, water-solubility, biocompatibility, and the possibility for functionalization to enable tissue-specific targeting are requirements to be met by the nanopartilces for in vivo imaging application. This can be achieved by the molecular and biomolecular functionalization of the particles. However, different approaches have been suggested for such modifications. In contrast to quantum dots, very little “tailor-made” coatings are published for of rare earth oxides and especially gadolinium oxide. In the majority of the cases common coatings for transition metal oxides are employed, whereas the coatings developed for iron oxide nanoparticles are of biggest relevance, due to their approved application in in vivo imaging [73].

Nevertheless, different coating methods and grafting groups are utilized for lanthanide oxide nanoparticles. The most prominent coating method is embedding of the metal oxide core in a silica shell. This inorganic network is yielded by the hydrolysis – condensation of tetraethylorthosilicate and aminopropyltriethoxysilane. However, the siloxane coating is mostly applied for ultra small nanoparticles fabricated by the above mentioned “polyol route”[44-47]. The particles are stabilized with the diethylene glycol, by grafting on the surface via the hydroxyl groups [74], as well as by stabilizing the particles in dispersion due to the high viscosity of this solvent. This fact saves the often delicate step of redispersion in an appropriate medium for functionalization. Furthermore, the silica shell provides the possibility of additional modifications. One is the incorporation of organic dyes into the matrix, another is the further binding of molecules, targeting ligands, or inert coatings on the surface [10]. Nevertheless, silica coating often entails the problem of significant increase in

particle size and the limited hydrolytical stability of the shell under physiological conditions [75].

Another method for rendering the particles water-soluble is the coating with acidic groups. Here, the carboxylic and phosphonic acid functinalities are the best investigated grafting groups, giving rise to a variety of different surface coatings. These groups graft on the nanocrystals via bridging binding modes, as displayed in figure 5

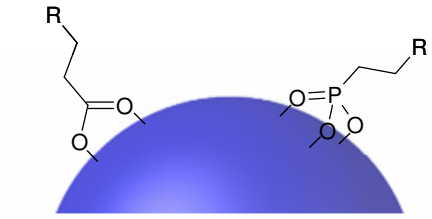

Figure 5: Binding of carboxylic acid and phosphonic acid on the nanocrystal surface.

The adsorbed molecules result in additional steric or electrostatic stabilization of the nanoparticles in aqueous medium. Some of the well known molecules applied for the solubilization of metal oxide particles are citric acid and poly(acrylic acid) [76,77]. These polyfunctional molecules (three carboxylic acids for citric acid and one per monomer for poly(acrylic acid)) form chelate complexes with the surface of the nanocrystals. However, in many examples it is not sufficient to simply add the dispersant. The redispersion is ensured by mechanical methods such as shear and high-energy ultrasound [78,79].

Table 1: Carboxylic acid containing ligands for coating of lanthanide oxide nanopaticles

Ligand	**Structure**	**Reference**
Citric acid	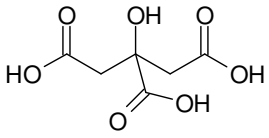	[76]
Poly(acrylic acid)	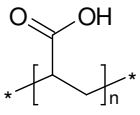	[77]
Poly(ethylene glycol) – b – poly(acrylic acid)	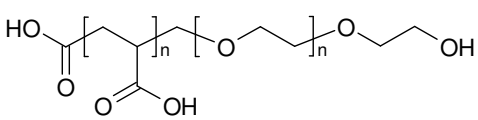	[80]

Furthermore, poly(ethylene glycol) modified poly(acrylic acid)s were employed for surface functionalization, giving a better stability over a broad pH range, preventing of undesirable protein adsorption on the surface and reducing of cross-sensitivty to salt containing solutions [80]. In table 1, examples of carboxylic acid containing ligands are displayed.

Alternatively to the carboxylic acid ligands used, also phosphonic acids are employed in many industrial applications as for corrosion inhibition or prevention of calcinations [81-83], due to their strong chelation properties. They react with a wide range of alkali and transition metals to form metal phosphonates. However, this grafting group binds strongly to different metal oxide surfaces, as zirconium oxide, yttrium oxide, or cerium oxide, forming strong M – O – P bonds. By the choice of the attached organic part of the phosphonic acid, the hydrophilic characteristics of the resulting coating can be controlled. The bonding occurs at room temperature, yielding a stable ligand film on the surface, without formation of phosphonate salts. This surface modification also can be easily be performed in water, due to the extraordinary high stability of the phosphonic acid – metal bond [84]. Another possible functionalization is, again, the use of poly(ethylene glycol) terminated phosphonates, adding some biological stealth properties and steric stabilization to the metal oxide nanoparticles [85,86]. In table 2, examples of carboxylic acid containing ligands are displayed.

Table 2: Phosphonic acid containing ligands for coating of lanthanide oxide nanoparticles

Ligand	Structure	Reference
Phenylphosphonate	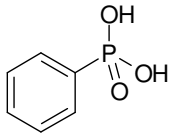	[84]
Poly(ethylene glycol) phosphonate	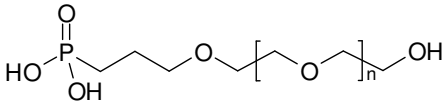	[85] [86]

6.5. Applications of Gadolinium Oxide Nanoparticles and conclusion

The small size of luminescent inorganic nanoparticles allows for replacing fluorescent molecules or complexes in analytical applications. Doped gadolinium oxide nanoparticles have the advantage of large Stokes´ shifts, narrow emission spectra, and long luminescence lifetimes. Furthermore, they do not undergo photobleaching and show no “blinking”, as for example single quantum dots, due to the fact that each particle contains a lot of luminescent

centers and is protected by the host lattice and a coating layer. In contrast to semiconductor quantum dots, their emission wavelength is independent of the particle size, and therefore, monodispersity is less crucial for a successful application, leading to lower costs in synthesis. Moreover, their optical properties are not much influenced by the surface coating used and can be tuned by controlled doping of lanthanide ions into the host material. Another advantage over, for example lanthanide complexes, is the reduced luminescence quenching by water, which normally does not acess the fluorescent centers in the crystal.

There are two fast evolving biological areas these particles are applied in. One is the development of fluorescent assays, because multiplexed techniques are essential to satisfy the growing demands of many fields in bioanalytics, including immunology, drug screening, disease diagnosis, and defense against biological threats. The ability to simultaneously measure multiple proteins in a single assay offers several advantages, such as higher throughput than single-target systems. Nevertheless, multicolor detection and analysis is often obstructed by high background signals, the requirement of complicated excitation and/or detection schemes, and challenging data collection and analysis [87,88]. Therefore, doped and functionalized gadolinium oxide nanoparticles seem to be ideal for these applications. For example, particles with double luminescence, i.e. a terbium doped gadolinium oxide core with a fluorescein functionalized siloxane shell for biological labeling was designed [10]. Moreover, immunoassays detecting phenoxybenzoic acid [89] or particles coated with IgG proteins for detection and visualization of antibodies patterned by microcontact printing [90] were developed. Another possibility to enhance the detection is the functionalization of the nanoparticles with a sensitizing dye molecule for a DNA assay [91]. As well, magnetic particles with a shell of europium doped gadolinium oxide were produced to benefit from both advantages (the luminescence and the magnetic properties) to detect DNA or IgG [92,93].

The second research area is the mono- or bi-modal in vivo imaging, utilizing the outstanding luminescent properties as well as the MRI activity of these particles. During the last few decades, MR imaging has become a well-established technique for clinical diagnosis. Today there are mainly two contrast agents used in MRI: superparamagnetic iron oxide particles (SPIOs) and paramagnetic chelates. However, gadolinium chelates have low relaxivity compared to what is theoretically possible, and SPIOs usually generate negative contrast, both leading to a loss of signal. Therefore, a particulate agent that generates positive contrast and enhanced relaxivity could be an important complement to the existing contrast agents. A combination of several detection techniques, provided by the application of bimodal

particulate agents ensures a better reliability of the recived data. As a result, benefits can be expected for small animal in vivo imaging which is a prerequisite step for clinical application but also a very useful tool for biomedical investigation.

Therefore a range of ultra small (< 5 nm) gadolinium oxide nanoparticles for MRI contrast enhancement were developed. Most of these particles, synthesized via the "polyol route" are coated with diethylene glycol [8]. Nevertheless, also apoferritin-encapsulated particles [94] and nanocrystals with glucoronic or lactobionic acid coating [7] were fabricated. All of these particles showed improved relaxivities compared to common gadolinium chelates. For bimodal detection in vivo, gadolinium oxide nanoparticles doped with terbium and coated with a poly(ethylene glycol) functionalized, dye-labelled siloxane layer were designed. It could be shown that these particles exhibit very good relaxivities and fluorescence properties in mice and rats [95].

A further utilization of the various properties of gadolinium containing nanoparticles is the combination of imaging and therapy. The potential of gadolinium neutron capture therapy has been suggested in recent years. However, the in vivo performance of commercially available gadolinium chelates is not satisfying yet, because they are eliminated rapidly from tumor tissues, even if intra tumor injected. This may probably be due to their high hydrophilicity, resulting in poor accumulation and retention in tumor. Thus, one of the keys for success in gadolinium mediated neutron capture therapy is to develop a device, which is able to maintain a sufficient gadolinium concentration in the tumor during treatment [70]. The number of gadolinium ions per nanoparticle is relatively high. As a result, the accumulation of these particles in cancerous cells is expected to have great potential for therapy. Moreover, these particles can combine fluorescence imaging, magnetic resonance imaging and therapy in one device. It was shown that the treatment of EL4 cells with the (above mentioned) doped gadolinium oxide nanoparticles coated with a poly(ethylene glycol) functionalized dye doped siloxane shell, generates a significant cytotoxic effect and leads to cell death [96]. Summarizing, doped gadolinium oxide nanoparticles exhibit great potential in various biological, analytical and medical applications and can, due to their various orthogonal properties, overcome many obstacles of other nanoparticlulate systems.

6.6. References

[1] K.N. Raymond, V.C. Pierre, Next generation, high relaxivity gadolinium MRI agents, Bioconjug. Chem. 16 (2005) 3--8.

[2] S.R. Bull, M.O. Guler, R.E. Bras, T.J. Meade, S.I. Stupp, Self-assembled conjugated to MRI contrast agents, Nano Lett. 5 (2005) 1--4.

[3] S.R. Bull, M.O. Guler, R.E. Bras, P.N. Venkatasubramanian, S.I. Stupp, T.J. Meade, Magnetic Resonance Imaging of Self-Assembled Biomaterial Scaffolds, Bioconjugate Chem. 16 (2005) 1343--1348.

[4] E.A. Anderson, S. Isaacman, D.S. Peabody, E.Y. Wang, J.W. Canary, K. Kirshenbaum, Viral Nanoparticles Donning a Paramagnetic Coat: Conjugation of MRI Contrast Agents to the MS2 Capsid, Nano Lett. 6 (2006) 1160--1164.

[5] S. Langereis, Q.G. de Lussanet, M.H.P. van Genderen, W.H. Backes, E.W. Meijer, Multivalent contrast agents based on gadolinium-diethylenetriaminepentaacetic acid-terminated poly-(propyleneimine) dendrimers for magnetic resonance imaging, Macromolecules 37 (2004) 3084--3091.

[6] V.S. Talanov, C.A.S. Regino, H. Kobayashi, M. Bernardo, P.L. Choyke, M.W. Brechbiel, Dendrimer-based nanoprobe for dual modality magnetic resonance and fluorescence imaging, Nano Lett. 6 (2006) 1459--1463.

[7] W.J.M. Mulder, G.J. Strijkers, A.W. Griffioen, L. van Bloois, G. Molema, G. Storm, G.A. Koning, K.A. Nicolay, A liposomal system for contrast-enhanced magnetic resonance imaging of molecular targets, Bioconjugate Chem. 15 (2004) 799--806.

[8] J.C. Frias, K.J. Williams, K.A. Fisher, Z.A.J. Fayad, HDL-like nanoparticles: a specific contrast agent for MRI of atherosclerotic plaques, Am. Chem. Soc. 126 (2004) 16316--16317.

[9] J. C Frias, Y. Ma, K.J. Williams, Z.A. Fayad, E.A. Fisher, Properties of a Versatile Nanoparticle Platform Contrast Agent To Image and Characterize Atherosclerotic Plaques by Magnetic Resonance Imaging, Nano Lett. 6 (2006) 2220--2224.

[10] A. Accordo, D. Tesauro, P. Roscigno, E. Gianolio, L. Paduano, G. D'Errico, C. Pedone, G. Morelli, Physicochemical Properties of Mixed Micellar Aggregates Containing CCK Peptides and Gd Complexes Designed as Tumor-Specific Contrast Agents in MRI, J. Am. Chem. Soc. 126 (2004) 3097--3107.

[11] T. N. Parac-Vogt, K. Kimpe, S. Laurent, C. Pierart, L. VanderElst, R.N. Muller, K. Binnemans, Gadolinium DTPA-monoamide complexes incorporated into mixed micelles as possible MRI contrast agents, Eur. J. Inorg. Chem. 17 (2004) 3538--3543.

[12] C.H. Reynolds, N. Annan, K. Beshah, J.H. Huber, S.H. Shaber, R.E. Lenkinski, J.A. Wortman, Gadolinium-Loaded Nanoparticles: New Contrast Agents for Magnetic Resonance Imaging, J. Am. Chem. Soc. 122 (2000) 8940--8945.

[13] J.L. Turner, D. Pan, R. Plummer, Z. Chen, A.K. Wittaker, K.L. Wooley, Synthesis of gadolinium-labeled shell-crosslinked nanoparticles for magnetic resonance imaging applications, Adv. Funct. Mater. 15 (2005) 1248--1254.

[14] C. Platas-Iglesias, L. Vander Elst, W. Zhou, R.N. Muller, C.F.G. Geraldes, T. Maschmeyer, J.A. Peters, Zeolite GdNaY nanoparticles with very high relaxivity

for application as contrast agents in magnetic resonance imaging, Chem. Eur. J. 8 (2002) 5121--5131.

[15] E. Toth, R.D. Bolskar, A. Borel, G. Gonzalez, L. Helm, A.E. Merbach, B. Sitharaman, L.J. Wilson, Water-Soluble Gadofullerenes: Toward High-Relaxivity, pH-Responsive MRI Contrast Agents, J. Am. Chem. Soc. 127 (2005) 799--805.

[16] B. Sitharaman, K.R. Kissell, K.B. Hartman, L.A. Tran, A. Baikalov, I. Rusakova, Y. Sun, H.A. Khant, S.J. Ludtke, W. Chiu, W. Laus, E. Toth, L. Helm, A.E. Merbach, L. Wilson, Superparamagnetic gadonanotubes are high-performance MRI contrast agents, J. Chem. Commun. (2005) 3915--3917.

[17] K.J. Balkus Jr., J. Shi, A Study of Suspending Agents for Gadolinium(III)-Exchanged Hectorite. An Oral Magnetic Resonance Imaging Contrast Agent, Langmuir 12 (1996) 6277--6281.

[18] Y.S. Lin, Y. Hung, J.K. Su, R. Lee, C. Chang, M.L. Lin, C.Y. Mou, Gadolinium(III)-incorporated nanosized mesoporous silica as potential magnetic resonance imaging contrast agents, J. Phys. Chem. B 108 (2004) 15608--15611.

[19] W.J.M. Mulder, R. Koole, R.J. Brandwijk, G. Storm, P.T.K. Chin, G.J. Strijkers, C. de Mello Donega, K. Nicolay, A.W. Griffioen, Quantum Dots with a Paramagnetic Coating as a Bimodal Molecular Imaging Probe, Nano Lett. 6 (2006) 1--6.

[20] G.A.F. van Tilborg, W.J.M. Mulder, P.T.K. Chin, G. Storm, C.P. Reutelingsperger, K. Nicolay, G.J. Strijkers, Annexin A5-Conjugated Quantum Dots with a Paramagnetic Lipidic Coating for the Multimodal Detection of Apoptotic Cells, Bioconjugate Chem. 17 (2006) 865--868.

[21] K. Vuu, J. Xie, M.A. McDonald, M. Bernardo, F. Hunter, Y. Zhang, K. Li, M. Bednarski, S. Guccione, Gadolinium-Rhodamine Nanoparticles for Cell Labeling and Tracking via Magnetic Resonance and Optical Imaging, Bioconjugate Chem. 16 (2005) 995--999.

[22] C. Louis, R. Bazzi, M.A. Flores, W. Zheng, K. Lebbou, O. Tellement, B. Mercier, C. Dujardin and P. Perriat, Synthesis and characterization of Gd_2O_3:Eu^{3+} phosphor nanoparticles by a sol-lyophilization technique, J. Solid State Chem. 173 (2003) 335--341.

[23] S.E. Seltzer, M.A. Davis, P.F. Judy, A. Havron, Absorption of polyenergetic X-rays in a CT scanner by elements of high atomic number: Implications for development of improved contrast agents, Invest. Radiol. 14 (1979) 400.

[24] S.E. Seltzer, Int. Congr. Ser. Excerpta Medica (EXMDA4) 561 (1981) 76.

[25] S.E. Seltzer, D.F. Adams, M.A. Davis, S.J. Hessel, A. Hurlburt, A. Havron, N.K. Hollenberg, Development of selective hepatic contrast agents for CT scanning, Invest. Radiol. 14 (1979) 356.

[26] S.E. Seltzer, D.F. Adams, M.A. Davis, S.J. Hessel, A. Havron, P.F. Judy, A.J. Pashins-Hurlburt, N.K. Hollenberg, Hepatic contrast agents for computed tomography: high atomic number particulate material. J. Comput. Assist. Tomogr. 5 (1981) 370--374.

[27] A. Havron, M.A. Davis, S.E. Seltzer, A.J. Paskins-Hurlburt, S.J. Hessel, Heavy metal particulate contrast materials for computed tomography of the liver, J. Comput. Assist. Tomogr. 4 (1980) 642--648.

[28] D.K. Williams, B. Bihari, B.M. Tissue and J.M. McHale, Preparation and Fluorescence Spectroscopy of Bulk Monoclinic Eu^{3+}:Y_2O_3 and Comparison to Eu^{3+}:Y_2O_3 Nanocrystals, J. Phys. Chem. B 102 (1998) 916--920.

[29] A.M. Pires, M.F. Santos, M.R. Davolos and E.B. Stucchi, The effect of Eu^{3+} ion doping concentration in Gd_2O_3 fine spherical particles, J. Alloys Compound. 344 (2002) 276--279.

[30] Y.C. Kang, H.S. Roh, E.J. Kim and H.D. Park, Synthesis of Nanosize Gd_2O_3:Eu Phosphor Particles with High Luminescence Efficiency under Ultraviolet Light, J. Electrochem. Soc. 150 (2003), H93--H97.

[31] K.S. Hong, R.S. Meltzer, B. Bihari, D.K. Williams and B.M. Tissue, Spectral hole burning in crystalline Eu_2O_3 and Y_2O_3 : Eu^{3+} nanoparticles, J. Lumin. 76/77 (1998) 234--237.

[32] J.-L. Bridot,A.-C. Faure, S. Laurent, C. Riviere, C. Billotey, B. Hiba, M. Janier, V. Josserand, J.-L. Coll, L. Vander Elst, R. Muller, S. Roux, P. Perriat, O. Tillement, Hybrid Gadolinium Oxide Nanoparticles: Multimodal Contrast Agents for in Vivo Imaging, J. Am. Chem. Soc. 129(16) (2007) 5076--5084.

[33] J.Y. Park, E.S. Choi, M.J. Baek, G.H. Lee, S. Woo, Y. Chang, Water-Soluble Ultra Small Paramagnetic or Superparamagnetic Metal Oxide Nanoparticles for Molecular MR Imaging, Eur. J. Inorg. Chem. (2009) 2477--2481.

[34] A. Klasson, M. Ahren, E. Hellqvist, F. Soederlind, A. Rosen, P.-O. Kaell, K. Uvdal, M. Engstroem, Positive MRI contrast enhancement in THP-1 cells with Gd_2O_3 nanoparticles, Contrast Media Mol. Imaging 3(3) (2008) 106--111.

[35] M. Nichkova, D. Dosev, S.J. Gee, B.D. Hammock, I.M. Kennedy, Multiplexed immunoassays for proteins using magnetic luminescent nanoparticles for internal calibration, Anal. Biochem. 369(1) (2007) 34--40.

[36] C. Louis, R. Bazzi, C.A. Marquette, J.-L. Bridot, S. Roux, G. Ledoux, B. Mercier, L. Blum, P. Perriat, O. Tillement, Nanosized hybrid particles with double luminescence for biological labeling, Chem. Mater. 17(7) (2005) 1673--1682.

[37] I. Hemmila, V.M. Mukkala, Time-resolution in fluorometry technologies, labels, and applications in bioanalytical assays, Crit. Rev. Clin. Lab. Sci. 38 (2001), 441--519.

[38] R.S. Niedbala, H. Feindt, K. Kardos, T. Vail, J. Burton, B. Bielska, S. Li, D. Milunic, P. Bourdelle, R. Vallejo, Detection of Analytes by Immunoassay using up-converting phosphor technology, Anal. Biochem. 293 (2001), 22--30.

[39] G.A.M. Hussein. Formation, Characterization, and Catalytic Activity of Gadolinium Oxide. Infrared Spectroscopic Studies, J. Phys. Chem. 98 (1994) 9657--9664.

[40] J. Miyawaki, M. Yudasaka, H. Imai, H. Yorimitsu, H. Isobe, E. Nakamura, S.Iijima, Synthesis of Ultrafine Gd_2O_3 Nanoparticles Inside Single-Wall Carbon Nanohorns, J. Phys. Chem. B 110 (2006) 5179--5181.

[41] E.M. Goldys, K.D. Tomsia, S. Jinjun, D. Dosev, I.M. Kennedy, S. Yatsunenko, M. Godlewski, Optical Characterization of Eu-Doped and Undoped Gd_2O_3 Nanoparticles Synthesized by the Hydrogen Flame Pyrolysis Method, J. Am. Chem. Soc. 128 (2006) 14498--14505.

[42] T. Matsumoto; Transport calculations of depth-dose distributions for gadolinium neutron capture therapy, Phys. Med. Biol. 37 (1992) 155--162.

[43] Y. Akine, N. Tokita, K. Tokuuye, M. Satoh, H. Churei, C. Le Pechoux, T. Kobayashi, K. Kanda, Suppression of rabbit VX-2 subcutaneous tumor growth by gadolinium neutron capture therapy, Japn. J. Cancer Res. 84(8) (1993) 841-843.

[44] J.L.A. Shih, R.M. Brugger, Gadolinium as a neutron capture therapy agent, Med. Phys. 19(2) (1992) 733--744.

[45] R.F. Martin, G. D'Cunha, M. Pardee, B.J. Allen, Induction of DNA double-strand breaks by gadolinium-157 neutron capture, Pigm. Cell Res. 2(4) (1989) 330--332.

[46] M. Ou, V. Mauchamp, B. Mutelet, T. Epicier, J. C. Le Bosse, S. Roux, O. Tillement, P. Perriat, Delocalization of 4f Electrons in Gadolinium Oxide on the Nanometer Scale, J. Phys. Chem. C 113 (10) (2009) 4038--4041.

[47] R. Bazzi, M. A. Flores-Gonzalez, C. Louis, K. Lebbou, C. Dujardin, A. Brenier, W. Zhang, O. Tillement, E. Bernstein, P. Perriat, Synthesis and luminescent properties of sub-5-nm lanthanide oxides nanoparticles, J. Lumin. 102-103 (2003) 445--450.

[48] F. Fievet, J.P. Laguier, B. Blin, B. Beaudoin, M. Figlarz, Homogeneous and heterogeneous nucleations in the polyol process for the preparation of micron and submicron size metal particles, Solid State Ionics 32/33 (1989), 198--205.

[49] C.-S. Park, M.-G. Kwak, S.-S. Choi, Y.-S. Song, S.-J. Hong, J.-I. Han, D.Y. Lee, Influence of Eu^{3+} doping content on photoluminescence of Gd_2O_3:Eu^{3+} phosphors prepared by liquid-phase reaction method, J Lumin 118(2) (2006) 199-204.

[50] F. Soederlind, H. Pedersen, R.M. Petoral, P.-O. Kaell, K. Uvdal, Synthesis and characterization of Gd_2O_3 nanocrystals functionalized by organic acids, J. Colloid Interf. Sci. 288 (1) (2005) 140--148.

[51] A. Müller, C.S. Karthikeyan, M. Neukam, M. Willert-Porada, Mikrowellen-unterstützte herstellung von TiO2 und Gd2O3 Nanopartkeln und deren Charakterisierung, Mat.-wiss. u. Werkstofftechn. 37(4) (2006) 298--300.

[52] G. K. Das, T.T.Y. Tan, Rare earth-doped and codoped Y_2O_3 nanomaterials as potential bioimaging probes, J. Phys. Chem. C 112(30) (2008) 11211--11217.

[53] Y. Li, G. Hong, Synthesis and luminescence properties of nanocrystalline Gd_2O_3:Eu^{3+} by combustion process, Journal of Luminescence 124(2) (2007) 297--301.

[54] L. Sun, J. Yao, C. Liu, C. Liao, C. Yan, Rare earth activated nanosized oxide phosphors: synthesis and optical properties, J. Lumin. 87-89 (2000) 447--450.

[55] J. McKittrick, L.E. Shea, C.F. Bacalski, E.J. Bosze, The influence of processing parameters on luminescent oxides produced by combustion synthesis. Displays 19(4) (1999) 169--172.

[56] Y. Li, G. Hong, Y. Zhang, Y. Yu, Red and green upconversion luminescence of Gd_2O_3:Er^{3+}, Yb^{3+} nanoparticles, J. Alloy Comp. 456(1-2) (2008) 247--250.

[57] C. Louis, R. Bazzi, M.A. Flores, W. Zheng, K. Lebbou, O. Tillement, B. Mercier, C. Dujardin, P. Perriat, Synthesis and characterization of Gd_2O_3:Eu^{3+} phosphor nanoparticles by a sol-lyophilization technique, J. Solid State Chemi. 173(2) (2003) 335--341.

[58] W. Widiyastuti, W.N. Wang, A. Purwanto, I.W. Lenggoro, K. Okuyama, A pulse combustion-spray pyrolysis process for the preparation of nano- and submicrometer-sized oxide particles. J. Am. Ceramic Soc. 90(12) (2007) 3779--3785.

[59] P. Ghosh, A. Patra, Understanding the influence of nanoenvironment on luminescence of rare-earth ions, Pramana 65(5) (2005) 901--907.

[60] G.T. Pott, W.H.J. Stork, Transition metal ion photoluminescence as a technique for the study of structures of oxidic catalysts, Catal. Rev.12(2) (1975) 163--199.

[61] M. Stavola, D.L. Dexter, Energy transfer and two-center optical transitions involving rare-earth and hydroxide ion impurities in condensed matter, Phys. Rev. B 20(5) (1979) 1867--1885.

[62] M. Buijs, A. Meyerink, G. Blasse, Energy transfer between europium$^{(3+)}$ ions in a lattice with two different crystallographic sites: europium$^{(3+)}$-doped yttrium oxide (Y_2O_3), europium$^{(3+)}$-doped gadolinium oxide (Gd_2O_3) and europium oxide (Eu_2O_3). J. Lumin. 37(1) (1987) 9--20.

[63] U. Rambabu, A. Mathur, S. Buddhudu, Fluorescence spectra of Eu^{3+} and Tb^{3+}-doped lanthanide oxychloride powder phosphors, Mater. Chem. Phys. 61(2) (1999) 156--162.

[64] U. Rambabu, K. Annapurna, T. Balaji, S. Buddhudu, Fluorescence spectra of Er^{3+} : REOCl (RE = La, Gd, Y) powder phosphors. Mater. Lett. 23(1,2,3) (1995) 143--146.

[65] M. Engström, A. Klasson, H. Pedersen, C. Vahlberg, P.-O. Käll, K. Uvdal, High proton relaxivity for gadolinium oxide nanoparticles, Mag. Res. Mater. Phy. 19(4) (2006) 180--186.

[66] E.J. Werner, A. Datta, C.J. Jocher, K.N. Raymond, High-Relaxivity MRI Contrast Agents: Where Coordination Chemistry Meets Medical Imaging, Angew. Chem. Int. Ed. 47 (2008) 8568--8580.

[67] S.P. Lin, J.J. Brown, MR contrast agents: physical and pharmacologic basics, J Magn Reson Imaging 25(5) (2007) 884--899.

[68] S.-B. Yu, A.D. Watson, Metal-Based X-ray Contrast Media, Chem. Rev. 99(9) (1999) 2353--2377.

[69] T. Albrecht, P. Dawson, Gadolinium-DTPA as X-ray contrast medium in clinical studies, Br. J. Radiol. 73(872) 878--882.

[70] F. Shikata, H. Tokumitsu, H. Ichikawa, Y. Fukumori, In vitro cellular accumulation of gadolinium incorporated into chitosan nanoparticles designed for neutron-capture therapy of cancer, Eur. J. Pharm. Biopharm. 53(1) (2002) 57--63.

[71] Y. Kubota, S.I. Takahashi, G. Patrick, Different cytotoxic response to gadolinium between mouse and rat alveolar macrophages. Toxicol. in Vitro 14(4) (2000) 309--319.

[72] I.-F. Li, C.-H. Su, H.-S. Sheu, H.-C. Chiu, Y.-W. Lo, W.-T. Lin, J.-H. Chen, C.-S. Yeh, $Gd_2O(CO_3)_2$ H_2O particles and the corresponding Gd_2O_3: Synthesis and applications of magnetic resonance contrast agents and template particles for hollow spheres and hybrid composites, Adv. Funct. Mater. 18 (2008) 766--776.

[73] Y. Zhang, N. Kohler, M. Zhang, Surface modification of superparamagnetic magnetite nanoparticles and their intracellular uptake, Biomaterials 23(7) (2002) 1553--1561.

[74] H. Pedersen, L. Ojamaee, Towards Biocompatibility of RE_2O_3 Nanocrystals - Water and Organic Molecules Chemisorbed on Gd_2O_3 and Y_2O_3 Nanocrystals Studied by Quantum-Chemical Computations, Nano Lett 6(9) (2006) 2004--2008.

[75] B.M. Silverman, K.A. Wieghaus, J. Schwartz, Comparative Properties of Siloxane vs. Phosphonate Monolayers on A Key Titanium Alloy, Langmuir 21(1) (2005) 225--228.

[76] S. Biggs, P.J. Scales, Y.-K. leong, T.W. Healy, Effects of citrate adsorption on the interactions between zirconia surfaces, J. Chem. Soc. Farad T 91(17) (1995) 2921--2928.

[77] A. Sehgal, Y. Lalatonne, J.-F. Berret, M. Morvan, Precipitation-Redispersion of Cerium Oxide Nanoparticles with Poly(acrylic acid): Toward Stable Dispersions, Langmuir 21(20) (2005) 9359--9364.

[78] S. Desset, O. Spalla, P. Lixon, B. Cabane, From Powders to Dispersions in Water: Effect of Adsorbed Molecules on the Redispersion of Alumina Particles, Langmuir 17(21) (2001) 6408--6418

[79] S. Desset, O. Spalla, B. Cabane, Redispersion of Alumina Particles in Water. Langmuir 16(26) (2000) 10495--10508.

[80] M. Kamimura, D. Miyamoto, Y. Saito, K. Soga, Y. Nagasaki, Design of Poly(ethylene glycol)/Streptavidin Coimmobilized Upconversion Nanophosphors and Their Application to Fluorescence Biolabeling, Langmuir 24(16) (2008) 8864--8870.

[81] M. Duprat, A. Shiri, Y. Derbali, N. Pebere, An electrochemical impedance approach to the corrosion inhibition of a carbon steel in neutral media, Mater. Sci. Forum 8 (1986), 267--279.

[82] M. Aguilar, N. Miralles, A.M. Sastre, Metal complexes with phosphonic and phosphinic acids, Rev. Inorg. Chem. 10(1-3) (1989) 93--119.

[83] M.D. Francis, R.G.G. Russell, H. Fleisch, Diphosphonates inhibit formation of calcium phosphate crystals in vitro and pathological calcification in vivo, Science 165(3899) (1969) 1264-1266.

[84] P.H. Mutin, G. Guerrero, A. Vioux, Organic-inorganic hybrid materials based on organophosphorus coupling molecules: from metal phosphonates to surface modification of oxides. Cr Acad. Sci II C 6(8-10) (2003) 1153--1164.

[85] L. Qi, A. Sehgal, J.-C. Castaing, J.-P. Chapel, J. Fresnais, J.-F. Berret, F. Cousin, Redispersible Hybrid Nanopowders: Cerium Oxide Nanoparticle Complexes with Phosphonated-PEG Oligomers, ACS Nano 2(5) (2008) 879--888.

[86] C.A. Traina, J. Schwartz, Surface Modification of Y_2O_3 Nanoparticles, Langmuir 23(18) (2007) 9158--9161.

[87] E.E. Swartzman, S.J. Miraglia, J. Mellentin-Michelotti, L. Evangelista, P.-M Yuan, A homogeneous and multiplexed immunoassay for high-throughput screening using fluorometric microvolume assay technology, Anal. Biochem 271(2) (1999) 143--151.

[88] E.R. Goldman, A.R. Clapp, G.P. Anderson, H.T. Uyeda, J.M. Mauro, I.L. Medintz, H. Mattoussi, Multiplexed Toxin Analysis Using Four Colors of Quantum Dot Fluororeagents, Anal. Chem 76(3) (2004) 684--688.

[89] M. Nichkova, D. Dosev, S.J. Gee, B.D. Hammock, I.M. Kennedy, Microarray Immunoassay for Phenoxybenzoic Acid Using Polymer Encapsulated Eu:Gd_2O_3 Nanoparticles as Fluorescent Labels, Anal. Chem. 77(21) (2005) 6864--6873.

[90] M. Nichkova, D. Dosev, R. Perron, S.J. Gee, B.D. Hammock, I.M. Kennedy, Eu^{3+}-doped Gd_2O_3 nanoparticles as reporters for optical detection and visualization of antibodies patterned by microcontact printing, Anal Bioanal Chem 384(3) (2006) 631--637.

[91] Y. Chen, Y. Chi, H. Wen, Z. Lu, Sensitized Luminescent Terbium Nanoparticles: Preparation and Time-Resolved Fluorescence Assay for DNA, Anal Chem 79(3) (2007) 960--965.

[92] M. Nichkova, D. Dosev, S.J. Gee, B.D. Hammock, I.M. Kennedy, Multiplexed immunoassays for proteins using magnetic luminescent nanoparticles for internal calibration, Anal Biochem 369(1) (2007) 34--40.

[93] A. Son, D. Dosev, M. Nichkova, Z. Ma, I.M. Kennedy, K.M. Scow, K.R. Hristova, Quantitative DNA hybridization in solution using magnetic/luminescent core-shell nanoparticles, Anal. Biochem 370(2) (2007) 186-194.

[94] Sanchez, Purificacion; Valero, Elsa; Galvez, Natividad; Dominguez-Vera, Jose M.; Marinone, Massimo; Poletti, Giulio; Corti, Maurizio; Lascialfari, Alessandro. MRI relaxation properties of water-soluble apoferritin-encapsulated gadolinium oxide-hydroxide nanoparticles. Dalton Transactions (2009), (5), 800-804.

[95] M.-A. Fortin, R.M. Petoral Jr., F. Soederlind, A. Klasson, M. Engstroem, T. Veres, P.-O. Kaell, K. Uvdal, Polythylene glycol-covered ultra-small Gd_2O_3 nanoparticles for positive contrast at 1.5 T magnetic resonance clinical scanning. Nanotechnol. 18(39) (2007) 395501/1--395501/9.

[96] J.-L. Bridot, D. Dayde, C. Riviere, C. Mandon, C. Billotey, S. Lerondel, R. Sabattier, G. Cartron, A. Le Pape, G. Blondiaux, M. Janier, P. Perriat, S. Roux, O. Tillement, Hybrid gadolinium oxide nanoparticles combining imaging and therapy, J. Mater Chem 19(16) (2009) 2328--2335.

Chapter 7

Gadolinium Oxide Nanoparticles - Materials and Methods

Materials

7.1. Particles synthesis

The gadolinium chloride hexahydrate (+99.9%), gadolinium nitrate hydrate (+99.9%), erbium chloride hexahydrate (+99.9%), terbium chloride hexahydrate (+99.9%), europium chloride hexahydrate (+99.9%), diethlyene glycol (ultra), (3-aminopropyl)triethoxysilane (98%), triethylamine (p.a.), polyacrylic acid sodium salt, etidronic acid (purum), was obtained from Sigma-Aldrich (Sigma-Aldrich Chemie GmbH, Munich, Germany). The hexa(ethylene glycol) bisphosphonate was synthesized by Surfactis Technologies (Surfactis Technologies SAS, Angers, France). Sodium hydroxide (p.a.), dimethlysulfoxide (p.a), citric acid (p.a.), glycin (p.a.) and urea (p.a.) were provided from Merck (Merck KGaA, Darmstadt, Germany).

7.2. Cytotoxicity test

Fetal Bovine Serum (FBS) was purchased from Biochrom (Biochrom KG, Berlin, Germany), 0.25% Trypsin-EDTA was obtained from Invitrogen (Invitrogen GmbH, Karlsruhe, Germany). 3-[4,5-Dimethylthiazol-2-yl]-2,5- diphenyltetrazolium bromide (MTT) was purchased from AppliChem (AppliChem GmbH, Darmstadt, Germany). Dulbecco´s modified Eagle´s medium (EMEM) and nutrient mixture F-12 HAM were obtained from Sigma-Aldrich (Sigma-Aldrich Chemie GmbH, Munich, Germany). Titriplex® III (ethylendinitrilotetraacetic acid disodium salt dihydrate) (p.a.) was obtained from Merck (Merck KGaA, Darmstadt, Germany).

Methods

7.3. DEG-mediated Synthesis of Gadolinium Oxide particles

7.3.1. Synthesis of sub-10 nm Gadolinium Oxide particles

For the synthesis of sub-5 nm gadolinium oxide particles, 2.0 mmol gadolinium chloride (741 mg, 1eq) was heated up to 60 °C in 10 mL diethylene glycol for half a hour, subsequently, the mixture was heated to 140 °C and held for one hour, until all gadolinium salt has dissolved. Then 500 µL of 3 N sodium hydroxide solution (1.5 mmol, 0.75eq) was added, and the reaction temperature was raised to 180 °C and held for 4 hours (see figure 1). The clear solution was cooled to room temperature and dialysed 3 days against diethylene glycol for purification [1].

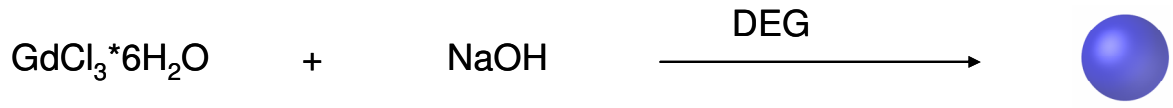

Figure 1: Reaction scheme of sub-10 nm gadolinium oxide nanoparticle formation.

7.3.2. Coating of sub-10nm Gadolinium Oxide particles with Silica

The gadolinium oxide particles synthesized according 2.1.1 were coated with a silica shell using silicate precursor for encapsulation. First, 0.075 mmol (3-aminopropyl)triethoxysilane (17.5 mL) were mixed with 500 µL dimethlysulfoxide, 2.5 mL of the purified gadoliniumoxide dispersion and 7.5 mL diethylene glycol, and stirred for 20 min at 40 °C. Afterwards, 4.5 µL 0.1 M triethylamine solution (0.45 mmol) were added and the reaction was stirred for one hour. Thereafter, 0.38 mmol (3-aminoproply)triethylsilane (88.5 µL) and 0.3 mmol tetraethyl orthosilicate (66.8 µL) were mixed with the dispersion and all was stirred again for 1 hour °C. At last, 2.3 mmol water were added and the reaction mixture was stirred for 48 hours (see figure 2) [2].

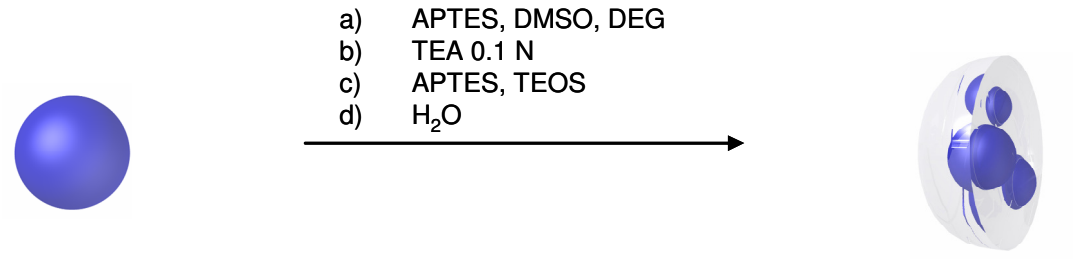

Figure 2: Reaction scheme of silica coating of sub-10 nm gadolinium oxide nanoparticles.

The purification was archived via three days dialysis against diethylene glycol followed by 3 days dialysis against water.

7.3.3. Synthesis and coating of Gadolinium Oxide Nanoparticles

The gadoliunium hydroxide particles were prepared via a synthesis route related to the sub-5nm gadolinium oxide particles. For this synthesis 1.0 mmol gadolinium chloride (371 mg, 1eq) was dissolved in 15 mL diethylene glycol by heating up the dispersion to 160 °C for 10 min. Subsequently, 500 µL of a 3 N sodiumhydroxide solution (1.5 mmol, 1.5eq) was added, the temperature of the reaction mixture was raised to 210 °C and held for half an hour. At the same time, the ligand for particle coating was dissolved. For citric acid were 1.0 mmol (211

mg, 1eq), for polyacrylic acid 0.025 mmol (M_w=2000, 500mg, 0.025eq) and for hexa(ethylene glycol) bisphosphonate 0.5 mmol (386mg, 0.5eq) dissolved in 5 mL diethylene glycol and 500 µL 3N sodium hydroxide solution (1.5 mmol, 1.5 eq); etidronic acid (1.0 mmol, 224 mg, 1eq) was dissolved in 500 µL 3N sodium hydroxide solution (1.5 mmol, 1.5 eq). The respective ligand solution was added to the particle dispersion at 210 °C and the reaction mixture was cooled to room temperature (see figure 3) [3].

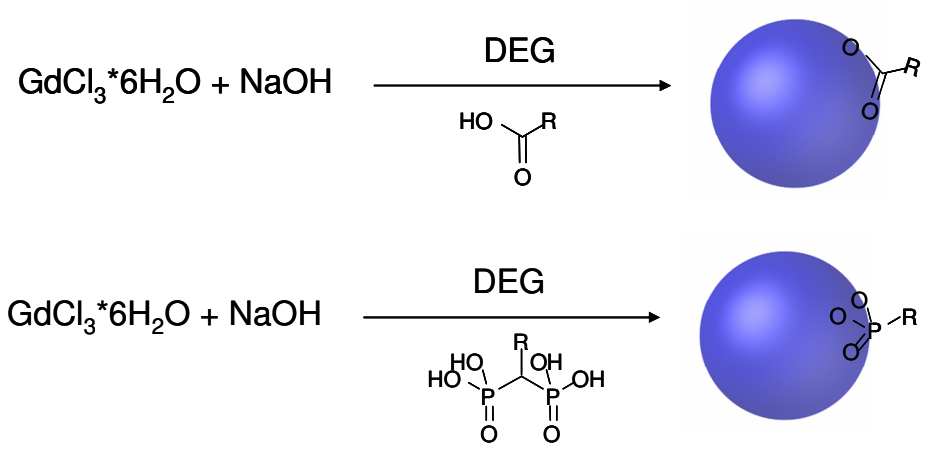

Figure 3: Reaction scheme of gadolinium oxide nanoparticle formation and subsequent coating with carboxylic and phosphonic acid derivatives.

For purification of the particles, methanol was added to the reaction mixture for precipitation of the gadolinium hydroxide particles. Subsequently, the particles were centrifuged (8000 g, 10 min, 18 °C) and the supernatant was removed. The particles were again dispersed in methanol, centrifuged (12000 g, 15 min, 18 °C) and the supernatant was removed. At last, the particles were dispersed in water or buffer solution.

After the purification of the particles, the aqueous dispersion was high pressure homogenizied with a Gaulin High Pressure Homogenizer three times at 1000 bar.

7.4. Synthesis of doped Gadolinium Oxide Nanoparticles

The doping of the particles was obtained by replacement of a given percentage of the gadolinium salt with either erbium chloride, terbium chloride or europium chloride. This results in different emission colors of the gadolinium oxide nanopaticles.

7.4.1. Combustion synthesis

The gadolinium oxide nanoparticles were synthesized via an ignition of the educts. 1.0 mmol gadolinium nitrate (451 mg, 1eq) and 1.0 mmol glycin (75 mg, 1eq) were dissolved in 10 mL of water. Afterwards, the water was evaporated under heat until a solid precipitate results, this precipitate was heated up further until combustion. The so obtained nanopaticles were collected and put in a muffle furnace at 450 °C for 4 h (see figure 4). No further purification was needed [4-6].

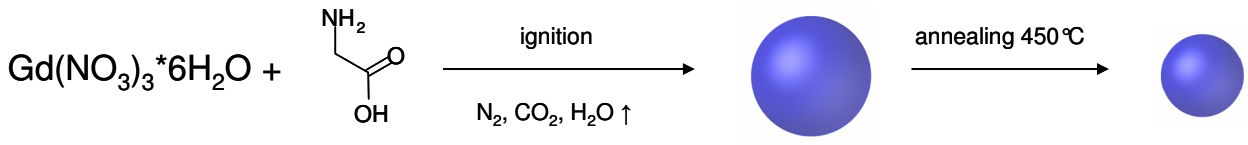

Figure 4: Reaction scheme of combustion synthesis.

7.4.2. Precipitation synthesis

For the synthesis of gadolinium oxide nanoparticles via the precipitation method, 1.0 mmol gadolinium chloride (371 mg, 1eq) and 1.0 mmol urea (61 mg, 1eq) were dissolved in 40 mL of water. This solution was refluxed for one hour, resulting in a nanoprecipitaion of gadolinium oxide.

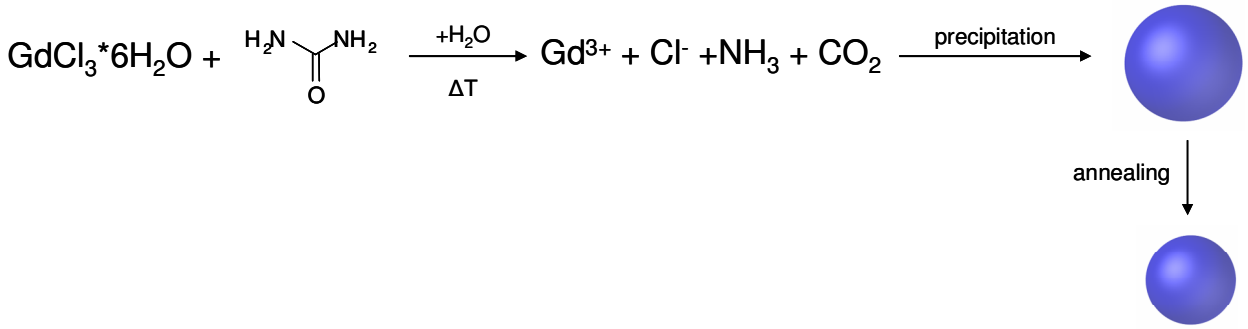

Figure 5: Reaction scheme of precipitation synthesis.

The precipitate was collected via centrifugation (15000 g, 30 min, 18 °C), and heated up in a muffle furnace to dedicated temperatures (450 °C for undoped, 200 °C for terbium doped, 700 °C for erbium and europium doped particles) (see figure 5). The obtained nanoparticulate powder needed no further purification [7].

7.4.3. Coating of particles

The particles obtained via the synthesis in 2.2.2 can be coated with hexa(ethylene glycol) bisphosphonate utilizing a procedure related with the nanoparticles synthesis in 7.2.3. 1.0 mmol of the nanoparticulate powder (362 mg, 1eq) was dispersed in 20 mL diethylene glycol and heated up to 210 °C, subsequently, a solution containing 0.75 mmol hexa(ethylene glycol) bisphosphonate (363 mg, 0.75eq) in 5 mL diethylene glycol was added. The dispersion was cooled to room temperature and purified.

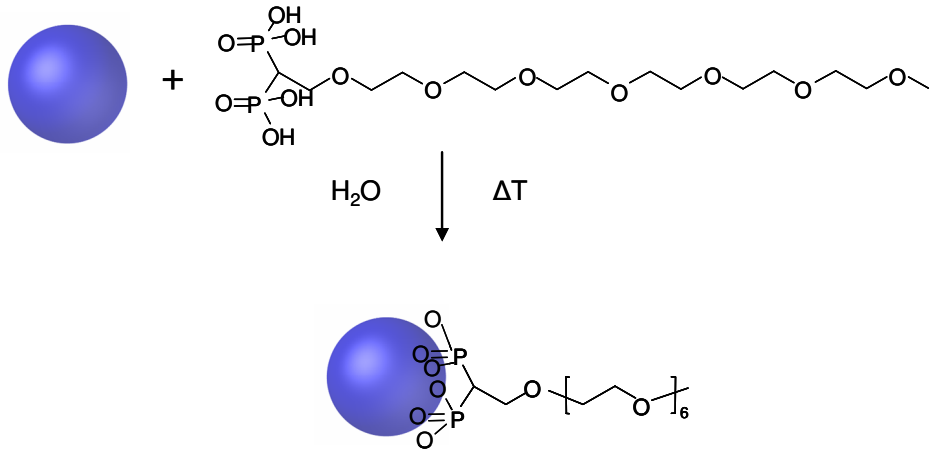

Figure 6: Reaction scheme of gadolinium oxide coating.

For the purification the nanoparicles were precipitated with methanol and centrifuged (15000 g, 10 min, 18 °C), the supernatant was removed and the procedure was repeated once. Then, the purified particles were dispersed in water (see figure 6).

7.5. Analysis of particles

7.5.1. Spectroscopic analysis

The absorbance spectra of the gadolinium oxide particles were measured with a UVIKON 941 two-beam spectrophotometer (Kontron Instruments). The excitation and emission spectra were measured with a Perkin-Elmer LS 55 (Perkin-Elmer) equipped with a R928 red-sensitive photomultiplier and the FL WinLab V4.00.03 software. For all measurements in aqueous solution 1 cm quartz cuvettes were used, for measurements of powders a self-made specimen holder for powders with a quartz pane was applied.

7.5.2. Size and zeta potential analysis with PCS

The hydrodynamic diameter and the zeta potential of the particles were measured with a ZetaSizer 3000 A (Malvern Insruments Inc.) photon correlation spectrometer (PCS). Purified water or buffer was used as solvent for the nanaoparticles. Furthermore, all samples were filtrated through a 1.0 µm glass fiber syringe filter. All measurements were carried out at 20 °C.

7.5.3. Morphological analysis with TEM

For the morphological analysis a Zeiss EM 10 C/CR (Carl Zeiss AG) transmission electron microscope (TEM) with 60 kV operating voltage was used. The samples were prepared on 3.05 mm formvar/carbon coated copper grids (300 mesh). The water-soluble particles were spreaded on the grids and dried using a vacuum pump.

7.5.4. Determination of gadolinium content

The samples for the gadolinium content determination were prepared by dissolving a dispersion of gadolinium nanopartilces in 0.5 µL concentrated nitric acid and diluting was up to 10 mL in a volumetic flask.

The content of the samples containing no bisphosphonate contamination were determined with a Jobin Yvon 70 P (S+S) (Horiba Yovin Ivon GmbH) inductively coupled plasma optical emission spectrometer (ICP-OES) in a sequential analysis mode. The standard stock solution was composed of 1000 ppm gadolinium chloride in 3% nitric acid.

The samples containing bisphosphonates were analyzed by ICP-MS according to DIN EN ISO 17294-2 (E29) (UST) at the Umweltanalytische Labor Dr. Mehrer.

7.5.5. Analysis of crystal structure with P-XRD

The crystal structure analysis was achieved by powder x-ray diffraction of the dry, grinded samples in a flat specimen holder. The measurement was carried out on a Stadip STOE powder diffractometer with Cu K_α radiation (λ = 1.54056 Å) and a germanium monochomator. The samples were analyzed in a transmission geometry and a PS detector. The data were evaluated with the WinXPow 1.08 software.

7.5.6. Determination of radio-opaqueness with CT Imaging

For the determination of the radio-opaqueness of the gadolinium oxide nanoparticles a 1.5 T Siemens Sensation 16 CT scanner (Siemens AG) computer tomograph (CT) was used. The data was evaluated with the SIENET sky software. The gadolinium oxide samples were prepared by dispersing coated or uncoated gadolinium oxide nanoparticles in water. The dispersions were transferred to 2 mL eppendorf cups and put into a cryo box. This cryo box was then placed in the computer tomtograph and the data were recorded. The evaluation of the CT images was done with the SINET Sky – DICOM CD-viewer and all HU values were calculated as average of HU values of 10 different layers throughout the whole cup.

7.5.7. Cytotoxicity test

The used cell lines for the cytotoxicity test were L929 and CHO cells. The L929 cells were grown in T-75 cell culture flasks containing 20 mL EMEM supplemented with 10% FBS. The CHO cells were grown in T-75 cell culture flasks containing 20 mL of HAM supplemented with 10% FBS. Both cell lines were cultured at standard cell culture conditions (37°C, 95%) relative humidity, and 5% CO_2. The growth medium was changed every third day. The cells were harvested at 90% confluence by exposure to a 0.25% trypsin-EDTA solution (3 mL/flask) and resuspended at a densitity of 50000 cells/mL for the MTT assay.
This colorimetric assay was based on the conversion of yellow, water-soluble MTT [3-(4,5-dimethylthiazol-2-yl)-2,5-diphenyl tetrazolium bromide] by the mitochondrial dehydrogenases of viable cells, to the purple, water insoluble, end-product formazan.

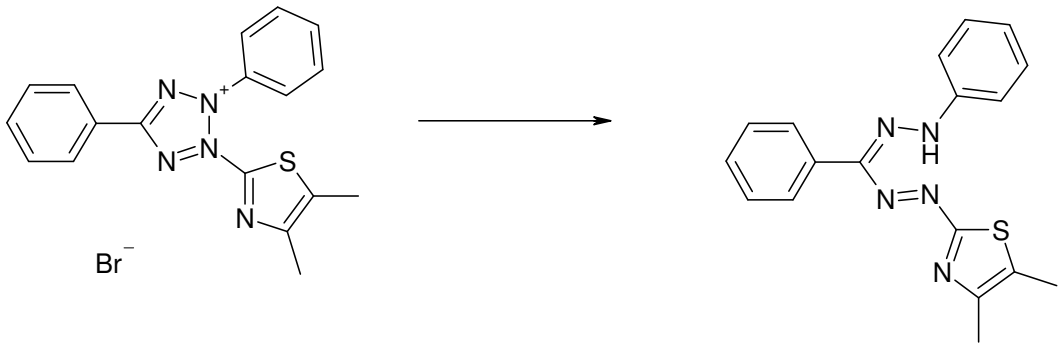

Figure 7: Reaction scheme of MTT to MTT formazan.

All MTT assays were carried out in 96-well plates. The cells were seeded at a density of 10,000 cells/well and solution of MTT was prepared by dissolving 2.5 MTT/mL in sterile

PBS. The L929 cells were grown for 24 h in 200 µL EMEM supplemented with 10% FBS at standard cell culture conditions; the CHO cells were grown for 24 h in 200 µL HAM supplemented with 10% FBS at standard cell culture conditions. 200 µL of nanoparticle dispersions of different concentrations in the respective medium containing 10% FBS were added to the cells and incubated for 4h at standard cell culture conditions. After incubation the nanoparticles were removed and the cells were washed with 200 µL sterile PBS. The MTT stock solution was diluted to a concentration of 0.625 mg/mL with the according medium, added to the cells and incubated for 4 h at standard cell culture conditions. Afterwards, the MTT solution was removed carefully and finally, 200 µL of 10% SDS in PBS were added to each well for further 24 h [8-10]. The absorbance of each well was determined on a TitertekPlus Microplate Reader (Friedrich S. Bartolomey) with 550 nm as test wavelength and 630 nm as reference wavelength.

7.6. References

[1] R. Bazzi, M. A. Flores-Gonzalez, C. Louis, K. Lebbou, C. Dujardin, A. Brenier, W. Zhang, O. Tillement, E. Bernstein, P. Perriat, Synthesis and luminescent properties of sub-5-nm lanthanide oxides nanoparticles, J. Lumin. 102-103 (2003) 445--450.

[2] C. Louis, R. Bazzi, C.A. Marquette, J.-L. Bridot, S. Roux, G. Ledoux, B. Mercier, L. Blum, P. Perriat, O. Tillement, Nanosized hybrid particles with double luminescence for biological labeling, Chem. Mater. 17(7) (2005) 1673--1682

[3] F. Soederlind, H. Pedersen, R.M. Petoral, P.-O. Kaell, K. Uvdal, Synthesis and characterization of Gd2O3 nanocrystals functionalized by organic acids, J. Colloid Interf. Sci. 288 (1) (2005) 140--148

[4] Y. Li, G. Hong, Synthesis and luminescence properties of nanocrystalline Gd2O3:Eu3+ by combustion process, Journal of Luminescence 124(2) (2007) 297--301.

[5] L. Sun, J. Yao, C. Liu, C. Liao, C. Yan, Rare earth activated nanosized oxide phosphors: synthesis and optical properties, J. Lumin. 87-89 (2000) 447--450.

[6] J. McKittrick, L.E. Shea, C.F. Bacalski, E.J. Bosze, The influence of processing parameters on luminescent oxides produced by combustion synthesis. Displays 19(4) (1999) 169--172.

[7] Y. Li, G. Hong, Y. Zhang, Y. Yu, Red and green upconversion luminescence of Gd2O3:Er3+, Yb3+ nanoparticles, J. Alloy Comp. 456(1-2) (2008) 247--250.

[8] T. Mosmann, Rapid Colorimetric Assay for Cellular Growth and Survival: Application to Proliferation and Cytotoxicity Assays, J. lmmunol. Methods 65 (1983) 55--63.

[9] J.A Plumb, R. Milroy, S.B Kaye, Effects of the pH Dependence of 3-[4,5 Dimethylthiazol-2-yl]-2,5-diphenyltetrazolium bromide – Formazan. Absorption on Chemosensitivity Determined by a Novel Tetrazolium-based Assay. Cancer Res. 49 (1989) 4435--4440.

[10] M. Shiau, H. Chiou, Y. Lee, T. Kuo, Y. Chang, Establishment of a consistent L929 bioassay system for TNF- α quantitation to evaluate the effect of lipopolysaccharide, phytomitogens and cytodifferentiation agents on cytotoxicity of TNF-α secreted by adherent human mononuclear cells. Mediat. Inflamm. 10 (2001) 199--208.

Chapter 8

Gadolinium Oxide Nanoparticles - Results

Synthesis of Gadolinium Oxide Nanoparticles

8.1. DEG mediated synthesis of Gadolinium Oxide Nanoparticles

As already mentioned in chapter 6.2, the "polyol" route is a very comfortable way for synthesizing ultra small, dispersable nanoparticles. Nevertheless, it also can yield particles of bigger sizes, depending on the chosen reaction parameters. Herein, nanocrystals with two different were synthesized and differently coated.

8.1.1. Synthesis and coating of sub-10 nm Gadolinium Oxide particles

Particles of about 10 nm diameter were produced adding a sub-stoichiometric amount of sodium hydroxide to the dissolved gadolinium chloride in diethylene glycol. The resulting reaction mixture was heated for 4 h to 180°C to achieve particle formation as described in chapter 7.3.1. In figure 1 the results of PCS and TEM analysis are shown. The measured solvatodynamic diameter of the nanoparticles in diethylene glycol is about 10 nm, which is in good accordance to the TEM results.

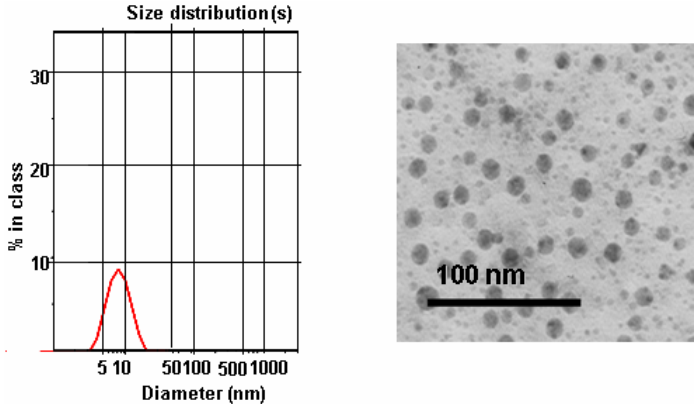

Figure 1: PCS measurement and TEM image of Gd_2O_3 nanoparticles after synthesis in diehtylene glycol

Nevertheless, the nanocrystals obtained are still dispersed in diethylene glycol, always causing problems with size measurement due to the high viscosity of the solvent. Furthermore, the bare gadolinium oxide nanoparticles are not dispersable in aqueous medium without subsequent aggregation and degradation. To render the particles water soluble, a coating with a stable, protecting, and hydrophilic shell is mandatory. A very common way of stabilizing nanoparticles is the incorporation into an additional silica shell. This silica shell is grown on the surface of the particles in a Stöber-like process [1], using the gadolinium oxide

nanoparticles as condensation nuclei. In figure 2 the PCS and TEM picture of as synthesized silica coated gadolinium oxide nanoparticles are displayed.

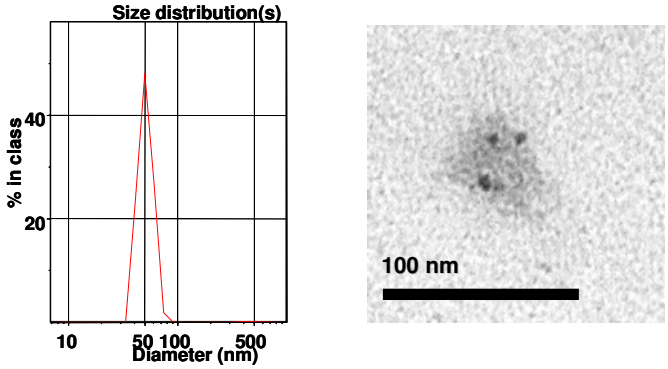

Figure 2: PCS measurement and TEM image of Gd_2O_3 nanoparticles in a silica shell

The core/shell gadolinium oxide/silica particles have an overall hydrodynamic diameter of about 50 nm, which is also visible in the TEM images. Nevertheless, more than one gadolinium oxide particle seems to be incorporated in the silica shell. Furthermore, not all nanocrystals are embedded and a lot of bare silica particles were formed, causing problems with sufficient purification of the particle dispersions. As a result of these purification problems, a thixotropic gel was formed after transferring the particles into aqueous solution, indicating a swelling of the silica shells and consequently an incomplete separation of the bare silica particles [2]. Therefore, another variation of the "polyol" route with an integrated coating step was performed, yielding "bigger" particles. Additionally, other coating possibilities were also investigated, to avoid the problems with the silica shell. Therefore, four different ligands with either carboxy- or phosphonic acid groups were chosen [3-7].

8.1.2. Synthesis and coating of Gadolinium Oxide Nanoparticles

The synthesis of "bigger" (~ 50-80 nm) gadolinium oxide nanoparticles was achieved by adding a higher amount of sodium hydroxide to the reaction mixture. Furthermore, the temperature was raised to 210°C for the reaction of the starting materials, as described in chapter 7.3.3. The formed particles can be coated in the same reaction vessel by only adding the dissolved ligand solution to the hot reaction mixture.

Influencing the size of coated Gadolinium Oxide particles

In figure 3 a TEM image of the obtained non-coated gadolinium oxide nanoparticles is displayed. The particles are in the size range between 20 and 80 nm with an almost spherical morphology. Nevertheless, an agglomeration of the particles is observable upon coating. Therefore, an additional high pressure homogenization step was necessary in order to destroy the particle aggregates and achieve a homogenous particle distribution. The working principle of high pressure homogenization is the destruction of aggregates by pressing particles with high pressure in a dispersion medium through a tight nozzle [8]. Due to the construction of the opening cavitation can occur, which breaks up the aggregates. This homogenization principle depends on the viscosity and boiling point of the solvent. The higher the boiling point of the solvent is, the higher the applied pressure has to be. Hence, the particle aggregates, which are held together by electrostatic and steric interactions of the ligands, should be destroyed. Nevertheless, the gadolinium oxide nanoparticles itself are not broken up due to their high solidity.

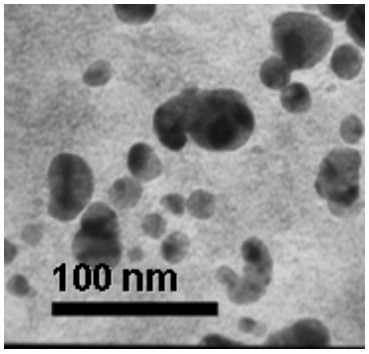

Figure 3: TEM image of uncoated Gd_2O_3 nanoparticles

In figure 4 three diagrams are displayed, showing the development of differently homogenized particle dispersions with repeated treatment. The influence of homogenization pressure and solvents were tested. The first diagram illustrates the particle development in diethylene glycol as solvent with a homogenization pressure of 500 bar. In this experiment, the unpurified particle dispersion after synthesis was used. However, it is obvious that homogenization in this solvent is not appropriate, maybe due to the high viscosity and boiling point, making cavitation impossible. The aggregate destruction in water was achieved after purification of the samples. Herein, pressures of 500 and 1000 bar were used. The diagrams visualize the good homogenization of etidronic acid, PEG-bisphosphonate and poly(acrylic acid) coated particles with both pressures. A lowering of the hydrodynamic diameters with

repeated homogenization steps is observable and all finally obtained diameters of the particles are below 200 nm. Moreover, the polydispersity indices of these homogenized particle dispersions drop with on going processing. For the etidronic acid coated particles they are below 0.1, indicating monodispersity. On the other hand, the citric acid coated particles show strong flocculation after homogenization. Breaking up the aggregates may influence their surface charge disadvantageously. However, no reasonable hydrodynamic diameters could be measured due to the obtained strong aggregation and sedimentation of the particles after homogenization. Therefore, high pressure homogenization in water was not suitable for citric acid coated particles.

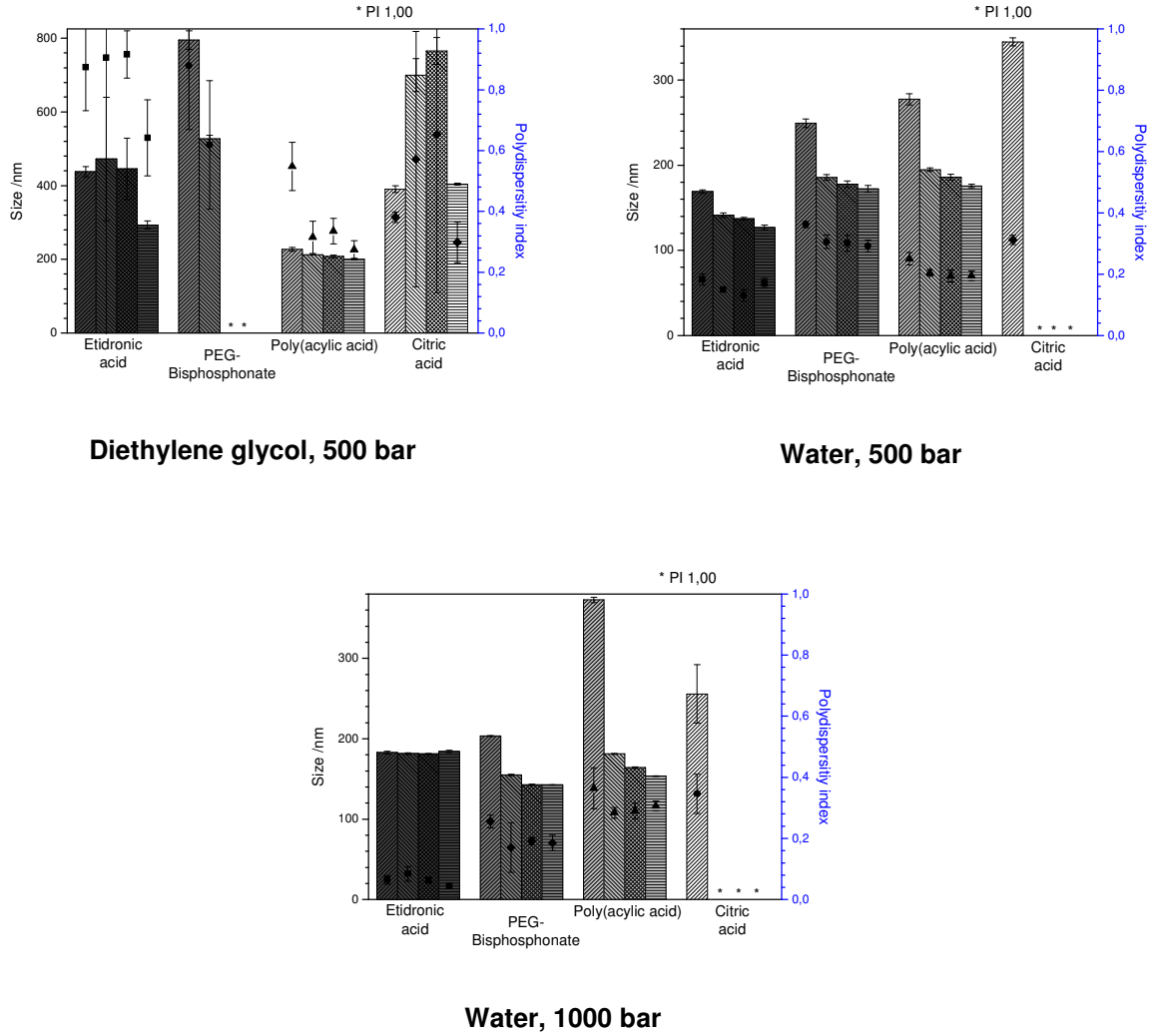

Figure 4: Influence of pressure (500, 1000 bar) and dispersant (dethylene glycol, water) during high pressure homogenization of differently coated Gd_2O_3 nanopartilces.

The TEM images of the nanoparticles coated with all four ligands, respectively, are displayed in figure 5. The coated crystals demonstrate a slightly rough surface compared to the non-

coated particles, indicating the presence of the ligands on the surface. Moreover, the diameters of the different coated particles visible in TEM show differences in size, maybe due to the different amount of dry ligand or adhering salts on the surface. The etidronic acid coated particles are the smallest, whereas those coated with the poly(acrylic acid) are the biggest in size. The particles functionalized with etidronic acid, poly(acrylic acid), and citric acid are not aggregated in contrast to the PEG-bisphosphonate coated particles. Nevertheless, an already mentioned problem with the preparation of TEM specimen is the drying of the samples on the TEM grid. This can lead to the formation of artifacts or "drying aggregates" and a distinction between "real" aggregates and aggregates caused by drying can not easily be done. Considering the PCS analysis of the PEG-bisphosphonate particles, no aggregation was detectable. Therefore, the formation of these aggregates due to the drying process is very likely.

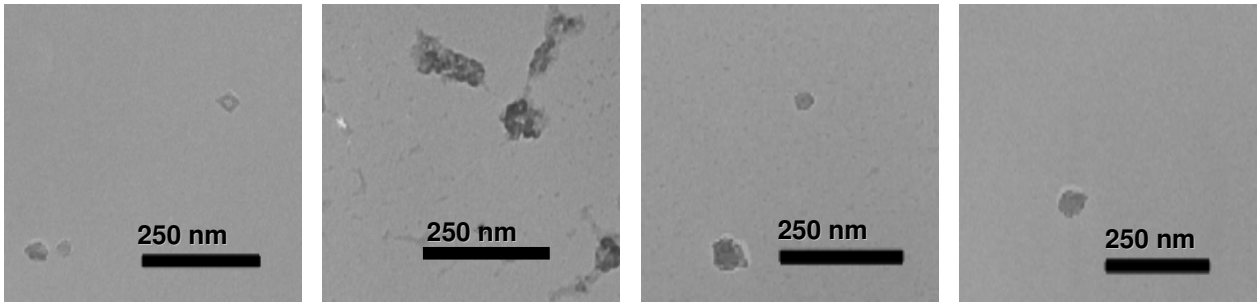

Figure 5: TEM images of coated Gd_2O_3 nanoparticles with etridronic acid, PEG-bisphosphonate, Poly(acrylic acid) and citric acid (left to right).

Another striking disagreement is the visible size in TEM and the according PCS hydrodynamic diameters as shown in table 1. The TEM sizes appear to be only half as large as the hydrodynamic diameters obtained by PCS. This is on the one hand, due to the hydration of the ligand corona in aqueous environment, which is, of course, not visible in the dried TEM samples.

Nevertheless, the hydrodynamic diameters should not be twice as high. It is also possible that the results of PCS analysis affected by a systematic error due to the strongly pronounced core-shell nature of the produced particles. The "soft" hydrated ligand shell has a considerable different refractive index than the "dense" particle core, and therefore an imprecise measurement and an inherent bias can be caused by the nature of the particles.

Table 1: Comparision of hydrodynamic diameters and TEM determined size

Sample	Hydrodynamic diameter /nm	Polydispersity index	Diamenter by TEM /nm
Gd_2O_3@ES	126 nm	0,171	~ 60
Gd_2O_3@Bp-PEG	175 nm	0,194	visible agglomerates
Gd_2O_3@PA	172 nm	0,292	~90
Gd_2O_3@CA	274 nm	0,238	~80

However, the error always should be the same for the differently coated particles and their aggregates, and hence the PCS results can still be used as an indicator for size estimation and aggregation during the preparation and processing of the particles.

Testing the particle stability after drying in different media

For the application of these particles as CT contrast agents, the preparation of stable, superposable powders is necessary, allowing redispersion right before application. Therefore, the particle stability concerning irreversible aggregation after drying in different media and the subsequent redispersability was examined. First of all, an experiment on the drying behavior was performed, as shown in figure 6.

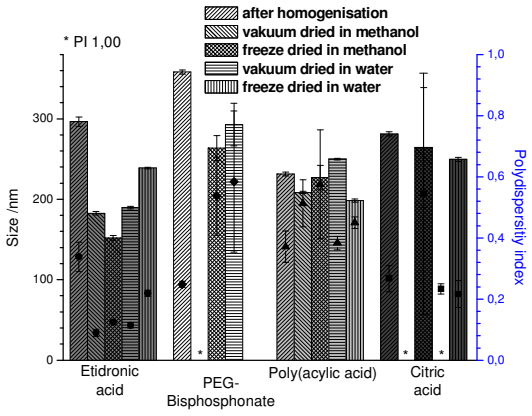

Figure 6: Influence of different drying methods in two dispersants on the aggregation of coated Gd_2O_3 nanoparticles.

Herefore, the hydrodynamic diameter of differently coated particles before and after drying was recorded. The drying was performed from water or methanol, which is used during the purification step. Moreover, vacuum drying and freeze drying were contrasted with each other. To summarize the most appropriate method for all coated particles, the freeze drying in

water provides the best results. Freeze drying seems to be the only suitable alternative for citric acid, due to the strong aggregation after vacuum dying for all samples. The other kinds of particles show no overall tendency.

The next step was to investigate the stability of the coated particles upon freeze drying in water and buffer solution (PBS) and the subsequent redispersion in one of these media. The dispersability in isotonic buffer is a prerequisite for the in vivo application. Therefore, the particles were homogenized in water or buffer solution and freeze dried subsequently. Afterwards, these lyophilized samples were redispersed in water or buffer solution. Additionally, the reaction time as a parameter for the size of the particles was investigated. As a result, all experiments were conducted with particle formation times of half an hour and 1 ½ hours, respectively, as shown in figure 7.

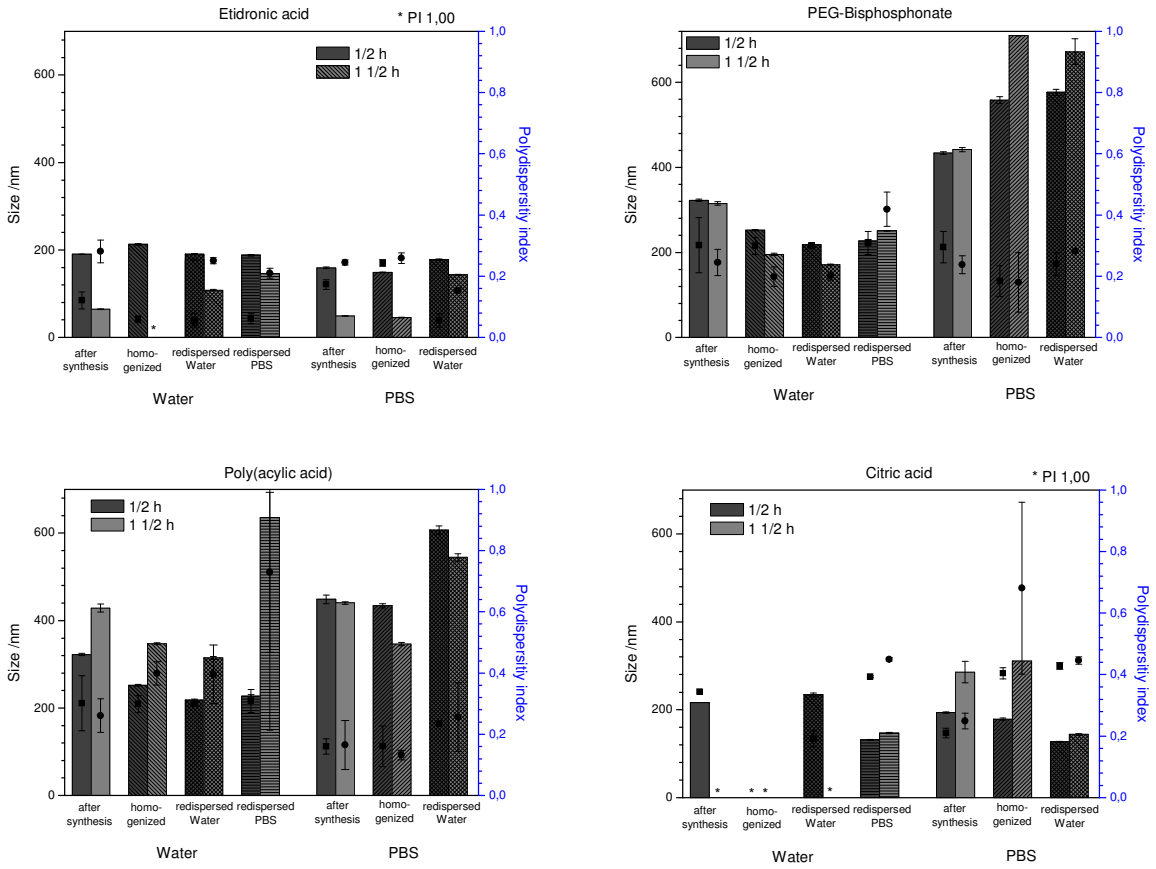

Figure 7: Influence of freeze drying and redispersion in different media on the aggregation of coated Gd_2O_3 nanoparticles

The particles coated with etidronic particles show good redispersability under all tested conditions. However, the freeze drying in water causes the lowest increase in polydispersity, at least for the samples reacted for ½ hour. Intersetingly, the influence of the reaction time on

the etidronic acid coated particles is exceptional and not comparable to the particle systems with the other ligands as coating material. For the PEG-bisphosphonate coated particles, the freeze drying in water causes significantly less aggregation after redispersion compared to the processing in buffer, correlating with the results for poly(acrylic acid). A contrary result is obtained for the citric acid coated particles. Here, the buffer solution seems to stabilize the particles during homogenization and freeze dying, which is maybe founded in the high surface charge and low stabilization of the coated crystals, as already assumed before. Moreover, the zeta potential for all tested particles and parameters was determined, giving quite low values of about -40 mV for etidronic acid, poly(acrylic acid), and citric acid and high values of ~+40 mV for PEG-bisphosphonate. The positive zeta potential for the PEG-bisphosphonate coated particles, is due to the shielding of the negative acidic charge of the bisphosphonate group achieved by the PEG part of the ligand.

Summarizing, the particles coated with either ligand are small, stable, and storable, enabling them for application as CT contrast agents. Nevertheless, the luminescent feature has still to be introduced to the nanoparticles, to achieve bimodal imaging with CT and additionally optical fluorescence detection. Unfortunately, this can hardly be achieved by the “polyol” mediated synthesis, due to the often observed amorphous structure of the particles. This is likely to prevent the formation of effective luminescent centers [9]. A new synthesis route yielding more crystalline particles for this purpose was mandartory.

8.2. Annealing based Gadolinium Oxide Nanoparticles

As already mentioned in chapter 6.2, there are different methods to prepare gadolinium containing precursor particles with high temperature annealing based syntheses routes. Two of the most prominent preparation methods are the combustion and the precipitation route, resulting in gadolinium oxide carbonate particles. These particles are then annealed at temperatures up to 900°C for 30 min to 4 hours, yielding gadolinium oxide nanoparticles of quite different size and morphology, depending on the reactants and the synthesis route used.

8.2.1. Combustion synthesis

One way of fabricating the precursor particles is the combustion synthesis. Here, the starting materials, gadolinium nitrate and an organic reducing agent are mixed in aqueous solution. Subsequently, the mixture is evaporated to dryness and overheated until combustion occurs. The precursor particles form a fluffy white powder of gadolinium oxide carbonate, which can

subsequently be annealed in a muffle furnace for conversion into gadolinium oxide nanoparticles.

As can be seen in figure 8, the TEM images of oxide nanoparticles synthesized with urea, glycine and citric acid as reducing agents turn out to be quite different in size and shape. The particles fabricated with urea are fairly homogenous, odd shaped with a size ranging from 20 to 150 nm, whereas the glycine based nanocrystals seem to be sintered together with a primary nanoparticle size of about 50 to 100 nm. Last, the citric acid prepared crystals are highly inhomogeneous with mostly not observable discrete particles up to a size of 250 nm. Therefore, the nanoparticles formed with the urea as reaction partner are the most promising particles achieved in those three experiments. Unfortunately, the hydrodynamic sizes of the as-obtained uncoated nanoparticles can not be measured due to the strong aggregation in water.

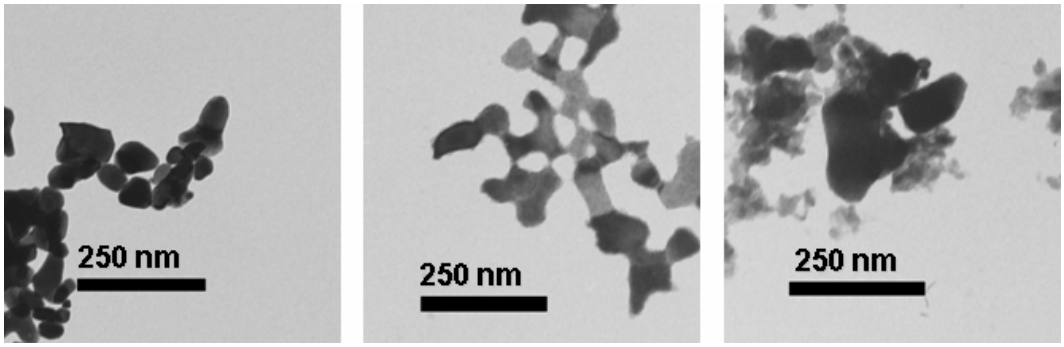

Figure 8: TEM images of Gd_2O_3 nanoparticles synthesized via combustion synthesis with urea, glycine and citric acid as reaction partner (left to right).

Nevertheless, figure 9 displays the PCS analysis of uncoated and PEG-bisphosphonate coated gadolinium oxide nanoparticles pointing out the above mentioned problem with aggregation. The expected result would have been the uncoated particles being smaller in size than the coated ones. However, the uncoated particles seem to form quite homogenous aggregates (PI ~ 2.1) of over 300 nm in size and no big improvement with coating of the particles is visible.

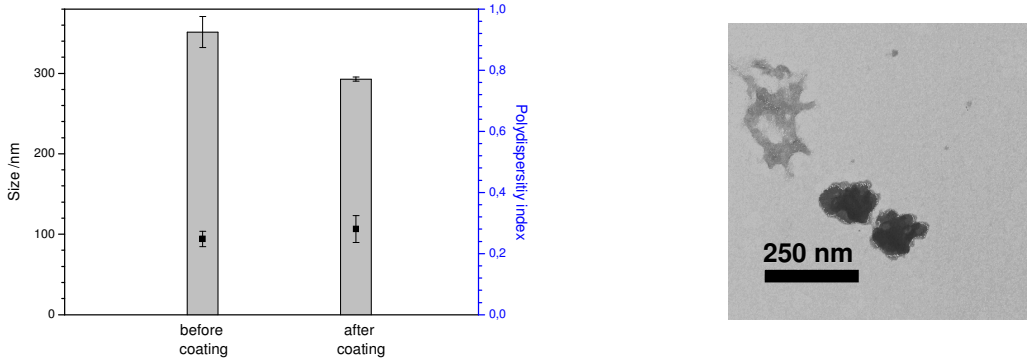

Figure 9: PCS analysis of Gd_2O_3 nanoparticles before and after coating with PEG-bisphosphonate; TEM image of coated Gd_2O_3 aggregates.

Therefore, the particles formed by combustion synthesis seemed not to be suitable for further investigations, due to their strong aggregation tendency. This may be founded in a disadvantageous surface charge and their quite irregular shape caused by the "uncontrolled" combustion process.

8.2.2. Precipitation synthesis

Another way of fabricating precursor particles for the formation of gadolinium oxide nanocrystals is the precipitation method. This synthesis route relies on the nanoparticle formation in aqueous solution, achieved by the reaction of gadolinium chloride, again, with a reducing agent like urea. This synthesis also yields gadolinium oxide carbonate particles, which can subsequently be annealed at high temperatures to form gadolinium oxide.

Influencing the size of Gadolinium Oxide particles

A big advantage over the combustion route is the possibility to influence the particle size via the chosen reaction conditions. Due to the fact that the synthesis has to be carried out in boiling water, and therefore the reaction temperature can not be altered, the two influenced parameters of particles the size are the educt concentration and the applied equivalents of the reducing agent.

The figure 10 shows the development of the particle size and their size distribution with reaction time and different educt concentrations. As can be seen, the lower the concentration of reactants used is, the lower the resulting particle diameter after sufficient reaction time. Additionally, the reaction time plays a role upon size development.

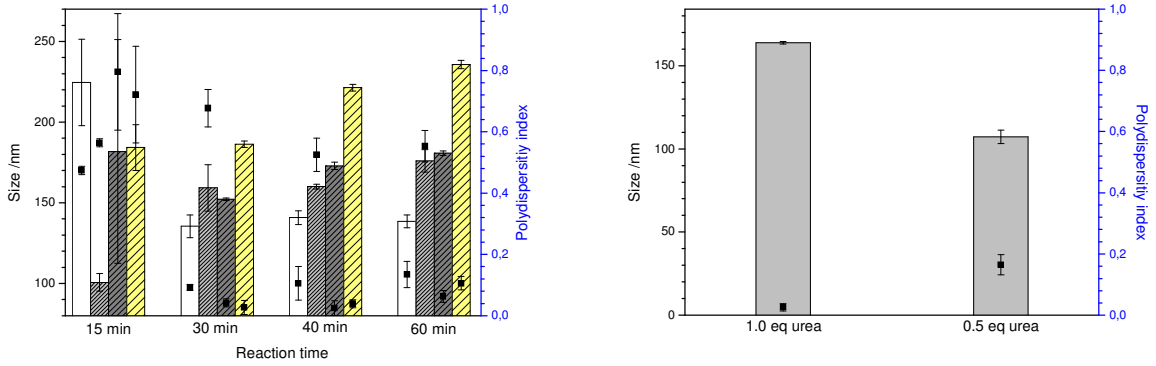

Figure 10: Size development of Gd_2O_3 precursor nanoparticles synthesized via precipitation synthesis in increasing reactant concentrations: (white) 16.6 mM; (grey) 25.0 mM; (dark grey) 50.0 mM; (yellow) 100 mM; and with different equivalents of reducing agent.

As can be seen by the obtained polydispersity indices, under all reaction conditions, after 15 min of "boiling", the particle formation is not yet completed, whereas after 30 min the PI values drop under 0.1 indicating that discrete particles of a low dispersity have been formed. Continuing the reaction, the particles show further increase in size. Concerning the second parameter, the higher the equivalent of reducing agent the higher the size of the particles is. Nevertheless, the measured hydrodynamic diameters resemble only the non annealed precursor particles, because the final gadolinium oxide nanocrystals are not dispersable in aqueous medium without further stabilizing coating. Consequently, upon annealing a further reduction of size can still be expected, which can not be investigated without the necessary coating.

Influencing the emission properties of doped Gadolinium Oxide particles

Another advantage of the precipitation synthesis used is the easiness of a controlled doping of the produced particles. The doping is achieved by mixing the different lanthanide educts in the respective amount and subsequently, the synthesis route described in chapter 7.4.2. is performed. As doping elements europium, terbium and erbium were chosen, to obtain particles luminescing in the blue, green and red range of the spectrum. To find out the optimal doping amount for these elements, experiments with increasing ratios of doping agent were carried out and the resulting fluorescence spectra were recorded.

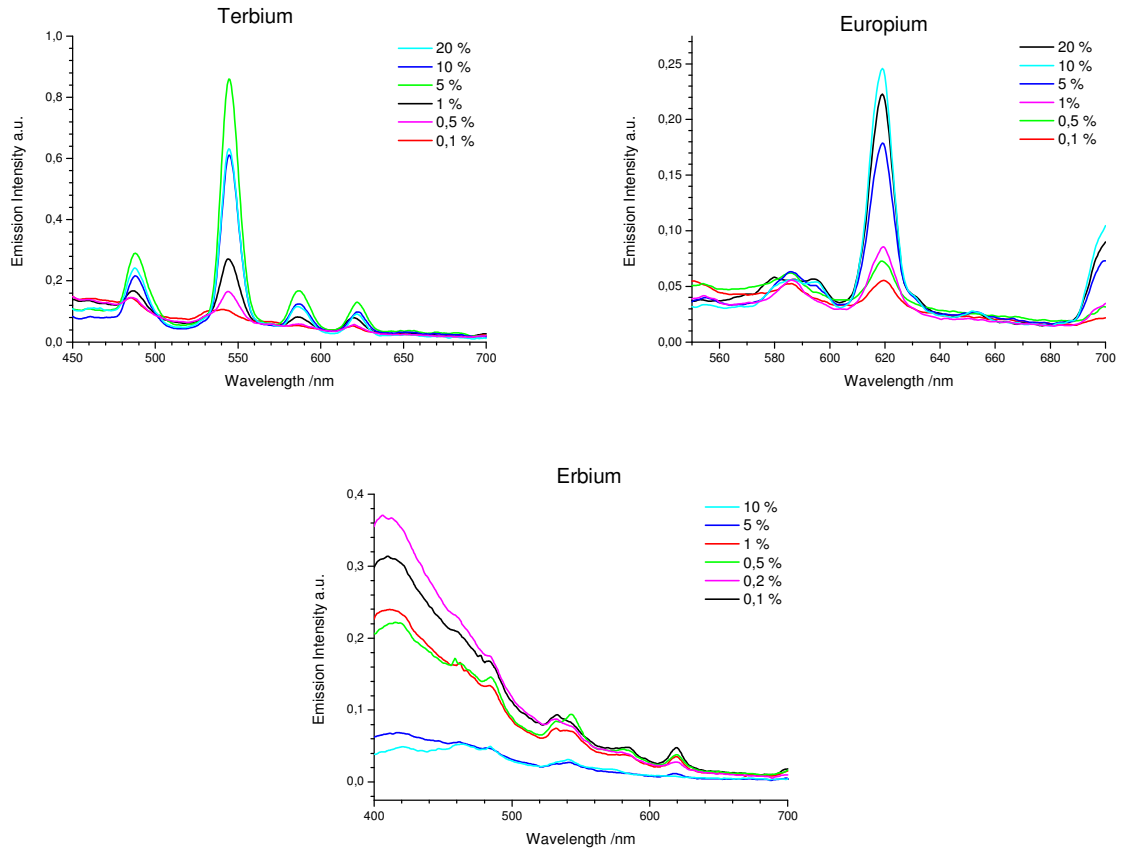

Figure 11: Development of the emission characteristics of Gd_2O_3 nanoparticles with different doping agents and doping amounts

Figure 11 shows three different diagrams with spectra of gadolinium oxide nanoparticles doped with different agents in increasing amounts from 0.1 to 10 or 20%. For terbium the maximal emission is reached at 5%, with europium at 10% and for erbium the optimal doping amount is 0.2%. Furthermore, the best annealing temperature for all three dopands was tested as shown in figure 12. As well as the doping amount, the annealing temperature has a great influence on the emission intensity. Depending on the doping element, different optimum temperatures were found. For terbium an annealing temperature of 200°C was the most favorable in contrast to europium and erbium, where 700°C gave the best results. The measured emission spectra resemble quite well emission lines of the respective elements known from literature [10,11]. Terbium doped gadolinium oxide shows several emission lines at 485, 544, 585 and 620 nm originating from the $^5D_4 \rightarrow ^7F_6$, $^5D_4 \rightarrow ^7F_5$, $^5D_4 \rightarrow ^7F_4$ and $^5D_4 \rightarrow ^7F_3$ transitions. The europium emission is composed of lines at 586, 595, 618, 653 and 700 nm resembling to the transitions of $^5D_0 \rightarrow ^7F_0$, $^5D_0 \rightarrow ^7F_1$, $^5D_0 \rightarrow ^7F_2$, $^5D_0 \rightarrow ^7F_3$ and $^5D_0 \rightarrow ^7F_4$. An, on the first sight, anomaly can be seem in the emission spectra of erbium, where a strong change in the intensity weighting of the emission lines occurs upon annealing. Nevertheless, this

alteration of the spectrum is founded in a change in the crystal structure of the gadolinium environment. The most of the found emission lines at 418, 484, 530, 543 and 618 nm can be dedicated to transitions of the $^2G_{9/2} \rightarrow {}^4I_{15/2}$, $^4F_{7/4} \rightarrow {}^4I_{15/2}$, $^2H_{11/2} \rightarrow {}^4I_{15/2}$, $^4S_{3/2} \rightarrow {}^4I_{15/2}$ and $^4F_{9/2} \rightarrow {}^4I_{15/2}$ states.

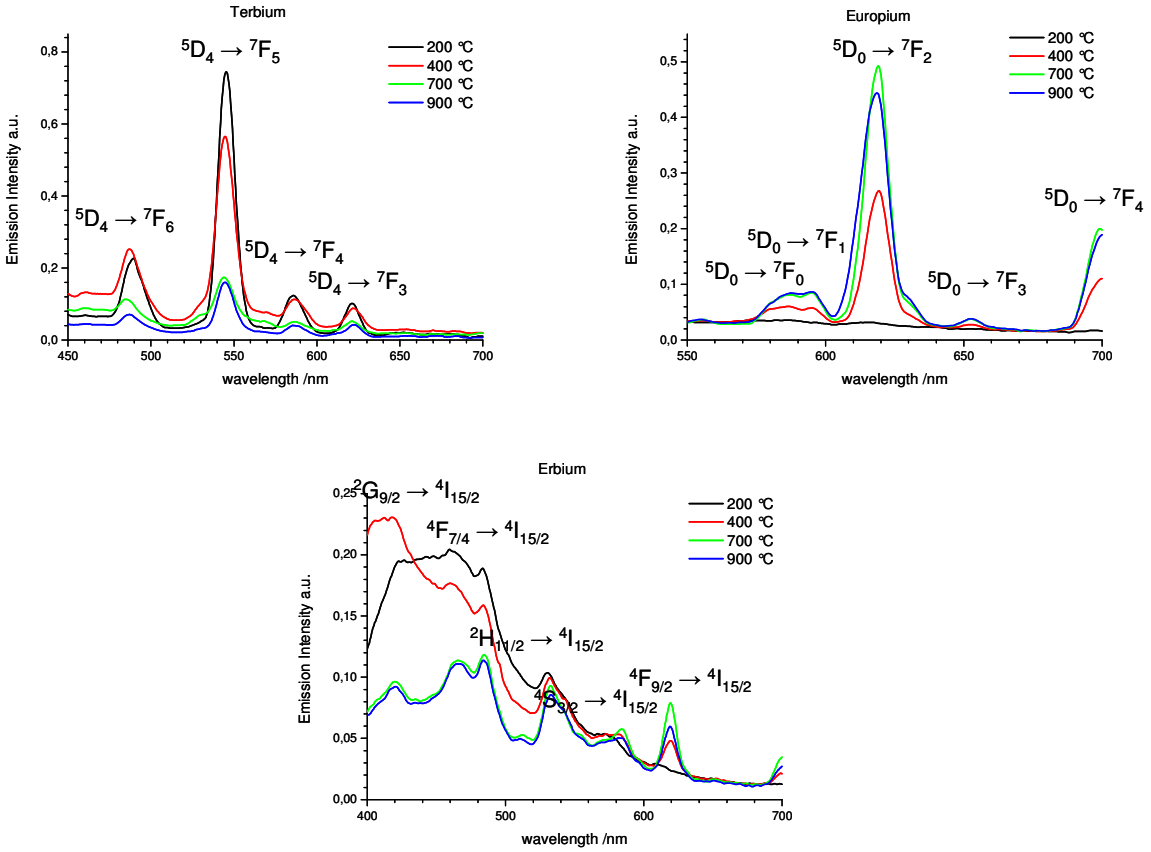

Figure 12: Development of emission characteristics of Gd_2O_3 nanoparticles with different annealing temperatures

The change in the crystal structure upon annealing was further investigated with powder x-ray diffraction. The respective diffractogramms of samples annealed at 200, 400, 700 and 900°C were recorded, as shown in figure 13. A clear development of amorphous to crystalline nanoparticles can be seen. As expected, the higher the annealing temperature, the higher the crystallinity of the samples get. The XRD patterns of the crystalline samples are similar to gadolinium oxide chloride (GdOCl, JCPDS no. 85-1199), a unit cell and crystal symmetry information is given in this JCPDS file. The literature gives the parameters for GdOCl as follows, a tetragonal phase with a = 3.95 Å, c = 6.67378 Å and volume = 104.1 Å^3 and a space group of P4/nm. The fitting of the as derived results gave the same unit cell (see supplement), nevertheless there is only a small amount of indexable lines given in the

diffractogramms. Unfortunately, the XRD diffractograms show, that not Gd_2O_3 but the corresponding chloride is formed indicating that the precipitated nanocrystals had considerable amount of chloride impurities.

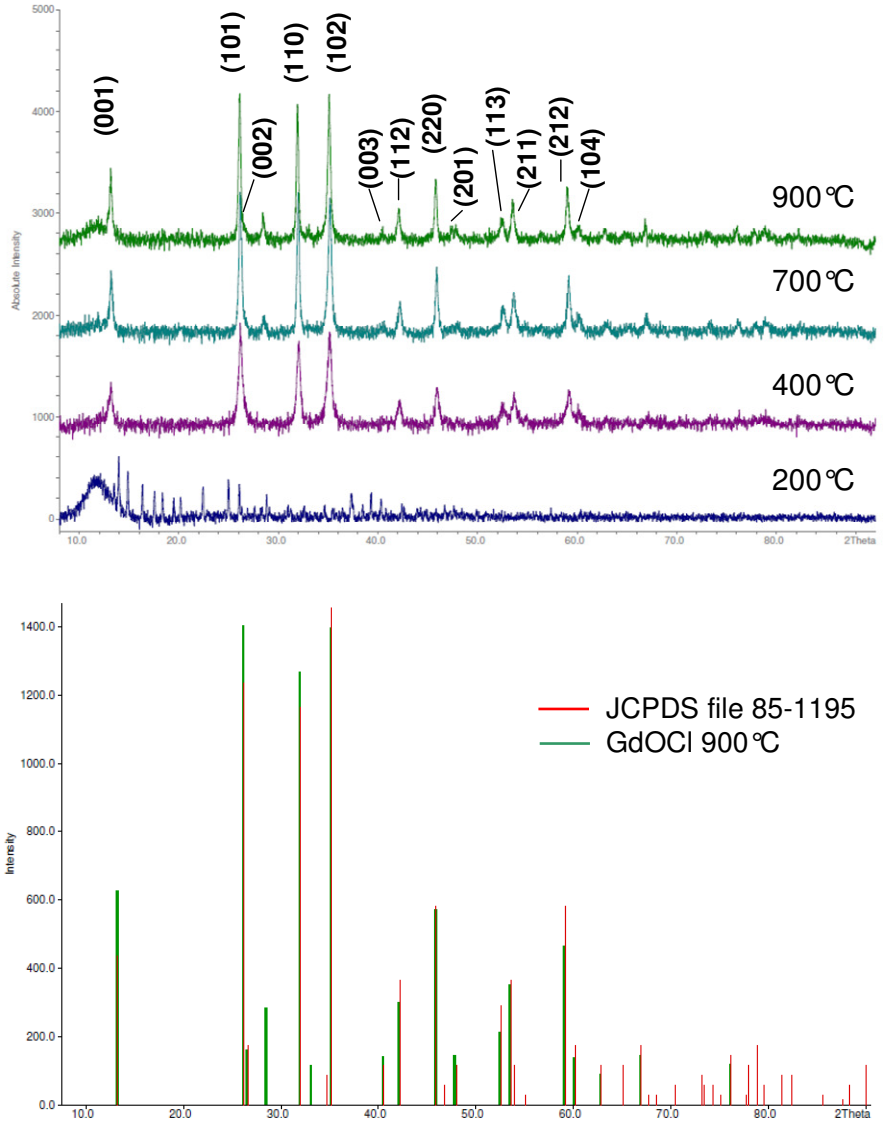

Figure 13: P-XRD pattern of the gadolinium oxide chloride nanoparticles with increasing annealing temperature; comparison of peak patterns of literature and as-synthesized particles.

Nevertheless, the advantageous characteristics of the particles are not influenced by the composition [12]. The particles are luminescent, in the case of terbium doping, the amorphous structure even seem to be better for the emission intensity, and the CT attenuation also should not be influenced significantly by the composition of the particles. Nevertheless, the particles will still be referred to as “gadolinium oxide” nanoparticles.

Coating of Gadolinium Oxide Nanoparticles with PEG-bisphosphonate

As already mentioned earlier, for an application of the nanoparticles in aqueous environment, coating with a water-soluble ligand is necessary to obtain stable particle dispersions. To avoid particle aggregation, the coating was performed using the poly(ethylene glycol) biphosphonate ligand, which was already used in chapter 8.1.2. to render the "polyol" route synthesized particles water dispersable. In figure 14 TEM images of the non coated and coated particles are displayed.

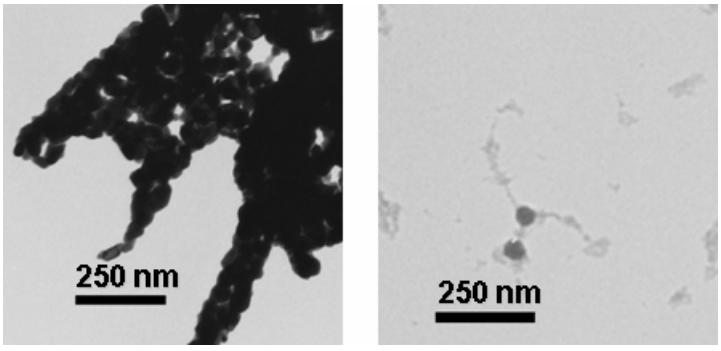

Figure 14: TEM images of uncoated and PEG-bisphosphonate coated Gd_2O_3 nanoparticles

The uncoated particles are, as expected, strongly aggregated due to the disadvantageous preparation method of the TEM specimen. In contrast, the coated particles are discrete, round shaped nanocrystals with visible, less contrasted, ligand on the surface, indicated by the particle roughness. Again, as already mentioned, the problem of the correlation between TEM and PCS analysis is given, suggesting once more the inherent problem of the performed PCS analysis. The particles shown on the TEM image (~ 80 nm) give a size of about 170 nm for their hydrodynamic diameter as shown in figure x, second bar. Nevertheless, it was possible to synthesize coated nanoparticles of different sizes by varying the reaction parameters as exemplary shown in figure 15. The lowest measurable hydrodynamic diameter was about 50 nm in size indicating that the measured particles are even smaller.

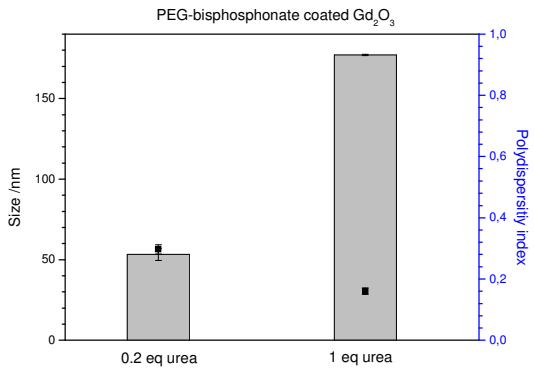

Figure 15: PCS analysis of PEG-bisphosphonate coated Gd_2O_3 nanoparticles synthesized in two different sizes.

These as coated particles of different diameters were applied in an in vitro CT experiment. For this experiment particles of different sizes coated with PEG-bisphosphonate and dispersed in water, were filled into small vessels of 2 mL volume and put into the computer tomograph. The as-derived HU amounts for the samples were correlated to the gadolinium content of the samples in table 2.

Table 2: CT contrast, corresponding gadolinium content and HU per mg gadolinium of in vitro CT experiment.

Composition of sample	**Hydrodynamic diameter /nm**	**CT contrast of sample /HU**	**Concentration /mg/mL**	**HU per mg Gd**
$GdCl_3$ in H_2O	-	209	3.28	64
H_2O	-	71	0	-
Air	-	0	0	-
Gd_2O_3@PEG-bisphosphonate	~ 170	244	4.14	59
	~ 80	234	3.72	63
	~ 50	255	4.24	60

All concentrations of the gadolinium samples were checked with ICP-MS and put into relation to their CT contrast. Furthermore, the attenuation of water and air, which must be

zero, was measured. The coated nanoparticles give good in vitro CT contrast, with about 60 HU per mg gadolinium. These, about 60 HU correspond to the HU values of gadolinium chloride in aqueous solution, and marks the inherent attenuation of gadolinium. Therefore, the measured CT contrast of the particulate samples is in very good accordance to the expected values, and no alteration with particle formation and particle size is visible. In figure 16, a cross section of the investigated samples with the respective HU values is shown.

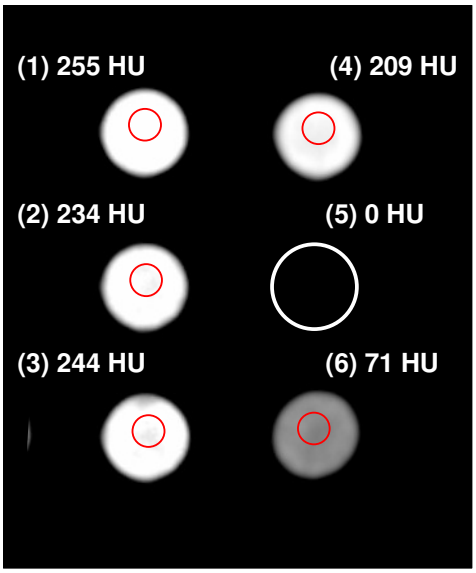

Figure16: CT image of nanopariclulate G_2O_3@PEG-bisphosphonate in 3 different sizes and the corresponding control vials (1) Gd_2O_3 50 nm; (2) Gd_2O_3 80 nm; (3) Gd_2O_3 170 nm; (4) $GdCl_3$ in H_2O; (5) air; (6) water.

The brightness of the samples marks their attenuation, and therefore a good visibility of the nanoparticle dilutions in vivo is expected. Moreover, the particles, functionalized with targeting functions, will give remarkably higher contrast at the site of interest and longer circulation times due to the targeting function. A last thing to investigate is the cytotoxicity of these nanoparticles.

8.2.3. Cytotoxicity tests of Gadolinium Oxide Nanoparticles with different coatings

The cytotoxicity of the coated gadolinium oxide nanoparticles and free gadolinium ions was tested according to the MTT cytotoxicity test described in chapter 7.5.7. For the assay freshly prepared dispersions of coated nanoparticles in medium, using two different serial dilutions were applied. The chosen concentrations of the nanoparticulate samples and the gadolinium ion concentrations are based on the known toxic gadolinium amount [13]. The amount of particles used was only related to the overall gadolinium concentration in the sample detected

by ICP-OES or ICP-MS, due to the imprecise PCS data. According to this data, no accurate determination of the particle diameter is possible, and therefore, no calculation of the particle concentration. However, all investigated particles had hydrodynamic diameters of about 200 nm, making the experiment comparable. Moreover, the investigated range of gadolinium ion concentration well covers the theoretical amounts of the element in all of the nanoparticulate samples (0.5 – 0.01 µM). The variations of the used nanoparticle amounts, respecting gadolinium concentration, result from the preparation procedure of the particles.

Table 3: Concentrations of nanopartilulate and gadolinium ion samples and their respective cytotoxicity

Composition of sample	**Concentration Gd^{3+}**		**Cytotocicity /%**	
	/µmol/L	**/µg/mL**	**L929**	**CHO**
Gd_2O_3@PA	0.539	85.0	1.2	15.7
	0.054	8.5	-6.8	12.0
Gd_2O_3@CA	0.119	18.8	6.2	2.8
	0.012	1.9	2.3	-5.4
Gd_2O_3@ES	0.445	70.0	5.7	4.5
	0.045	7.0	0.1	-10.3
Gd_2O_3@PEG-bisphosphonate	0.774	121.8	11.7	6.6
	0.077	12.2	-8.0	-10.2
Gd^{3+}	6.5	$1.03 \cdot 10^3$	66.3	32.4
	0.65	103.0	2.2	-13.8
	0.07	10.3	10.7	-2.6
	0.01	1.0	9.8	-7.3

All investigated nanoparticulate concentrations show, as expected, only very low to no observable toxicity toward the chosen cell lines. In contrast, the highest gadolinium concentration shows a considerable effect on the viability of the cells. In table 3 the gadolinium ion concentrations of the nanoparticles and the control with their respective cytotoxicity on two different cell lines are shown. Figure 17 displays the viability of both cell lines under nanoparticulate and control treatment.

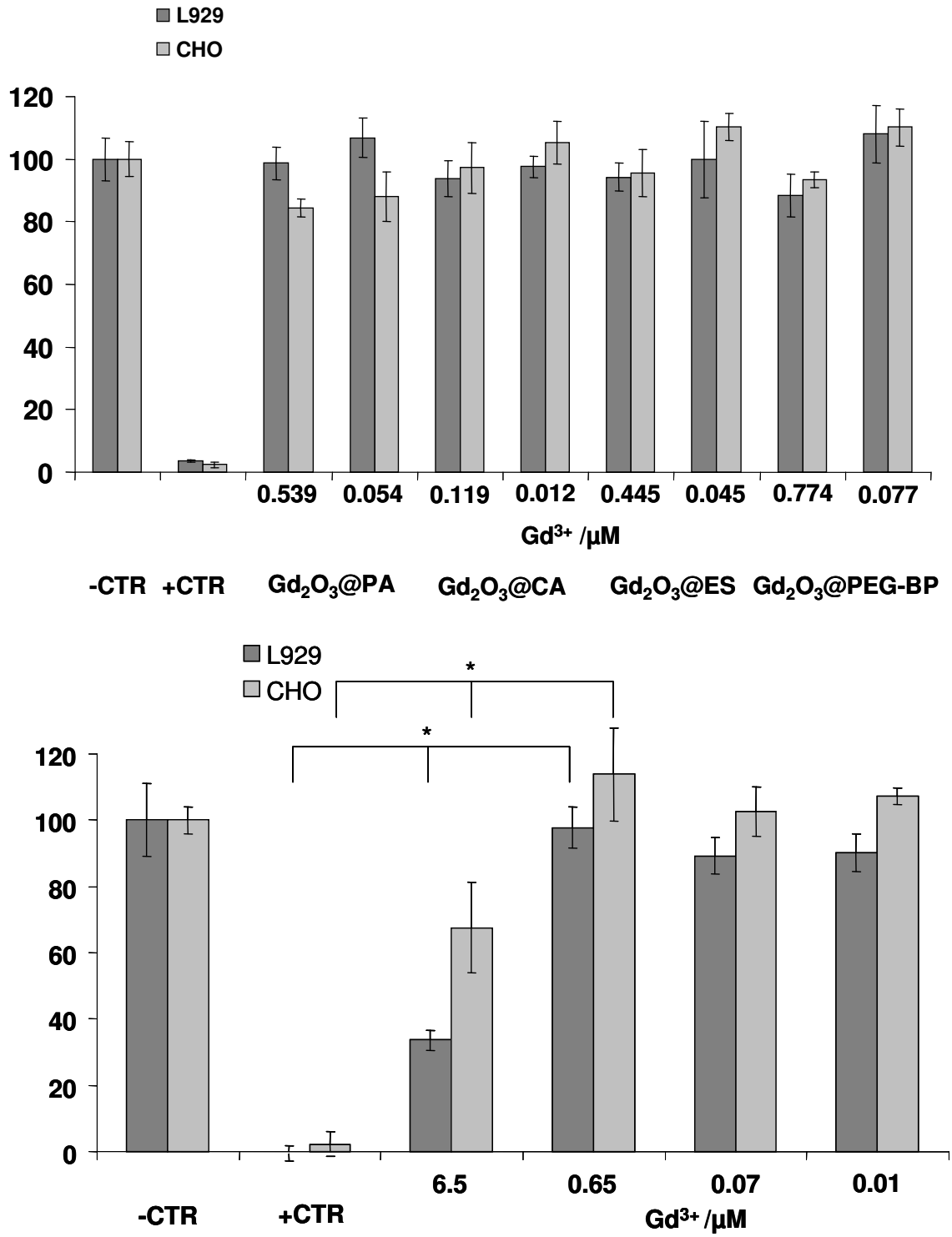

Figure 17: Viability of L929 and CHO cells under treatment with differently coated Gd_2O_3 nanoparticles and Gd^{3+}, * significantly different $p < 0.01$.

For the different gadolinium ion solutions, the faster proliferating and more robust CHO cells always showed a slightly lower response in comparison to the L929 cell line. In contrast, for the particulate sample no general trend was observed. This indicates that the observed variations are due to minor variations of the cell numbers or growth activity, but not founded

in toxic or proliferative effects. Therefore, the gadolinium oxide nanoparticles can be said to be not toxic in the tested concentration ranges.

9. References

[1] F. Caruso, Nanoengineering of Particle Surfaces, Adv. Mater. 13(1) (2001) 11--22.

[2] B.M. Silverman, K.A. Wieghaus, J. Schwartz, Comparative Properties of Siloxane vs. Phosphonate Monolayers on A Key Titanium Alloy, Langmuir 21(1) (2005) 225--228.

[3] S. Biggs, P.J. Scales, Y.-K. leong, T.W. Healy, Effects of citrate adsorption on the interactions between zirconia surfaces, J. Chem. Soc. Farad T 91(17) (1995) 2921--2928.

[4] A. Sehgal, Y. Lalatonne, J.-F. Berret, M. Morvan, Precipitation-Redispersion of Cerium Oxide Nanoparticles with Poly(acrylic acid): Toward Stable Dispersions, Langmuir 21(20) (2005) 9359--9364.

[5] M. Aguilar, N. Miralles, A.M. Sastre, Metal complexes with phosphonic and phosphinic acids, Rev. Inorg. Chem. 10(1-3) (1989) 93--119.

[6] P.H. Mutin, G. Guerrero, A. Vioux, Organic-inorganic hybrid materials based on organophosphorus coupling molecules: from metal phosphonates to surface modification of oxides. Cr Acad. Sci II C 6(8-10) (2003) 1153--1164.

[7] L. Qi, A. Sehgal, J.-C. Castaing, J.-P. Chapel, J. Fresnais, J.-F. Berret, F. Cousin, Redispersible Hybrid Nanopowders: Cerium Oxide Nanoparticle Complexes with Phosphonated-PEG Oligomers, ACS Nano 2(5) (2008) 879--888.

[8] A.A. Datea, V.B. Patravaleb, Current strategies for engineering drug nanoparticles, Cur Opin Colloid Interface Sci 9(3-4) (2004) 222--235.

[9] A.M. Pires, M.F. Santos, M.R. Davolos, E.B. Stucchi, The effect of Eu^{3+} ion doping concentration in Gd_2O_3 fine spherical particles, J Alloy Compounds 344(1-2) (2002) 276--279.

[10] U. Rambabu, A. Mathur, S. Buddhudu, Fluorescence spectra of Eu^{3+} and Tb^{3+}-doped lanthanide oxychloride powder phosphors, Mater. Chem. Phys. 61(2) (1999) 156--162.

[11] U. Rambabu, K. Annapurna, T. Balaji, S. Buddhudu, Fluorescence spectra of Er^{3+} : REOCl (RE = La, Gd, Y) powder phosphors. Mater. Lett. 23(1,2,3) (1995) 143--146.

[12] E. Antic-Fidancev, M. Lemaitre-Blaise, P. Porcher, J. Hölsä, Ovservation and Simulation of the Energy Levels of Trivalent Rare Earth Ions in RE Oxyhalide Matrices, Phys. Stat. Sol. A 130 (1992) K142--K153.

[13] Y. Kubota, S.I. Takahashi, G. Patrick, Different cytotoxic response to gadolinium between mouse and rat alveolar macrophages. Toxicol. in Vitro 14(4) (2000) 309--319.

Chapter 9

Gadolinium Oxide Nanoparticles - Discussion

9.1. Discussion

Two different synthesis methods for the fabrication of gadolinium oxide nanoparticles were successfully established to provide nanoparticulate gadolinium oxide for imaging applications. They both have advantages and disadvantages. It turned out that the different synthesis approaches result in different particles concerning size, optical properties, and detectability in the CT. The “polyol” mediated route yields coated particles immediately after synthesis, whereas the annealing based routes give luminescent nanocrystals after additional high temperature treatment.

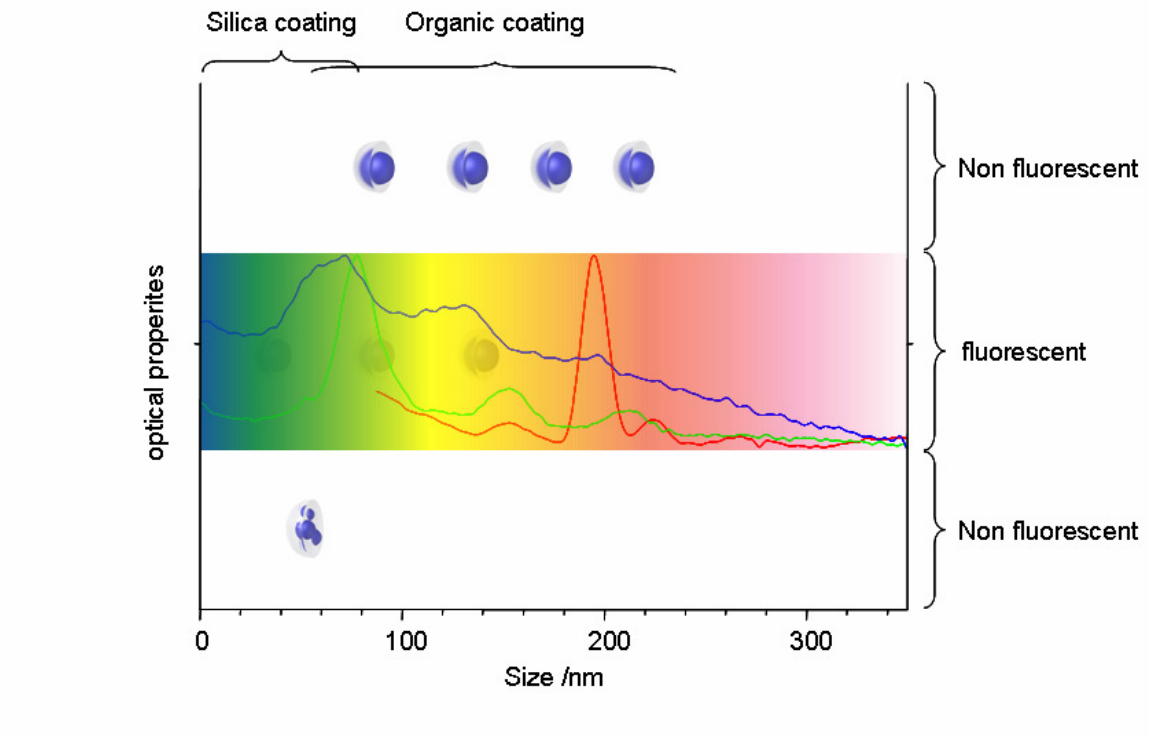

Figure 1: Diagramm of the size and the optical properties of the synthesized Gd_2O_3 nanoparticles.

The first investigated “polyol” route allowed synthesizing differently coated nanoparticles in a size range of 50 – 200 nm (see figure 1). A subsequent stable coating can be achieved very easily by only adding the dissolved ligand to the hot particle solution, immediately after the particle formation. Moreover, these as-coated nanoparticles can be further high pressure homogenized and freeze dried to give stable, storable, and redisperable powders, with ideal properties for the application as CT contrast agents. As shown in the first experiments (chapter 8.1.1.), the coating with a silica shell raises significant problems with purification

and subsequent swelling of the shell material, due to the excess of not removable silica formed during the particle preparation.

These drawbacks can be circumvented by applying more specific organic molecules as coating materials [1-5]. For this approach, hydrophilic and charged molecules with known high affinity to metal oxides were chosen, carrying either carboxylic acid or phosphonic acid groups. They turned out to be adequate stabilizers for the synthesized gadolinium oxide nanoparticles in dispersion either via a introduced surface charge (etidronic acid, citric acid, poly(acrylic acid)) or via a steric stabilization of the nanoparticles (PEG-bisphosphonate). Nevertheless, a slightly modified synthesis was applied, considering the additional sodium hydroxide consumption of the ligands, also yielding "bigger" particles with a diameter of about 50-80 nm (see figure 1). The bigger size of the particles is certainly founded in a higher concentration of sodium hydroxide added for the particle formation, resulting in a higher amount of gadolinium hydroxide. This gadolinium hydroxide precipitates and forms the particles, which are subsequently converted to gadolinium oxide. Moreover, the direct addition of the respective ligand to the reaction solution seems to influence the particle diameter as well. Therefore, it seems to be reasonable that the differing pK_a values of the ligands have to be taken into account. For example, etidronic acid has four pK_a values (1.35; 2.87; 7.03; 11.3) in contrast to citric acid, having three pK_a values (3.13; 4.76; 6.40) [6,7]. Hence, more sodium hydroxide is consumed to fully deprotonate the bisphosphonate containing ligand. Therefore, less sodium hydroxide is available for gadolinium hydroxide formation and the particles get smaller. Nevertheless, this may not be the only reason for the observed size variation of the particles. The etidronic acid coated particles were the smallest, likely due to the tight binding of the phosphonic acid group to the surface and the small size of the ligand molecule. On the other hand, the citric acid functionalized particles caused the biggest problems with stabilization against aggregation, although citric acid is a quite small ligand as well. These particles also have the biggest diameters in the TEM as well as in the PCS analytics. This may be founded in more unspecific aggregation of the citric acid molecules on the nanoparticle surface, resulting in an inferior stabilization. Moreover, the interaction of the ligand mediated excess surface charge with counterions in buffer solutions, stabilizing the particles to a satisfying extent, supports this assumption. On the one hand, the cations present in the buffer can interact with the citric acid molecules, which are well known for their metal-complexing properties, and therefore stabilizing the surface charge. On the other hand, the phosphate ions of the buffer salt can replace the citric acid, due to their superior binding affinity, and hence stabilizing the particles to a greater extent. The crystals

coated with the bigger polymeric ligands, poly(acrylic acid) and PEG-bisphosphonate, exhibited hydrodynamic particle diameters of about 150 - 250 nm, and displayed a good steric stabilization. No significant differences in particle size under homogenization and drying could be observed, suggesting that the longer chains of the ligands protect the particle core more efficiently.

The "polyol" synthesized particles coated with citric acid were already applied in a preliminary animal experiment with female rats at Bayer Schering Pharma, giving very good intra-uterine CT contrast, as it can be seen in figure 2. The citric acid coated particles used were developed especially as a model to image the intra-uterine transport of nanoparticles. Therefore, no additional targeting function was necessary, because the particles were applied with a syringe via the vagina directly into the rat uterus. The citrate coated particles were used due to the assumed best biocompatibility of excess citrate ions in the acidic milieu. CT images of citric acid coated Gd_2O_3 nanoparticles (size = 330 nm, concentration = 200 mg/mL) in rat uteri with give an in vivo contrast 450 HU (see figure 2).

amimal 2 (midestrus rat)

(midestrus rat = very dry uterus)

V_{appl} = 150 µL, after 1min

animal 4 (estrus rat)

(estrus rat = liquid filled uterus)

V_{appl} = 100 µL, after 1 min

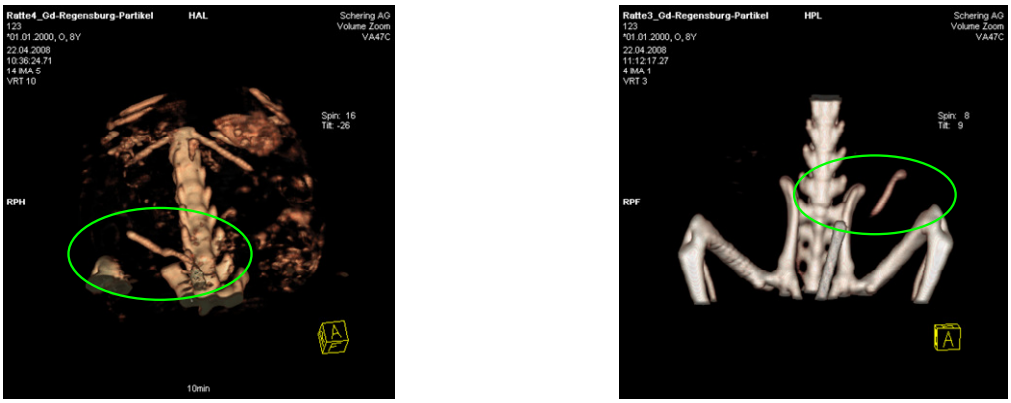

Figure 2: CT images of 330 nm citric acid coated Gd_2O_3 nanoparticles in rat uteri with a concentration of 200 mg/mL particles; in vivo contrast 450 HU.

A drawback for the analysis of the coated particles were the inconsistent results obtained by the PCS measurements, not allowing to compare the obtained hydrodynamic diameters with the TEM results. The very pronounced core/shell structure of the particles probably caused an inherent bias in the data for the measured diameters. As already mentioned in chapter 8.1.2, the strongly differing refractive indices of the "hard" inorganic core and the "soft" organic

shell may be an explanation for the observed mismatch. The soft shell, of course, contributes about 20 to 30 nm to the overall hydrodynamic diameter, but should not completely double it. Another possible source of error for the calculation of the hydrodynamic radii may also be the viscosity of the chosen dispersion medium. All measurements were carried out in purified water or buffer solution. Thus the viscosity of water was considered for the calculation of the diameters of the particles. However, the influence of the desorbed ligand molecules from the nanoparticles is not fully understood. This effect may additionally alter the viscosity of the dispersion medium, which could not be taken into account for the size calculations. A concentration dependent formation of bigger particle aggregates was excluded by size measurement of the particles at various dilutions, always yielding similar particle diameters. Moreover, the good polydispersity indices obtained for most particle types (except citric acid) indicate that there is only one single particle species in the samples. Hence, the hydrodynamic diameters obtained with PCS were only taken as an indicator for the aggregation tendency and the size development of the nanoparticles. Nevertheless, TEM images were taken as often as possible to verify the absolute particle sizes.

The preparation of small, stably coated, fluorescent, and CT active nanoparticles was successful, applying the secondly investigated “annealing based” synthesis methods. These advantageous properties can compensate the additional reaction step needed, compared to the “polyol” route, to achieve the coating of the nanocrystals,. Due to the annealing step, the nanocrystals exhibit bare oxidic or carboxylic surfaces, making coating procedures more difficult. Hence, the PEG-bisphosphonate ligand was chosen as coating material, since the phosphonic acid groups provide a very good and stable grafting on the nanoparticulate surface. Moreover, an effective stabilization against aggregation and reduced adsorption of counterions from the medium is provided by the uncharged PEG chains of the ligand.
The combustion synthesis route with urea as reducing agent yielded appropriate particles. Nevertheless, coating procedures turned out to be rather difficult. The nanoparticles had a strong tendency to stick together, and therefore build aggregates of about 250 nm in size. This is likely due to the quite irregular shape and disadvantageous surface charge of the particles caused by the combustion. Moreover, the reaction offered no possibilities to influence the particle size in an appropriate manner, due to the “uncontrollable” combustion event.
The nanoparticles synthesized by means of the alternative precipitation method, on the one hand, display very good optical properties. On the other hand, this synthesis method provides the possibility to tailor size of the particles. Hence, the precipitation synthesis was applied for

further particle preparation. Three different emission colors could be obtained via doping of the nanocrystals, using europium, terbium, and erbium ions. Particles with blue, green, and red emission were successfully prepared. They display sharp emission lines and a broad excitation spectrum, due to the surrounding host lattice. The gadolinium oxide host lattice can also absorb in a broad spectral range, subsequently transferring the energy to the dopand centers [8]. Moreover, a successful optimization of the emission properties with respect to the doping concentration and the annealing temperature could be achieved. It was proved that the synthesized particles display the typical emission lines of the respective doping agents [9,10]. A significant reduction in emission intensity was observed when exceeding the optimal doping amount. This decrease in emission can be dedicated to a direct interaction of the luminescent centers in the nanocrystal, thus giving rise to non-radiative deactivation processes [11]. The dependence of luminescence intensity on the annealing temperature also could be seen. This dependence is based on a change in crystallinity of the particles. The europium and erbium doped particles have an optimum emission intensity when an annealing temperature of 700 °C is applied. As a result, it can be stated, that these dopands need a high crystallinity to exhibit high luminescence intensity. On the other hand, the terbium doped nanoparticles have their highest emission intensity, when annealed at low annealing temperatures, resulting particles with an amorphous structure. This result suggests an oppression of luminescence due to the symmetry of the dopand centre in the respective structure.

Another result of the powder x-ray diffraction patterns was the assignment of the crystalline diffractogramms to the structure of gadolinium oxide chloride [12]. The matlockite-type PdFCl structure of the lighter lanthanide oxide chlorides (Ln = La – Er, Y) belongs to the crystal system space group with P4/nmm – D_{4h}^7 (no. 129, Z = 2) [9]. The overall structure is formed by altering layers of $[LnO]_n^{n+}$ complex cations and Cl^- anions in a typical way for all tetragonal lanthanide oxycompounds such as oxybromide, -iodides, -sulfates, -nitrates and some oxycarbonates [13]. In GdOCl the Gd^{3+} cation is coordinated to four oxygens and five chlorides yielding a monocapped square antiprism for coordination polyhedron. This arrangement results in C_{4v} point symmetry of the Gd^{3+} site. Moreover, the presence of a sensitive forbidden transition $^5D_0 \rightarrow {}^7F_0$ in the spectra of the europium doped crystals supports the lanthanide oxychloride structure [9]. The result shows clearly, that even the highest annealing temperature for the particles is not sufficient enough to form pure gadolinium oxide, and significant amounts of chloride impurities are present after precipitation. Nevertheless, this does not alter the properties of the emission, as the $[LnO]_n^{n+}$ cation has been shown to play the dominant role in determining the crystal field effect on the

energy level scheme of the doped ions in several lanthanide oxysalts [13]. Besides, the GdOCl composition is known to form luminescent materials very efficient upon doping. Moreover, it has been proved in another experiment that the CT-contrast for the coated GdOCl nanoparticles is not altered compared to Gd_2O_3. Therefore, the particles are referred to as "gadolinium oxide" nanoparticles, even if there are some chloride impurities.

By tuning the reaction conditions, a straight forward procedure to tailor-make particles of about 50 to over 100 nm in diameter was developed. With tuning the concentration, amount of reducing agent and reaction time, the size of the particles can be influenced. This is, of course, based on in the reaction equilibrium, where lower concentrations and lower amounts of reducing agent lead to smaller particles. The investigation of the reaction times revealed that the reaction needs a certain time to form distinct particles, which are increasing in size with ongoing reaction.

Moreover, after coating of these particles with PEG-bisphosphonate, they showed no aggregation predisposition in dispersion. Particles of different hydrodynamic diamters (50, 80, 170 nm) were applied in an in vitro CT-experiment, illustrating the very good X-ray attenuation of gadolinium oxide chloride nanoparticles. The measured HU values correspond to the HU values for dissolved gadolinium chloride of the same concentration. Thus, it can be stated that no alteration of the attenuation properties upon particle formation or due to differently sized particles occurs.

Hence, a very good in vivo CT-contrast is to be expected for the particles, as already shown for the "polyol" derived particles. Moreover, a suitable tailoring of the nanocrystal size aiming for different applications is possible. With an additional targeting of the particles to a specific site of interest, a superior contrast compared to gadolinium chelates can be obtained due to the much higher local gadolinium concentration at one specific point. This targeting can be achieved by using an amino functionalized PEG-bisphosphonate ligand comparable to the ligand used herein. Therefore, this kind of coated nanocrsytals can easily be applied for multimodal imaging, combining CT and luminescent properties. Moreover, the gadolinium in the nanoparticle opens the door for further applications as MRI contrast agent [14], and in the described neutron capture therapy [15], resulting in superior results compared to e.g. gadolinium chelates due to their nanoparticulate nature.

The cytotoxicity tests of the prepared nanoparticles with the different coating materials, etidronic acid, citric acid, poly(acrylic acid), and PEG-bisphosphonate showed no significant toxicity in different cell cultures, neither due to the heavy metal nature, nor due to the size of

the particles. Therefore, a save application can be assumed, at least for cell based or small animal in vivo imaging.

9.2. References

[1] S. Biggs, P.J. Scales, Y.-K. leong, T.W. Healy, Effects of citrate adsorption on the interactions between zirconia surfaces, J. Chem. Soc. Farad T 91(17) (1995) 2921--2928.

[2] A. Sehgal, Y. Lalatonne, J.-F. Berret, M. Morvan, Precipitation-Redispersion of Cerium Oxide Nanoparticles with Poly(acrylic acid): Toward Stable Dispersions, Langmuir 21(20) (2005) 9359--9364.

[3] M. Aguilar, N. Miralles, A.M. Sastre, Metal complexes with phosphonic and phosphinic acids, Rev. Inorg. Chem. 10(1-3) (1989) 93--119.

[4] P.H. Mutin, G. Guerrero, A. Vioux, Organic-inorganic hybrid materials based on organophosphorus coupling molecules: from metal phosphonates to surface modification of oxides. Cr Acad. Sci II C 6(8-10) (2003) 1153--1164.

[5] L. Qi, A. Sehgal, J.-C. Castaing, J.-P. Chapel, J. Fresnais, J.-F. Berret, F. Cousin, Redispersible Hybrid Nanopowders: Cerium Oxide Nanoparticle Complexes with Phosphonated-PEG Oligomers, ACS Nano 2(5) (2008) 879--888.

[6] Römpp Chemikexikon 2.0

[7] I.M. Kolthoff, S. Bruckenstein, Acid-bases in analytical chemistry, New York : Interscience Publishers (1959).

[8] X.-Q. Zeng, G.-Y. Hong, H.-P. You, X.-Y. Wu, C.-H. Kim, C.-H. Pyun, B.-Y. Yu, H.-S. Bae, C.-H. Park, I.-E. Kwon, Luminescent Properties of Gd_3PO_7:Eu in UV/VUV Region, Chin, Phys. Lett. 18(5) 690--691.

[9] U. Rambabu, A. Mathur, S. Buddhudu, Fluorescence spectra of Eu^{3+} and Tb^{3+}-doped lanthanide oxychloride powder phosphors, Mater. Chem. Phys. 61(2) (1999) 156--162.

[10] U. Rambabu, K. Annapurna, T. Balaji, S. Buddhudu, Fluorescence spectra of Er^{3+} : REOCl (RE = La, Gd, Y) powder phosphors. Mater. Lett. 23(1,2,3) (1995) 143--146.

[11] G.T. Pott, W.H.J. Stork, Transition metal ion photoluminescence as a technique for the study of structures of oxidic catalysts, Catal. Rev.12(2) (1975) 163--199.

[12] GdOCl, JCPDS no. 85-1199

[13] E. Antic-Fidancev, M. Lemaitre-Blaise, P. Porcher, J. Hölsä, Ovservation and Simulation of the Energy Levels of Trivalent Rare Earth Ions in RE Oxyhalide Matrices, Phys. Stat. Sol. A 130 (1992) K142--K153.

[14] M. Engström, A. Klasson, H. Pedersen, C. Vahlberg, P.-O. Käll, K. Uvdal, High proton relaxivity for gadolinium oxide nanoparticles, Mag. Res. Mater. Phy. 19(4) (2006) 180--186.

[15] F. Shikata, H. Tokumitsu, H. Ichikawa, Y. Fukumori, In vitro cellular accumulation of gadolinium incorporated into chitosan nanoparticles designed for neutron-capture therapy of cancer, Eur. J. Pharm. Biopharm. 53(1) (2002) 57--63.

Chapter 10

Summary and Conclusion

10.1. Summary

The enhancement of existing and development of new nanoparticular probes is a promising field of research, emanating from the increasing demand on nanoparticular contrast agents for luminescence and CT imaging. Moreover, newly developed systems give the possibility of combining both to overcome the limitations of each. In this work, the synthesis and functionalization of two quite different inorganic nanoparticular systems for imaging applications, and moreover with the prerequisites for molecular imaging applications, were presented. The first developed system is an ultra small inorganic semiconductor based nanoparticle with unique optical properties, ranging from size tunable emission to very high photostability. These quantum dots have drawn tremendous attention in the field of in vitro and small animal in vivo fluorescence imaging in the last decade (part I of the thesis). The second investigated nanoparticulate system is a lot less prominent on the field of molecular imaging till now. Nevertheless, the inherent properties of gadolinium oxide nanoparticles are as unique as those of the quantum dots. These nanoparticles are not only applicable in fluorescence imaging, but open up the way to combined multi-modal imaging and therapy (part II of the thesis).

10.1.1. Quantum Dots

Following this evolution, herein, an organometallic synthesis for long-wavelength emitting quantum dots with an effective surface passivation of the semiconductor core was developed. The synthesis parameters were optimized with respect to the emission wavelength and quantum yield. Moreover the most prominent influence factors could be dedicated. The choice of the type of Te-precursor and its respective concentration in the reaction solution is a crucial factor. The reaction scale has great influence on the quality of the synthesized quantum dots. In contrast the effect of the Cd-precursor is quite low, and the influence of the temperature was not observable in this experiments. Nevertheless, for the trioctylphosphine precursor, the use of a high precursor concentration, low reaction scale and the oleic acid cadmium precursor gives the best results. The tributhylphosphine precursor based synthesis, on the other hand, yields the best particles, with respect to wavelength and quantum yield, with a comparably low precursor concentration.

The further modification of these particles rendering them water-soluble was achieved using different surface ligands. Within the tested ligands, the PEG based molecules gave the most promising stabilization of the inorganic particles against aggregation and oxidation in aqueous

environment. The developed procedure allowed the preparation of long-term stable, water-soluble quantum dots in a simple ligand exchange reaction. Furthermore, it could be shown that the coated nanocrystals have very small diameters of sub-10 nm. Moreover, the functionalization of the nanocrystal surface with amino groups, and therefore the prerequisite for further modification with e.g. targeting functions, was achieved.

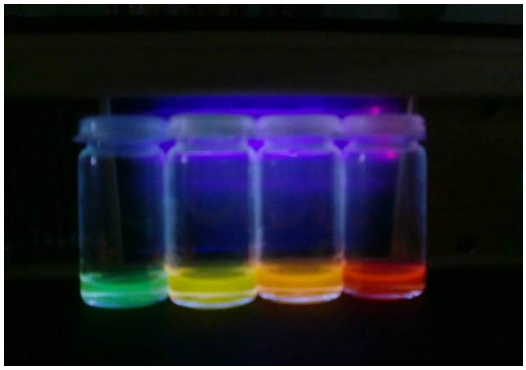

Figure 1: Picture of CdSe quantum dots with different emission wavelength under UV excitation.

Furthermore, a way to tune the amount of amino ligands, and hence, functionizable groups on the surface was developed. The examination of the cytotoxicity of as well the quantum dots, the ligands, as free cadmium ions, showed that the observed toxicity can be attributed to the attached ligands, and not to the released cadmium ions.

Table 1: Summary of all synthesized quantum dot compositions, reaction parameters, coating ligands, and tunable characteristics.

Composition	Parameters	Ligands	Characteristics
CdSe, CdSe/ZnS	Te-Precursor	Tributhylphosphine	Wavelength
CdTe, CdTe/CdSe, CdTe/CdZnS	Cd-Precursor	Trioctylphosphine	Quantum yield
	Precursor concetration	Mercaptoundecanol	Size
	Injection temperature	Dihydrolipoic acid	Hydrophilicity
	Shell growth temperature	Tri(ethylene glycol) mercaptoundecyl ether	Toxicity
	Reaction scale	Hexa(ethylene glycol) mercaptoundecyl ether	
		Amino poly(ethylene glycol)$_{750}$ mercaptoundecyl ether	
		Amino poly(ethylene glycol)$_{2000}$ mercaptoundecyl ether (PEG2000-NH_2)	

However, the tested dilutions of quantum dots exceeded the usually applied ones about three orders of magnitude, suggesting that the quantum dots can be regarded as non toxic for cellular experiments. Therefore, this preparation method turned out to be an easy way to stable biocompatible and functionizable quantum dots for biomedical applications. In table 1 a summary of all realized compositions, tested parameters, coating ligands, and the therefore tunable characteristics of these nanoparticles is displayed.

10.1.2. Gadolinium Oxide Nanoparticles

Concerning the second nanoparticulate system, two different routes were applied o synthesize those particles. One route yields bigger particles for CT contrast agent use only, the other synthesis procedure leads to particles for bimodal fluorescence- and CT-imaging. The “polyol” mediated synthesis yielded nanoparticles of bigger sizes. However, the coating step was already included into the particle formation. Herein, four ligands giving different particle properties were applied (citric acid, poly(acrylic acid), etidronic acid, PEG-bisphosphonate). All those particle species were investigated in terms stability after high pressure homogenization, freeze drying and redispersion in different media, to fabricate a stable, storable and redisperable powder for CT imaging applications. One of those as-coated

nanoparticle systems was investigated in an animal experiment, resulting in very good contrast properties in vivo.

The precipitation synthesis, on the other hand, gave smaller nanoparticles with very good luminescent properties (see figure 2). The luminescence was achieved by doping the nanocrystals with different lanthanide elements, yielding blue, green and red emission wavelengths. The parameters for optimal doping amount and annealing temperature were investigated. Moreover, the influence of the reaction time, reducing agent concentration and overall concentration on the nanoparticle size was studied.

Therefore, highly luminescent and, independently size tunable, particles could be successfully prepared. The coating of these nanocrystals was achieved using a bisphosphonate functionalized PEG ligand, giving very good stabilization against aggregation of the particles. These coated particles were applied in an in vitro CT experiment, testing the X-ray attenuation of the nanocrystals in aqueous environment. This resulted in a very good CT contrast of about 60 HU per milligram of gadolinium.

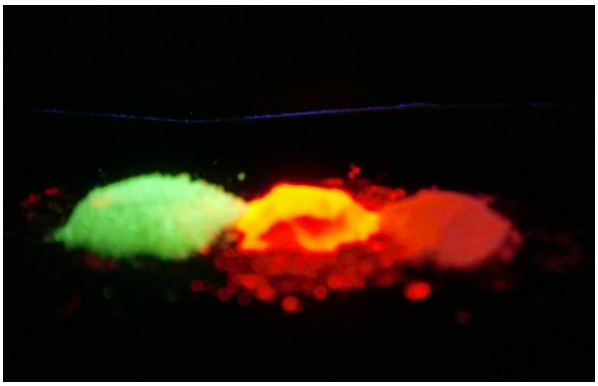

Figure 2: Picture of doped GdOCl nanoparticlulate powder under UV excitation

The testing of the cytotoxicity of all coated particles proved that there is no observable toxicity. Therefore, a successful preparation of stable, biocompatible, size-tunable, luminescence-tunable and CT active nanoparticles was achieved. In table 2 a summary of all prepared gadolinium containing nanoparticles, tested reaction parameters, applied coating ligands, used doping elements and the resulting tunable particle characteristics are shown.

Table 2: Summary of all synthesized gadolinium containing nanoparticles, synthesis parameters, coating ligands, doping elements, and tunable characteristics.

Composition	**Reaction Parameters**	**Coating ligands**	**Doping elements**	**Characteristics**
Gd_2O_3	NaOH equivalents	Silica	Europium	Size
GdOCl	Reaction temperature	Citric acid	Terbium	Wavelength
	Homogenization pressure	Poly(acrylic acid)	Erbium	X-ray attentuation
	Homogenization dispersant	Etidronic acid		Surface
	Freeze dying parameters	PEG-bisphosphonate		
	Reaction concentration			
	Equivalents reducing agent			
	Reaction time			

10.2. Conclusion

Summarizing, both of the developed systems have unique optical properties (see figure 1&2), such as “tunable” emission wavelength and high photostabilities. Within the quantum dots the emission is dependent on the size of the particles. Whereas, the emission of the gadolinium oxide nanocrystals is coupled to the respective dopand used, and the wavelength is size independent. The coated non functionalized quantum dots have remarkably low diameters giving the possibility to apply them as probes for particulate diffusion experiments into living tissues. The functionalized ones obviously offer the possibility to add targeting moieties, using them for cell experiments as well as for small animal in vivo imaging. Another research field, the nanocrystals with coatings of different hydrophilicites can be implemented in, is the incorporation into micro- or nanoparticulate dosage forms to image different processes during the formation and dissolution of these drug delivery systems. The luminescent gadolinium oxide nanoparticles, can, of course, also be used for the above mentioned approaches. Moreover, they provide a superior contrast in TEM compared to the semiconductor nanoparticles, giving the possibility to investigate the cellular fate of the particles on the nano-scale. Furthermore they open up an exciting way for new bi- or multimodal imaging applications. The non-doped particles proved to give very good CT contrast within rats, and therefore the luminescent nanocrystals can be applied for combined small animal in vivo CT

and fluorescence imaging. One promising feature, which has still to be investigated with the herein synthesized gadolinium oxide nanoparticles, is their MRI contrast. This is expected to be superior to those of the gadolinium chelates currently used. The second and even more, interesting feature is the application for neutron capture therapy, enabling this unique nanoparticulate system to overcome the limitations of diagnostics for a combination of imaging and therapy.

Chapter 11

Abbreviations

A	absorbance of sample
AIBN	α,α´azoisobutyronitril
APTES	(3-aminopropyl)triethoxysilane
A_R	integrated area under the corrected fluorescence spectrum of the reference fluorophore
A_S	integrated area under the corrected fluorescence spectrum of the tested substance
BOC	(tert-butly)carbonate
BP-PEG	hexa(ethylene glycol) bisphosphonate
BRET	bioluminescence resonance energy transfer
c	concentration of sample
CA	citric acid
CT	computer tomography
D	diameter of the nanaoparticles
d	length of penetratured medium
D±	size distribution of the diameter of the nanoparticles
DEG	diethylene glycol
DHLA	dihydrolipoic acid
DMSO	dimethlysulfoxide
DNA	desoxyribonucleic acid
EDTA	ethylendinitrilotetraacetic acid disodium salt dehydrate
EMEM	Dulbecco´s modified Eagle´s medium
E_R	absorbance at the excitation wavelength of reference fluorophore
E_S	absorbance at the excitation wavelength of the tested substance
ES	etidronic acid
FBS	fetal bovine serum
Fluram®	fluorecamine
FRET	Förster resonance energy trasnsfer

fwhm	full width at half maximum
HAD	hexadecylamine
HAM	nutrient mixture F-12 HAM
^{1}H NMR	proton nuclear magnetic resonance
HPLC	high pressure liquid chomatograpy
HU	Houndsfield unit
I	transmitted X-ray intensity
I_0	incident X-ray intensity
ICP-MS	inductively coupled plasma mass spectrometry
ICP-OES	inductively coupled plasma optical emission spectroscopy
K	magnification constant
k_{nr}	rate of non radiative processes
MRI	magnetic resonance imaging
MTT	3-[4,5-Dimethylthiazol-2-yl]-2,5- diphenyltetrazolium bromide
MWCO	molecular weight cut-off
n_R	refractive index of the solvent for the reference fluorophore
n_S	refractive index of the solvent for the tested substance
ODE	octadecene
PA	poly(acrylic acid)
PAMAM	poly(amidoamine)
PBS	phosphate buffered saline
PCS	photon correlation spectroscopy
PEG	poly(ethylene glycol)
PEG2000-NH_2	amino poly(ethylene glycol)$_{2000}$ mercaptoundecyl ether
PEG3	tri(ethylene glycol) mercaptoundecyl ether
PEG6	hexa(ethylene glycol) mercaptoundecyl ether
PEG750-NH_2	amino poly(ethylene glycol)$_{750}$ mercaptoundecyl ether
PEG-bisphosphonate	hexa(ethylene glycol) bisphosphonate

PEI	poly(ethylene imine)
PES	poly (ether sulfon)
PET	positron emission tomography
PXDR	powder X-ray diffraction
Q	quantum yield
QD	quantum dot
S_n	Singlet ground state
SPECT	single photon emission computed tomography
SPIO	superparamagnetic iron oxide
T_1	longitudinal relaxation time
TBP	tributylphosphine
TEA	triethylamine
TEM	transmission electron microscope/microscopy
TEOS	tetraethyl orthosilicate
THF	tretahydrofuran
T_n	Triplet ground state
TOP	trioctylphosphine
TOPO	trioctylphosphine
UD	mercaptouncdecanol
US	ultrasound
x	thickness of matter
XRD	X-ray diffraction
Z	atomic number
Γ	rate of luminescence of the fluorophore
δ	Compton effect
ε	decadic molar absorbance coefficient
λ_{max}	wavelength of the first absorbance maximum

μ	mass attenuation coefficient of the absorber
μ_p	linear attenuation coefficient of a pixel
μ_w	linear attenuation coefficient of water
τ	photoelectron effect
Φ_F	quantum yield
Φ_R	quantum yield of the reference
Φ_S	quantum yield of the substance to be determined
ω	coherent scattering

Chapter 12

Supplement

```
Peak File  : C:\Dokumente und Einstellungen\Anna\Desktop\hea001-1.pks
File title : Gd203 : Tb  200 °C   [79]  10.12.2009

Wavelength : 1.540598

Number of accepted peaks : 10

2Theta window : 0.050

2Theta zeropoint : -0.0377 ( refineable )

Symmetry   : Tetragonal P

Initial cell parameters :
Cell_A     : 3.9481
Cell_C     : 6.6742

Refined cell parameters :
Cell_A     : 3.9424(16)
Cell_C     : 6.677(4)
Cell_Volume: 103.78(11)

Number of single indexed lines : 8
Number of unindexed lines      : 2

2Theta zeropoint : -0.055(17)

Final 2Theta window : 0.0200
```

N	2Th[obs]	H	K	L	2Th[calc]	obs-calc	Int.	d[obs]	d[calc]
1	13.233	0	0	1	13.249	-0.0163	41.9	6.6854	6.6772
2	26.242	1	0	1	26.230	0.0126	100.0	3.3932	3.3948
3	32.093	1	1	0	32.081	0.0120	82.9	2.7867	2.7877
4	35.210	1	0	2	35.197	0.0131	93.5	2.5469	2.5478
5	42.190	1	1	2	42.198	-0.0079	22.3	2.1402	2.1398
6	45.991	2	0	0	46.006	-0.0149	38.5	1.9718	1.9712
7	52.574	1	1	3	52.574	-0.0002	22.8	1.7394	1.7393
8	53.730	2	1	1	53.728	0.0017	31.8	1.7046	1.7047
9	59.292	--- not indexed ---					35.3	1.5573	
10	60.242	--- not indexed ---					14.0	1.5350	

```
Average delta(2Theta) = 0.010
Maximum delta(2Theta) = 0.016 ( peak 1 ) = 1.7 * average

Figure of Merit F(8) = 40.6 ( 0.010, 20 )

Durbin-Watson serial correlation = 1.378

Sqrt[ sum( w * delta(q)^2 ) / ( Nobs - Nvar ) ] = 0.00011787
```

Chapter 13

Curriculum Vitae and List of Publications

Curriculum Vitae

Family Name:	Hezinger
Name :	Anna Franziska Elisabeth
Date of Birth :	20.05.1981
Place of Birth:	Ulm
Nationality :	German
Adress :	Deutschherrnweg 2, 93053 Regensburg

Studies

01/2006 - 04/2010	**PhD Thesis** Institut für Pharmazie, Lehrstuhl für Pharmazeutische Technologie, Prof. A. Göpferich, Universität Regensburg Topic: „Biocompatible Inorganic Nanoparicles for fluorescence and CT Imaging“
11/2005	Graduation: **Diplom Chemiker**
03/2005 - 11/2005	**Diploma Thesis** Institut für Analytische Chemie, Chemo- und Biosensorik, Prof. Otto S. Wolfbeis, Universität Regensburg Topic: „Design of New Iridium-based Metal-Ligand Complexes for Protein Labeling Approaches”
11/2000 - 12/2004	**Chemistry (Diploma)** Universität Regensburg, Regensburg

Education

06/2000	Graduation: **allgemeine Hochschulreife (Abitur)**
09/1991 - 06/2000	**Bertha-von-Suttner Gymnasium** Neu-Ulm / Pfuhl

List of publications

Poster Presentations

A.F.E. Hezinger, B. Kosog, J. Teßmar, A. Göpferich: CdTe/Cd_xZn_yS and $CdSe_xTe_y$/ZnS alloyed core-shell quantum dots - Control of composition and luminescent properties. NaNaX 3, Lecce, Italy (2008).

W. Hild, K. Zenger, C. Rose, A. Hezinger, J. Teßmar, A. Göpferich: Towards the optimization of quantum dot preparation for use in biological systems. NaNaX 3, Lecce, Italy (2008).

A.F.E. Hezinger, J. Tessmar, A. Goepferich: Control of shape and luminescent properties in CdTeZn/Cd_xZn_yS alloyed core-shell quantum dots. ACS National Fall Meeting, Boston, Massetusets (2007).

C. Rose, A. Hezinger, C. Becker, J. Teßmar, A. Göpferich: Imaging of particulate delivery systems - Quantum dots as sensitive fluorescent probes. DPhG Jahrestagung, Erlangen (2007).

C. Rose, A. Hezinger, C. Becker, J. Teßmar, A. Göpferich: Quantum Dots as tool for the long-term imaging of particulate drug delivery systems. CRS Annual Meeting, Long Beach, California (2007).

C. Rose, A. Hezinger, C. Becker, J.Tessmar, A. Goepferich: Quantum Dots – fluorescent markers for particulate delivery systems. CRS German Chapter, Freiburg i. Brsg. (2007).

A.F.E. Hezinger, J. K.Teßmar, A. Göpferich: Surface modified Quantum dots for the development of new drug delivery systems. Partec, Nürnberg (2007).

Oral Presentations

A.F.E. Hezinger, B. Kosog, A. Göpferich and J. Teßmar: Synthesis and Characterization of Long-Term Stable, Long-Wavelength Emitting and Water Soluble Quantum Dots. CRS Annual Meeting, Copenhagen, Denmark (2009).

Paper

A. F.E. Hezinger, A. M. Goepferich, J. K. Tessmar: Polymer coated quantum dots. Handbook of Nanophysics, in press

A.F.E. Hezinger, J. Teßmar, A. Goepferich: Polymer coating of quantum dots – A powerful tool toward diagnostics and sensorics. European Journal of Pharmaceutics and Biopharmaceutics 68, 138-152 (2008).

T. Nilges, C. Dreher, A. Hezinger: Structures, phase transitions and electrical properties of $Ag_5Te_{2-y}Se_yCl$ (y = 0–0.7). Solid State Sciences, 7(1), 79-88, (2005)

Erklärung

Hiermit versichere ich, dass ich die vorliegende Arbeit selbst verfasst und keine anderen als die angegebenen Quellen und Hilfsmittel verwendet habe.

Regensburg, den

_____

Anna Hezinger